ABSTRACT

Title of Dissertation: DEVELOPMENT OF BETA-LACTOGLOBULIN BASED PARTICLES AS COLLOIDAL STABILIZERS AND EVALUATION OF THEIR PERFORMANCE ON INTERFACES

Jinglin Zhang, Doctor of Philosophy, 2020

Dissertation directed by: Associate Professor, Qin Wang
Department of Nutrition and Food Science

Beta-lactoglobulin (Blg) is a major whey protein in bovine milk. The desirable functional properties of Blg make it a versatile material, which has been processed into various types of colloidal systems such as nanoparticles, microgels and emulsions. This dissertation first developed several stable colloidal systems using native Blg molecules or denatured Blg aggregates as stabilizers. The study then elucidated the stabilization mechanism by characterizing Blg microgels adsorption on the interface.

Firstly, novel selenium nanoparticles were developed using Blg as a stabilizer. The synthesized Blg-selenium nanoparticles were stable at pH 2.5-3.5 and 6.5-8.5 at 4ºC for 30 days as a result of electrostatic repulsions. Furthermore, the cell toxicity of selenium nanoparticles was significantly lower than that of sodium selenite on both cancerous and non-cancerous cells, implying their potential uses as anti-cancer medicines.

The second part of this study was to stabilize a novel water-in-water (W/W) emulsion system using self-assembled Blg microgels. The microstructure and stability of the W/W emulsion were investigated under different environmental conditions. Microgels accumulating at the liquid-liquid interface led to a stable emulsion at pH 3 to 5. When pH was increased above the pI of the microgels, the emulsion was destabilized because the microgels tended to stay in the continuous phase (i.e., dextran) rather than the interface. In addition to electrostatic interactions, interfacial tension and hydrophobic attraction between microgels and two polymer phases were investigated to better understand the driving force for particles' accumulation at the interface.

Lastly, we proposed a new method to study the interfacial properties of Blg microgel. Quartz crystal microbalance with dissipation (QCM-D) was employed to investigate adsorption behavior of Blg microgels on a hydrophobic solid surface, which was hypothesized to mimic the oil-water interface. Coupling with atomic force microscopy (AFM), QCM-D showed the ability to characterize the microgels adsorption efficiency and viscoelasticity of adsorbed layer on the solid surface. The application of QCM-D and AFM enabled us to generate insights into the fundamental behavior of soft particles at a solid-liquid interface.

DEVELOPMENT OF BETA-LACTOGLOBULIN BASED PARTICLES AS COLLOIDAL STABILIZERS AND EVALUATION OF THEIR PERFORMANCE ON INTERFACES

by

Jinglin Zhang

Dissertation submitted to the Faculty of the Graduate School of the
University of Maryland, College Park, in partial fulfillment
of the requirements for the degree of
Doctor of Philosophy
2020

Advisory Committee:
Professor Qin Wang, Chair
Professor Rohan V. Tikekar
Professor Seong-Ho Lee
Professor Amy J. Karlsson
Professor Taylor J. Woehl

Acknowledgements

I am grateful to my advisor, Dr. Qin Wang, for her guidance and support during my study. My graduate life has been a meaningful journey to have an advisor who inspired and helped me with her tremendous knowledge and patience, provided me with the best research conditions possible, as well as giving me the freedom to explore the world of unknown.

I would like to thank my dissertation committee members, Drs. Rohan V. Tikekar, Seong-Ho Lee, Amy J. Karlsson, and Taylor J. Woehl. I sincerely appreciate their time and effort in helping me throughout my research. This work would not be completed without their support and guidance.

Special thank goes to my labmates, Lei Mei, Zi Teng, Nannan Chen and Peihua Ma, as well as my friends in the department, Zhiyuan Lou, Qiao Ding, Qingyang Wang, Yinzhi Qu, Xuji Su, Si Fan, Jihye Lee, Surabhi Rani, Shraddha Karanth, and Yuan Li. These people offered me great advices and extensive assistance, not only in my research but also in every aspect of my life.

I owe my deepest gratitude to my family members for their endless love and support. I want to thank my parents, who raised, guided and supported me for decades. I am particularly thankful to my husband, Pengjun Xia, for his unconditional love. He is also the first person who inspired and encouraged me to start my PhD five years ago.

Last but not least, I would like to appreciate the University of Maryland for providing such a good academic environment. I want to thank University of Maryland NanoCenter, Surface Analysis Center, Imaging Core Facility, and Dr. Silvia Muro, for their kind technical supports. Special thanks go to Dr. Yaguang Luo and Dr. Bin Zhou from U.S. Department of Agriculture for their technical supports.

Table of Contents

List of Tables

List of Figures

1. Chapter I: Literature Review

1.1 Overview of colloidal systems

Colloidal systems such as dispersions and emulsions are highly prevalent in many food products. Colloids form when a substance is dispersed throughout another substance at a microscopic level. Colloidal systems are not stable, thus potentially resulting in adverse effects on food products; e.g., phase separation of an emulsion leads to undesirable texture and appearance of salad dressings. Hence, the ability to control the stability of structures containing colloidal systems is essential for improving the quality and prolonging the shelf-life of food products. To achieve this goal, a wide range of emulsifying and stabilizing agents, including small-molecule surfactants, proteins and polysaccharides are used. These compounds are surface active, and their main functions in emulsions are to lower the interfacial tension and/or form a viscoelastic film at the interface and protect newly formed droplets against unwanted flocculation and coalescence. Among the numerous candidate surfactants, proteins are the top choice because of their high biocompatibility and multiple functionalities. The desirable functional properties of proteins, including emulsifying and gelling properties, together with excellent solubility, make them a versatile material that can be processed into various types of colloidal systems, such as nanoparticles (NPs), microgels and emulsions.

1.2 β-lactoglobulin and β-lactoglobulin particles

1.2.1 β-lactoglobulin

Bovine β-lactoglobulin (Blg) comprises approximately 10-15% of the protein content in milk. The primary structure of Blg consists of 162 amino acids with a

molecular weight around 18.60 Kg/mol. Commercially available Blg products contain two variants, namely, variant A and B, which differ at two amino acid substitutions 64 (Asp/Gly) and 118 (Val/Ala) [1]. In both variants A and B, Blg contains two disulfide bonds and one free thiol group on cysteine residue, which are important for stable tertiary and/or quaternary structures and many biological functions of Blg. Blg comprises predominantly a β-sheet configuration containing nine antiparallel β–strands from A to I. The β–strands A-D form one surface of the barrel(calyx), whereas β-strands E-H form the other.

Blg is a member of lipocalin protein family, which is able to carry small hydrophobic molecules into their hydrophobic cavity and therefore may provide a transport for bioactive ingredient such as retinol, fatty acids, and vitamin D3 [2]. Furthermore, Blg demonstrates a significant resistance to peptic digestion because of the compactly folded conformation, which is originated from the abundance of rigid β-sheet structures. On the other hand, Blg is much more readily degraded by trypsin in small intestine [3]. Blg has been used as a model globular protein for a wide range of studies because of its well-defined molecular structure, abundance, and ease of extraction from milk.

1.2.2 Blg Nanoparticles

NPs from both inorganic and organic compounds offer the possibility of entrapping poorly soluble anti-cancer nutraceuticals/drugs, thus rendering them suitable for oral administration and modifying the blood circulation and tissue distribution of cargos to achieve preferential accumulation at selected tumor sites [4]. The unique optical and magnetic characteristics of inorganic NPs, such as Fe_3O_4 and AuNPs,

make them potential carriers for cancer therapy and imaging applications. However, toxicity has been reported for inorganic NPs, and their high tendency to aggregate may hinder their applications in cancer therapy. One way to overcome the pitfalls of inorganic NPs is to hybridize them with lipids, polysaccharides and proteins. Among these, proteins have various advantages, especially in tumor-targeted delivery for drugs and stimuli-responsive delivery systems. Below, some representative studies are discussed to illustrate advanced applications of Blg-NPs hybrids in drug delivery.

Target delivery

Blg contains multiple functional groups (e.g., NH_2, COOH and OH) available for drug conjugation or ligand-mediated tumor delivery. Carbodiimide coupling is the most commonly used reaction for protein-NP conjugation via an amide or an ester bond formation. Ethyl-3-(3-demethylaminopropyl) carbodiimide hydrochloride (EDC) as a linker for conjugation has been found to be comparable to bifunctional crosslinkers, e.g., glutaraldehyde, while avoiding their toxicity [4]. The active amino groups on Blg have been used for functionalization of Blg and doxorubicin (DOX) nanohybrids with two moieties: fluorescein isothiocyanate through a direct reaction with folic acid via EDC coupling. Conjugation of these NPs with folic acid has been found to enable an efficient receptor-mediated endocytosis and drug releasing in acidic endocytic organelles *in vitro*. The nanohybrids significantly inhibited cell proliferation in MCF-7 and MDA-MB-231 cells at much lower doses than those of free DOX [5].

Another common linker, succinic anhydride, has been used to conjugate mesoporous silica NPs (MNPs) to proteins [6]. In this approach, the MNPs were first functionalized with 3-aminopropyl triethoxysilane to yield NH_2-MNPs. Then, succinylated Blg was conjugated to the NH_2-MNPs via EDC coupling. The binding of succinylated Blg to functionalized mesoporous silica NPs resulted in a 3-D pore network and yielded an oral drug delivery system with high colloidal stabilities and sustained-release properties.

Stimuli-responsive delivery

As a charged macromolecule, Blg can interact electrostatically with oppositely charged inorganic NPs, thus forming a protein shell around the NPs. The pH differences between the systemic circulation and the tumor compartment can be used as a biological stimulus to trigger drug release from protein-NPs hybrids. Because proteins are composed of both acidic and alkaline units, they are amphiphilic, and the number and distribution of charges vary as a function of the pH of the surrounding aqueous solution. Above the isoelectric point (pI), which is 5.2 for Blg, the proteins are negatively charged, whereas at lower pH values, the net charge is positive. At the pI, the net charge is zero, but the Blg still contains positively and negatively charged patches. Instability of pure Blg NPs has been considered a drawback because of the formation of aggregate or precipitate at the protein's pI. Blg NPs coated by a polysaccharide (i.e. pectin) have been reported to improve their stability under a wider pH region because of electrostatic attraction between the anionic polysaccharide and the protein particles' positively charged patches, thus increasing the entropy of the system[7]. Moreover, the disruption of electrostatic attraction resulting from increasing the negative charges on the Blg

NPs has indicated a new structure pH-responsive sensitivity, the pectin coated Blg NPs is stable in acidic conditions but is able to release its cargo at pH 7[7].

1.2.3 Blg microgels

Thermal aggregation of Blg

When whey protein isolate (WPI) or pure Blg is heated above 60 ºC in an aqueous solution, the peptide chains become mobile and then interact with other protein molecules. Bonds can form between protein molecules, thus leading to aggregation. The morphology of the aggregates depends on the pH (Fig. 1.1). Curved strands with a diameter of several nanometers are formed when the effective charge density of WPI or Blg is high (at pH 7.0), whereas spherical particles with a radius of approximately 100 nm are formed when the pH is low (at pH 5.8, which close to the protein's pI). The spherical protein particles consist of a hydrated network of covalently crosslinked proteins and may therefore be considered microgels [8]. At very low pH levels (1.5–2.5) and low ionic strength, long rigid fibrils are formed when WPI or Blg is heated extensively. However, at this low pH, the proteins are hydrolyzed, and fibrils are formed in a fraction of the peptides. At higher protein concentrations, the strands or the microgels randomly associate into larger self-similar aggregates, and above a critical concentration, gels are formed. The details of the kinetics of Blg aggregation have been reviewed elsewhere [9] and are not the focus of this study.

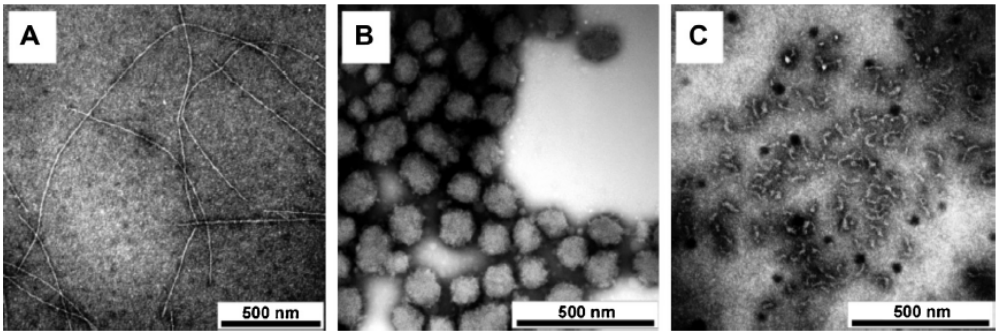

Figure 1.1 Negative-staining TEM images of aggregates formed after heating 10 g/L Blg in aqueous solutions at pH 2.0 (A), pH 5.8 (B) and pH 7.0 (C). Figure adapted from Literature[10]

The spherical particles, also called microgels, were studied herein. After heating of dilute protein solutions at temperatures up to 85 ºC under mildly acidic conditions (pH 5.8–6.2), stable microgel particles formed spontaneously in the absence of external cross-linking agents. Stable microgel suspensions can be formed through fine-tuning the protein's charge density, which has a narrow range between approximately three and five charges per protein. When the charge density is high, strands are formed, and when it is low, microgels associate into larger clusters[11]. The size of microgels is also affected by charge density, which increases with decreasing protein net charge. Whey protein microgels (WPMs) are considered to have many potential applications in food systems, such as interfacial and bulk functionality in the stabilization of aqueous foams, structural functionality in the fabrication of cold-set acid-induced gels and particularly the ability to stabilize oil-in-water (O/W) emulsions over a wide range of pH values and ionic strengths.

Characteristics of Microgels

An appealing feature of WPMs is their pH and ionic strength responsiveness. WPMs can form stable dispersions between pH 2 and 8, but are unstable and

undergo reversible aggregation in the pH range 4<pH<5.5. At pH values above 10, at which disulfide bridges are broken, microgel structure disintegrates. Zeta-potential measurements have indicated that WPMs exhibit a polyampholyte character around the pI of 4.82. Samples have been found to be stable against aggregation/precipitation when the zeta-potential value exceeds an absolute value of 20 mV, correspond to Blg solution at pH values below 4 and above 5.5. Thus the colloidal stability of WPMs appears to be controlled primarily by their overall charge [12]. Therefore, a similar trend has been observed in the presence of NaCl, in which the instability domain shifts toward an acidic pH (3.5<pH<5.0) with the addition of 150 mM NaCl [13].

Microgels are soft and poorly cross-linked particles swollen by water, and their swelling behavior is largely dependent on the degree of solvation of the constitutive protein units and on the attractive or repulsive electrostatic interactions between their charges. The minimum microgel size has been found to be close to the pI in the absence of salt, corresponding to the domain of charge neutralization. Microgels swell at higher and lower pH values, at which their net charges are higher. An asymmetric swelling behavior is observed on either side of the pI, and the swelling degree is more pronounced under acidic pH. Although the WPM size reflects the de-swelling and swelling cycle, as shown in Fig. 1.2, when the pH is increased, the polydispersity of the particle size does not change significantly with pH [12].

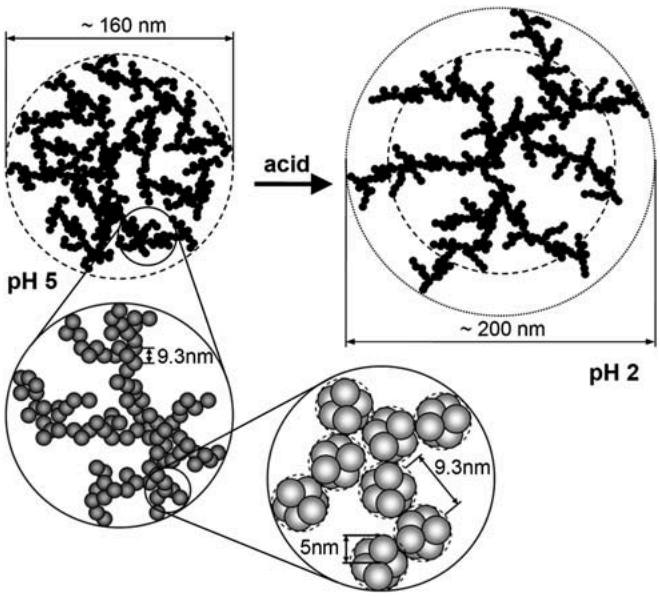

Figure 1.2 WPM particles of a hierarchically structured interior. (Figure adapted from literature[12])

When urea or SDS is combined with dithiothreitol, a reducing agent that breaks disulfide bonds, the WPM dissociates, thus leading to the formation of soluble aggregates exhibiting a hydrodynamic radius of approximately 40 nm. These soluble aggregates are thought to correspond to the WPM building blocks under denaturing conditions for microgels. A mechanism for WPM formation has been proposed[12]. After heat denaturation, the unfolded whey proteins expose the hydrophobic regions, which associate into small oligomers relatively rapidly; soluble aggregates then are formed and are primarily maintained by hydrophobic and hydrogen bonds. Subsequently, intra-particle disulfide bonds are formed, thus leading to covalent stabilization of the structure. In contrast to more uniform cross-linked networks of synthetic polymer microgels, WPMs have a complex hierarchical structure consisting of strands of clusters of the soluble protein aggregates, as shown in Fig. 1.2 [12].

1.3 Blg microgels in Pickering emulsions

1.3.1 Overview of Pickering emulsions

Pickering emulsion is emulsion stabilized by particles, it was termed after a publication by Pickering [14]. Colloidal particles such as microgels are inherently surface active at both oil-water and air-water interfaces, because of their amphiphilic polymer character. However, the colloidal particles function as emulsion stabilizers in a fundamentally different manner from small surfactants or molecules in traditional emulsions. The concept of food-grade Pickering emulsions attracts more and more attention from both theoretical and practical points of view, because they add exceptional values, as compared with inorganic particles or conventional emulsifiers.

Just as amphiphilic properties (defined as the hydrophilic-lipophilic balance) play an essential role in conventional emulsifiers, the wettability of solid particles is a key property governing the formation and stabilization of Pickering emulsions. Usually, the three-phase contact angle θ (formed at the three-phase boundary where solid particles, continuous phase and dispersed phase intersect) is used to semi-quantitatively determine this property. After a particle with radius r is attached to the oil-water interface, the free energy of spontaneous desorption, ΔG_d, is extremely high compared with the thermal energy:

$$\Delta G_d = \pi r^2 \gamma_{OW} (1 - \cos\theta)^2$$

where γ_{OW} is the oil-water interfacial tension, and θ is the three-phase contact angle of the particle between the solid and two liquids. As long as the contact angle

is not too far from 90°, for relatively small NPs (r = 5–10 nm), the process of particle adsorption at the oil-water interface is essentially irreversible ($\Delta G_d \gg 10\ kT$) [15].

1.3.2 Differences between solid particles and microgels in Pickering emulsions

General principles allowing solid particles to function as Pickering emulsion stabilizers have been summarized by Xiao et al. [16] as follows: i) particles should be partially wetted by both the continuous and dispersed phase, yet should not be soluble in either phase; ii) particles should preserve proper partial wettability to gain a sufficient interface absorption efficiency; iii) the particle size should be substantially smaller than the targeted emulsion droplet size (by at least one order of magnitude). Microgels differ considerably from solid particles in terms of their interfacial properties. After being localized to the oil-water interface, microgel particles undergo deformation and structural rearrangement, as subject to the topological constraints of the internal polymer network and colloidal interactions with other adsorbed particles. As mentioned above, the contact angle of solid particle surfaces at the oil-water interface is a key parameter for Pickering emulsions, but for deformable, porous microgels, the contact angle concept is ill-defined and inappropriate[17]. That is, the behavior of an adsorbed microgel particle should be characterized not by a single point (or line) of contact but instead by a continuous profile of the polymer density. Moreover, individual microgel particles deform on the interface depending on the local state of solvent penetration and their interactions with other adsorbing microgels on the interface.

Another difference between microgels and solid particles is that the interfacial layers of charged microgels are more easily compressed than the corresponding

layers of uncharged microgels, because of the difference in the swelling behavior of charged and uncharged states [18]. The presence of charges and thus of counterions inside microgels leads to enhanced swelling, which affects the viscoelastic properties of the interface. The stabilization of the microgel-stabilized emulsions does not depend on electrostatic repulsion, although the presence and location of charges are relevant. The ability of microgels to form a tightly packed monolayer of compressed microgel particles at the interface provides a mechanism basis for emulsion stabilization by microgel particles [19]. However, these conclusions have mostly been obtained from synthetic microgels.

To highlight the similarities and differences of Pickering emulsion systems stabilized by microgels versus by solid particles, the former have been given the nickname "Mickering emulsions" [17]. Here, the techniques and corresponding findings regarding the interfacial properties of microgels in Pickering emulsion systems are reviewed.

1.3.3 Interfacial properties of microgels by different techniques

Direct measurement of contact angles using an optical microscopy for particles attached to the liquid interface seems rather straightforward and simple. However, this method is suitable for only particles larger than 30 μm, which are rare in fabricated food-grade particles. In 2012, de Folter et al. [20] applied a captive drop method to measure the contact angle of zein colloidal particles. In their experiment, a homogeneous zein film was initially formed and then placed on top of the water subphase. Next, an oil droplet was attached to the film surface in the water phase with a bent needle tip. The static contact angle of the oil droplet at the zein film was

measured with a Data Physics OCA15 setup. The particle film-oil-water contact angle was clearly not a perfect replica of three-phase contact of a particle at the water-oil interface. Nevertheless, using this method it is easy to predict the wetting properties of zein particles because the measured contact value demonstrates the potential of zein particles as Pickering emulsifiers, and it is sensitive at different medium conditions (i.e., ionic strength and pH).

Of note, the three-phase contact angle concept is based on perfectly spherical and rigid particles, whereas in reality particles fabricated from edible materials are usually non-spherical and have deformable properties. Thus, the contact angle is more useful in theory than in real-world applications, such as food-grade particles. Consequently, in practice, researchers tend to use interfacial microstructure observations and rheometry as more appropriate criteria for evaluation. In this study, we also evaluated the possibility of using QCM-D to study the interfacial properties of microgels.

Confocal laser scanning microscopy (CLSM)

CLSM uses a laser beam to acquire in-focus images with a submicron resolution from selected depths. This instrument allows researchers to obtain two-dimensional structural images, three-dimensional image reconstruction, and quantitative measurements of the depth of the particle coating layer. To identify the position and morphology of particles at the interface, the particles should be autofluorescent or stained with fluorescent dye. In some cases, one of the two emulsion phases can be labeled with a fluorescent dye to aid in phase identification. In the field of emulsion droplets stabilized by food-grade particles, CLSM is extensively useful and widely

applied to collect direct evidences of adsorption of WPMs at droplet interfaces [21]. Interestingly, CLSM may be used to determine the contact angle by visualizing the fluorescently labeled particles at the interface [22], but it is suitable only for rigid spherical particles.

Cryogenic scanning electron microscopy (cryo-SEM)

Cryo-SEM is used to visualize packing structures of particles with average sizes below 100 nm at an interface, which enables *in situ* characterization of nanoscale particles at liquid-liquid interfaces. One of the most exciting case studies using cryo-SEM in food-grade particles stabilized Pickering emulsion was conducted by Destribats et al. [13]. Direct visualization of WPMs at interfaces of heptane-in-water emulsions by cryo-SEM has shown that the microgels adsorb differently depending on the pH and salinity, either forming a dense 2-D network of aggregated particles or leaving the drops poorly protected with sparsely distributed particle aggregates. In the latter case, bridging events have been observed between drops as the origin of the flocculation of the emulsions. The high resolution of SEM enables the discovery of different packing structures of particles at interfaces and the continuous protein thin films between protein aggregates.

Atomic force microscopy (AFM)

AFM is used to visualize Pickering emulsion droplets. Moreover, it enables measurement of the stiffness and strength of the interfacial shell, thus aiding in characterization of Pickering emulsions. Instead of directly characterizing Pickering emulsion droplets, AFM studies often measure the *in situ* adsorption of microgels on silica or gold surfaces [23, 24]. The topography and mechanical properties

of WPM particles have been investigated at pH 6.5, 5.5 and 3.0. AFM force-distance measurements enable quantification of the effective Young's modulus and have shown a significant increase in stiffness at pH 5.5 and 3.0, by more than 15-fold compared with that at pH 6.5 [24]. However, AFM data must be interpreted with caution, because the adsorption occurs on a flat surface rather than the droplet surface, and using a different immobilization strategy on an AFM chip may interfere with the microgel interaction on the surface.

Interfacial rheological behavior

Because of its susceptibility to gravity induced creaming during storage, the concentrated creaming layer of Pickering emulsions usually behaves like a weak gel-like emulsion with a viscoelastic rheological behavior. The presence of particles at emulsion interfaces with high droplet volume fractions then yields rigid interfaces with surface elasticity. The elastic storage modulus is contributed by the compression of emulsion droplets, which permits the storage of interfacial energy by deforming the droplet interfaces, and by interfacial elasticity resulting from the strong adhesion between solid particles adsorbed at the oil water interface. Measurements of dynamic surface pressure and dilational elastic modulus [25] have shown that the adsorption of Blg microgels is influenced by their sizes and their bulk concentrations: smaller microgel particles have faster adsorbing ability and generate layers with greater elasticity; Interfacial compression increases surface pressure but not elasticity, possibly due to mechanical disruption of inter-particle interactions.

Quartz crystal microbalance with dissipation (QCM-D)

QCM-D is a technology that enables real time measurement of biological materials' adsorption and/or interactions on various surfaces. This method relies on a voltage being applied to a quartz crystal, causing it to oscillate at a specific frequency. QCM-D is able to measure two individual parameters: the adsorbed mass, by changes in frequency (Δf) of the quartz crystal, and the structural (viscoelastic) properties of adsorbed layers, provided by the energy dissipation parameter (ΔD). In addition, through monitoring both Δf and ΔD, the viscoelastic variables relating to the shear viscosity and the storage modulus of adsorbed biological materials can be quantified [26]. QCM-D has been shown to be a powerful tool because of its ability to monitor the adsorption of microgel particles to a gold surface, their subsequent swelling and collapse due to pH changes, and the uptake of other functional particles by the microgel [27-29]. Simultaneously, the viscoelastic properties of the adsorbed microgel film are evaluated with a combination of two parameters (Δf and ΔD) from QCM-D. The gold coated quartz crystals used in QCM-D experiments have been modified with the alkane thiol molecule $(CH_3CH_2)_{14}CH_2SH$ to mimic the oil-water interface in real emulsions [30]. The thiol group in this molecule was immobilized onto gold surfaces through a covalent bond [31]; therefore a hydrophobic self-assembled monolayer containing CH_3 terminal groups on the quartz crystal surface is formed. This model surface has been used to study whey protein and lactoferrin interactions at an oil-water interface by QCM-D.

1.4 Blg microgels stabilized water-in-water emulsions

1.4.1 Formation of water-in-water emulsions

Mixtures of two hydrophilic polymers in an aqueous solution usually have three different phase behaviors: (a) complete miscibility, in the case of weak interactions

between the two types of polymers; (b) associative phase separation, with formation of a precipitate/coacervate, because of strong attractive interactions between the two polymers; or (c) segregative phase separation induced by repulsive interactions among polymers. The third case leads to the formation of aqueous two-phase systems (ATPS), in which two aqueous solutions in a thermodynamic equilibrium are formed. A depletion model gives the thermodynamic explanation for the phase separation of polymers in a solution based on an excluded volume [32]. The excluded volume effects, in which physical volume of one biopolymer molecule is not available to the other biopolymer molecule, are highly related to the size and shape of the biopolymers [33].

In these ATPS, water-in-water (W/W) emulsions are formed by mixing of two incompatible water-soluble macromolecules, thus leading to a dispersed phase enriched with one macromolecule and a continuous phase enriched with the other. These emulsions are characterized by extremely low interfacial tension, generally between 10^{-4} and 10^{-6} N/m (100–1000 times lower than the interfacial tension of a typical oil-water interface) [34]. In contrast to O/W emulsions, W/W emulsions cannot be stabilized by the addition of molecular surfactants, because the interface is expressed only on length scales larger than the correlation length of the macromolecule solutions [35]. Effective stabilization of an emulsion can be achieved by the accumulation of particles, such as quartz, latex, and protein microgels, at the water-water interface [34, 36]. Blg particles adsorbed spontaneously at the interface inhibit W/W emulsion coalescence [21], whereas an individual protein molecule is too small to adsorb at the water-water interface.

1.4.2 Factors affecting water-in-water emulsion stability

Particle morphology

The effects of Blg particle's morphology on the structure and stability of dextran and polyethylene oxide emulsion have been studied by Gonzalez-Jordan et al. [37]. Spherical microgels, fractal aggregates and rod-like fibrils were prepared by heating Blg solutions under different conditions. Fibrils were found to be the most effective stabilizer at pH 7, whereas the fractals were most effective at pH 3. At pH 3.0, creaming or sedimentation happened very slowly when the emulsions were stabilized by fractals. Fractals have a much lower density than fibrils and microgels and therefore can cover a large area at the same protein concentration.

pH and ionic strength

Microgels are characterized by their sensitivity to ionic strength and pH, thus leading to two behaviors of W/W emulsion. In the dextran/PEO emulsion system, protein particles partition to the dextran phase at pH > 4 but to the PEO phase at pH 3. The preference of protein particles for one phase or the other has important consequences in the stability and the structure of emulsions [37]. Consequently, microgels can stabilize PEO/dextran emulsion at pH 7; at pH 3 stable dextran/PEO emulsions are formed, whereas at pH 7, dextran/PEO emulsions are rapidly destabilized. However, the effect of pH on the net charge density of the protein cannot explain these preference changes. Therefore, other factors, such as the exposure of the hydrophobic units on the surface of the proteins, have been proposed to also play a role in the pH dependence of the emulsion behavior. Aggregation of protein particles can be induced by decreasing the net charge density of proteins or by increasing the ionic strength, in a process known as cold gelation

[38]. Therefore, the interfacial layer of protein particles becomes denser, and gelation occurs. Aggregation of droplets also happens, thus accelerating the creaming of PEO droplets or sedimentation of dextran droplets.

Surface modification of microgels

Protein microgels have been complexed with anionic or cationic polysaccharides, and the effects on their capacity to stabilize W/W emulsions have been investigated [39]. Small stable complexes can be formed with κ-carrageenan and chitosan around the pI of the microgels (pI=5.0), where the microgels flocculate in the absence of polysaccharides (pH 4.3–5.5). It is shown that the microgel-polysaccharide complex stabilizes emulsions in the pH range where emulsions containing only microgels flocculate. Formation of complexes between the microgels and polysaccharides can modify the capacity of the former to stabilize W/W emulsions, as also reported in other liquid phase separation systems [40]. Below pH 5.5, xyloglucan spontaneously binds with Blg microgels, thus stabilizing the W/W emulsions formed by aqueous mixtures of amylopectin and xyloglucan. Polysaccharides added in small quantities clearly do not drive phase separation but are specifically used to modify the wettability of protein microgel particles and usually improve the stability of W/W emulsions.

1.4.3 Stabilization mechanisms of W/W emulsions

For proper stabilization of W/W Pickering emulsions, the particles must be partially wetted by both aqueous phases, thus allowing the formation of a stabilizing layer of particles adsorbed on the interface. Interestingly, the same particles do not necessarily stabilize emulsions of phase A in phase B in the same manner as

emulsions of phase B in phase A. In fact, emulsions have been found to be more stable when the particles prefer the continuous phase, that is, when they protrude from the droplet surface [21]. This observation supports the idea that the protein particle layer at interfaces forms an effective barrier only if it is wetted more strongly by the continuous phase (Frinkle's rule). After localizing within a thick dense layer at the outer droplet surface, the adsorbed microgel particles formed a steric barrier that protected the emulsions against droplet coalescence [41].

The adsorption of protein particles at the interface can lead to the aggregation of particles, through a process probably driven by depletion attraction [42]. Aggregation of particles at the interface has also been reported by Sinn et al. [43] and has been proposed as an alternative mechanism for the Pickering stabilization of O/W emulsions in addition to the particle layer formation around the droplets. In this case, the steric particle-based barrier is a region of a network of particles adsorbed at the interface, and the whole aggregated structure is held together by attractive inter-particle forces.

The overall goal of this study was to develop stable colloidal systems based on Blg particles and to elucidate the stabilization mechanisms by characterizing Blg particles adsorption on the interface. The three specific aims were as follows: aim 1) development and characterization of selenium NPs stabilized by Blg; aim 2) investigation of Blg microgels as a colloidal stabilizer in a new W/W emulsion system; aim 3) investigation of Blg microgel adsorption onto a hydrophobic solid surface by QCM-D.

2. Chapter II: Development, Physicochemical Characterization and Cytotoxicity of Selenium Nanoparticles Stabilized by Beta-lactoglobulin

Adapted from Zhang, J., Teng, Z., Yuan, Y., Zeng, Q.Z., Lou, Z., Lee, S.H. and Wang, Q., 2018. Development, physicochemical characterization and cytotoxicity of selenium nanoparticles stabilized by beta-lactoglobulin. *International journal of biological macromolecules*, 107, pp.1406-1413.

2.1 Abstract

Novel Selenium nanoparticles (SeNPs) were developed using beta-lactoglobulin (Blg) as a stabilizer in redox systems of selenite and ascorbic acid in this study. Particle size, morphology, stability, and *in vitro* biological activity of synthesized Blg stabilized selenium nanoparticles (Blg-SeNPs) were characterized by dynamic light scattering (DLS), transmission electron microscopy (TEM), ultraviolet-visible spectrophotometry (UV/Vis), and cell toxicity assays, respectively. Stabilizing mechanisms of Blg-SeNPs were investigated by Fourier-transform infrared spectroscopy (FTIR) and protein fluorescence probe. The results revealed that the Blg-SeNPs were spherical with mean particle size of 36.8±4.1 nm. They were stable in acidic or neutral to basic solutions (pH 2.5-3.5 or 6.5-8.5) at 4ºC for 30 days as a result of electrostatic repulsions. FTIR results showed that functional groups of $–NH_2$ and –OH on Blg molecules were responsible for binding with SeNPs. Furthermore, decreases in protein surface hydrophobicity indicated that possible binding happened between Se and the hydrophobic domains of Blg. The cell toxicity of Blg-SeNPs was significantly lower than that of sodium selenite on both

cancerous and non-cancerous cells. This study provides a facile and green method for chemically synthesizing stable SeNPs which are suitable for further evaluation in medicinal applications.

Keywords: Selenium, Nanoparticles, Beta-lactoglobulin

2.2 Introduction

Selenium (Se) is an essential trace element in human and animal body. It is a necessary dietary constituent as 21st amino acid-selenocystein, which is required at the active site of all human selenoproteins and selenoenzymes.[44] Se has key functions in balancing redox systems, providing proper functions of body's immune systems, and having anticarcinogenetic effects. It is well known that Se displays a narrow margin between beneficial and toxic effects. Consumption of 200 μg Se per day in cancer patients reduced mortality and depressed the incidence of many types of cancer including lung, colorectal and prostate cancers. However, symptoms of selenosis in susceptible patients were found at or above an Se-intake of 910 μg/day, corresponding to a blood Se level of 1.05 mg/L.[45]

The beneficial and toxic effects of Se on human health are closely related to its chemical species [46], among which ionic selenite salt is the most toxic form. Selenium nanoparticles (SeNPs) with zero oxidation state have gained much attention recently because of their excellent bioavailability and low toxicity. SeNPs can be synthesized through physical [47], chemical [48], biological methods [49] and have a distinct bright orange-red color. The most widely used method for forming SeNPs is through the redox reaction between selenite and ascorbic acid or other reducing agents. However, the resultant nanoparticles are usually unstable and further

aggregate into grey and black elemental Se, which is biologically inert. Many efforts have been made to stabilize the red SeNPs including the use of polyphenols [50, 51], polysaccharides [52, 53], and proteins [54, 55]. Polyphenol suffered from auto-oxidization and aggregation at acidic pH in the stomach [51], and there are many advantages of proteins as encapsulants or stabilizers over polysaccharides including flexible structure, possession of multiple functional groups, amphiphilic nature, and desirable biodegradability.[3] It has been reported that bovine serum albumin (BSA) stabilized SeNPs (BSA-SeNPs) exhibited comparable efficacy to organic Se in upregulating selenoenzymes, but has much lower toxicity.[56] However, BSA could be completely digested under gastric condition [57], leading to changes of particle size and surface properties of the nanoparticles, which would influence the absorption of SeNPs in the human body.

Beta-lactoglobulin (Blg) is the most abundant whey protein in cow's milk, accounting for about 58% of the whey and 10% of the total milk protein. Consisting of 162 amino acids in its sequence, BLG exhibits an average molecular weight of 18 kDa and an isoelectric point (pI) of pH 5.1–5.2. As a member of lipocalin family, Blg is a small globular protein, and has a strong affinity for a variety of natural nutrient, including retinol, vitamin D, fatty acids, phenolic compounds, and cholesterol.[3] Furthermore, Blg has demonstrated a significant resistance to peptic digestion [58], while it is much more readily degraded by trypsin in the small intestine. These characteristics provide Blg-based encapsulation systems with desirable controlled release property. Blg was widely used as carriers in various delivery systems, including emulsion [59], nanoparticle [60], and nanocomplex [61]. However, to

the best of our knowledge, no study has been reported utilizing Blg as an *in situ* stabilizer for SeNPs.

In this work, a facile and green method to synthesize and stabilize SeNPs has been developed by using Blg as the stabilizing agent, in the redox system of selenite and ascorbic acid. The size, morphology, stability, and binding mechanisms were characterized by dynamic light scattering (DLS), transmission electron microscopy (TEM), ultraviolet-visible spectrophotometry (UV/Vis), and Fourier-transform infrared spectroscopy (FTIR). The *in vitro* cytotoxicity of the Blg-SeNPs was also studied and compared with selenite. Moreover, the stabilizing mechanism was discussed in detail.

2.3 Materials and methods

2.3.1 Materials

L-Ascorbic acid and 8-anilino-1-naphthalenesulfonic acid (ANS, 97% purity) were purchased from Sigma-Aldrich (St. Louis, MO, USA). Sodium selenite was purchased from Spectrum Chemical (Gardena, CA, USA); 2, 3-Diaminonaphalene (DAN) was purchased from Alfa Aesar (Heysham, England); Hydrochloric Acid (HCl, 36.5-38%) were of ACS grade from VWR (Radnor, PA, USA); Tris was purchased from Mallinckrodt Baker, Inc. (Phillipsburg, NY, USA)

Human colon adenocarcinoma cells (HCT116) and colon normal cell (CCD112) were purchased from American Type Culture Collection (Manassas, VA, USA). 3-(4, 5-dimethyltiazole-2-yl)-2, 5-diphenyltetrazolium bromide (MTT), and dimethyl sulfoxide (DMSO) were purchased from Sigma Aldrich (St. Louis, MO, USA).

DMEM/F-12 media, fetal bovine serum (FBS), penicillin streptomycin were purchased from Invitrogen (Carlsbad, CA, USA).

2.3.2 Preparation of protein solutions

Whey protein isolate was kindly donated by Davisco Foods International (Le Sueur, MN, USA) and further extracted for Blg based on an established procedure.[62] Extracted Blg has initial pH of 4.1 and high similarity compared to commercial pure Blg powder according to FTIR and sodium dodecyl sulfate polyacrylamide gel electrophoresis (SDS-PAGE) preliminary tests. Blg solution was prepared by dispersing the purified Blg powder in deionized water under gentle magnetic stirring at room temperature for at least 2 h. Solutions were stored overnight at 4±1ºC to allow complete protein hydration. Blg solution were then filtered through 0.22 μm Acrodisc syringe filter membrane (Pall Co., Newquay, UK) to remove impurity. The concentration of Blg solution was checked by UV/Vis spectrophotometer (Beckman Coulter, DU-730, Fullerton, CA) at 278 nm, using the specific extinction coefficient of 17,600 M^{-1} cm^{-1}.[63] The final concentration of Blg stock solution was 1 wt%.

2.3.3 Preparation selenium nanoparticles

Ascorbic acid (AA) was used as a reducing agent for synthesis of selenium nanoparticles. First, the solution of 0.3 M AA was freshly prepared by dissolving 0.529 g AA powder in 10 mL of deionized water. Then, a 1 mL of 1 wt% Blg solution was mixed with 5 mL of 0.3 M AA and 3 mL deionized water under magnetic stirring at the speed of 600 rpm. With the stirring speed reduced to 300 rpm, 1 mL of 0.06 M aqueous sodium selenite solution was added slowly into the

mixture to initiate the reduction. Upon adding the sodium selenite, the solutions converted from colorless into intense orange-red gradually. Intense red solution was formed at first ten minutes of mixing. However, the reaction was allowed for a total of 30 min to ensure high yield of SeNPs with homogeneous nano-size. The Blg concentration and mixing time were optimized by the particle sizes and polydispersity in preliminary tests.

The obtained Blg-SeNPs were clarified by 10K Microsep™ Advance Centrifugal Filter (Pall Corporation) and stored at 4ºC or lyophilized for further tests.

2.3.4 Se analysis

Se conversion rate in the presence and absence of Blg was quantified by measuring remaining sodium selenite in the reaction solution according to a reported method [64] with minor modification. The determination of Se was based on a measurement of the piazselenol formed when selenium (IV) reacts with 2, 3-Diaminonaphalene (DAN). A DAN working solution was prepared by dissolving 1.0 g of DAN in 1 L of 0.1 N HCl. Blg-SeNPs solution was filtered by 10K Microsep™ Advance Centrifugal Filter. Filtrate was added into DAN solution as ratio of 1:10 (Sample: DAN) and allowed to stand for 2 h at room temperature. Piazselenol was extracted by toluene and determined by UV/Vis Spectrophotometer (Beckman Coulter, DU-730, Fullerton, CA) at 380 nm. Selenite reduced by AA without Blg was used as a control.

Initial Se concentration was 470 μg Se/mL (0.006 M Selenite). The conversion rate of Se was calculated as follow:

Conversion % = $(Se_{initial}-Se_{remaining})/Se_{initial}$ %

2.3.5 Particle size and morphology characterization of Blg-SeNPs

Freshly prepared Blg-SeNPs were used for particle size measurement. Hydrodynamic diameters of different treatments were measured by a dynamic light scattering (DLS) instrument (BI-200SM, Brookhaven Instruments Corp., Holtsville, NY), which was equipped with a 35 mW HeNe laser beam at a wavelength of 637 nm. All DLS measurements were performed at 25 °C with triplicates. The morphology of Blg-SeNPs was observed using a JEOL JEM-2100 LaB6 Transmission electron microscopy (TEM, JEOL USA Inc., Peabody, MA, USA). Samples were dripped and dried on a copper grid coated with a thin amorphous carbon film. Representative images were reported.

2.3.6 Storage and pH stability

Appearance and particle size of SeNPs without Blg or with Blg in an aqueous solution were recorded by photographs and measured by DLS, respectively. The storage stability of Blg-SeNPs was compared for 30 days at 4 or 25±1ºC to represent refrigerating and room temperatures. Effect of pH on particle stability was also evaluated by DLS and UV/Vis Spectrophotometer at 500 nm. HCl and NaOH were used to adjust pH of Blg-SeNPs aqueous solution. Both particle sizes and OD_{500} absorbance of Blg-SeNPs were reported as an average of triplicates.

Laser Doppler velocimetry (Zetasizer Nano ZS90; Malvern Instruments LTD., Malvern, UK) was used to characterize the zeta potential of Blg-SeNPs in different pH levels. During the experiment, samples were well mixed, diluted and filled in a fold capillary cuvette (Folded Capillary Cell-DTS1070, Malvern, UK). The whole

cuvette was inserted into the chamber at 20ºC for measuring electrophoretic mobility. The zeta potential of the particles was obtained by application of the Henry equation:

$$U_E = \frac{2\varepsilon\zeta f(Ka)}{3\eta}$$

where:

ζ: Zeta potential.

U_E: Electrophoretic mobility.

ε: Dielectric constant.

η: Viscosity.

f(Ka): Henry's function.

Two values are generally used as approximation for the f(Ka) determination, either 1.5 or 1.0. If the electrophoretic determination of zeta potential is made in aqueous media and moderate electrolyte concentration, f(Ka) is 1.5 and is referred to as the *Smoluchowski* approximation. Non-aqueous measurement generally use f(Ka) of 1.0, and is referred to as the Huckel approximation. Since the Blg-SeNPs samples were prepared in aqueous solution, the *Smoluchowski* approximation was used to calculate the zeta potential. For each sample, three replicates were obtained and the results were analyzed statistically.

2.3.7 FTIR

FTIR spectra of different samples were recorded on a Thermo Nicolet NEXUS 670 FTIR spectrometer (Thermo Scientific, West Palm Beach, FL, USA) with an Attenuated Total Reflectance (ATR) cell in the range of 4000-400 cm^{-1}, resolution

4 cm^{-1} . For each sample, three replicates were obtained and spectra were further analyzed by Omnic software (Therno Scientific, West Palm Beach, FL, USA).

2.3.8 Surface hydrophobicity

The specific surface hydrophobicity of Blg was determined using 8-anilino-1-naphthalenesulfonic acid (ANS) as a protein fluorescence probe.[65] Stock solution of Blg-SeNPs or Blg only (both containing 1 mg/mL of Blg) and ANS (150 μg/mL) was prepared in deionized water and 0.1 M tris/HCL pH 8.0 buffer. The resultant solution was then mixed and diluted to achieve a fixed ANS concentration of 75 μg/mL and protein concentrations ranging from 0 to 50 μg/mL. After 1 h of incubation at 25°C, the fluorescence intensity (FI) of each sample was obtained on a SpectraMax M5 plate reader (Molecular Devices, Sunnyvale, CA, USA). The excitation and emission wavelengths were 355 and 460 nm, respectively. For each sample, a linear regression equation was established for FI versus protein concentration ($R^2 > 0.99$), and the slope (S_o) was used as an index for surface hydrophobicity.

2.3.9 *In vitro* cytotoxicity

Non-cancerous (CCD-112) and cancerous (HCT-116) colon cell lines were used for evaluating the cytotoxicity of sodium selenite and Blg-SeNPs (twice dialysis). Cells were maintained in DMEM/F-12 media supplemented with 10% fetal bovine serum (FBS), and a mixture of penicillin (100 U/mL) and streptomycin (100 μg/mL) under a humidified atmosphere of 5% CO_2 at 37ºC.

Cell viability were measured to compare the *in vitro* cytotoxicity of Blg-SeNPs and sodium selenite on CCD-112 and HCT-116. Both cell lines were seeded at 5×10^4 cells/well into 96-well plates. The cells were allowed to recover for 36 h at 37ºC in an incubator (CO_2 Incubator symphony 5.3 A, VWR, Radnor, PA, USA). The medium in each well was then replaced with either Blg-SeNPs or Sodium selenite solution diluted with DMEM/F-12 media to obtain an equivalent concentration of Se element. The addition of Blg-SeNPs or sodium selenite did not cause any changes on media's pH as confirmed by the preliminary measurement. DMEM/F-12 media without any treatment was used as a control. After 24 and 48 h incubation, the cell viability was evaluated by MTT assay as follows: supernatant was removed and 100 μL of mixture of MTT and serum free media (ratio of 1:5) was added to each well. Plates were covered with foil and incubated for 4 h at 37ºC, followed by removal of the medium and addition of 200 μL DMSO to each well. After overnight incubation, the plates were read at 540 nm using a microplate reader (Bio-Tek Instruments Inc., Winooski, VT, USA)

2.3.10 Statistics

All experiments and analysis were conducted in triplicate with data reported as mean ± standard error. Experimental statistics were performed using a SPSS 22 software (IBM). The analysis of variance (ANOVA) with Duncan's multiple-comparison test was used in the analysis of differences. The significance level (*P*) was set at 0.05.

2.4 Results and discussion

2.4.1 Morphology and stability of Blg-SeNPs

The chemical reaction of selenious acid with ascorbic acid in water was formulated in Scheme 2.1. The formation of colloidal dispersions of selenium using ascorbic acid as the reducing agent was first introduced by David Mees.[48] Agreed with Mees, the suspension was not stable in the absence of added stabilizers, brick-red precipitate was clearly observed after a few minutes of mixing (Fig.2.1a). The color of the precipitate turned into black after 2 days, indicating that the structure of selenium compound rearranged from either amorphous or monoclinic selenium particles into trigonal selenium.[52] The crystallization of elemental selenium might be the reason that grey or black elemental selenium is biologically inert.

Scheme 2.1 Chemical reaction of selenious acid with ascorbic acid in water.

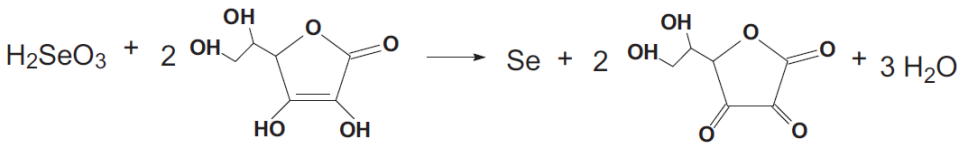

On the other hand, the SeNPs solution in the presence of Blg exhibited an orange-red color, which might be due to a nano-size effect (Fig.2.1b). The uniform Blg-SeNPs were synthesized after 30 mins of magnetic stirring. Extended mixing (30-180 mins) did not affect the particle size and size distribution of SeNPs particle confirmed by DLS measurement (data not shown). The particle size of Blg-SeNPs was 36.8±4.1 nm based on DLS result of size distribution with relatively small polydispersity. Blg, therefore, played an indispensable role in stabilizing the nanoparticles. Because of the nanosize of the selenium particles and interference of ascorbic acid in the redox system, no specific UV-Vis absorption peak was observed for Blg-SeNPs in tested wavelength region of 250-600 nm (Fig.2.2), which is in agreement with the nature of the spectra reported in the literature[66].

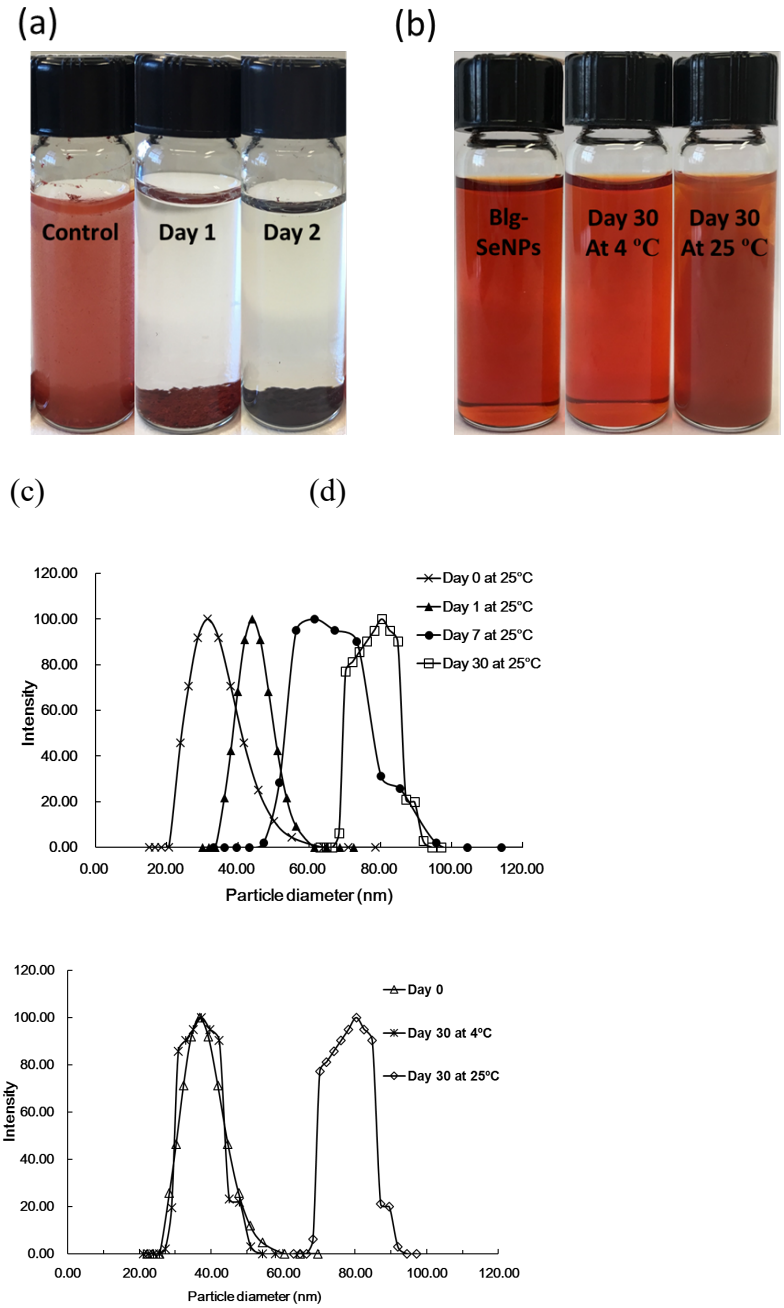

Figure 2.1 (a) SeNPs aqueous solutions in the absence of Blg (b) SeNPs aqueous solutions in the presence of Blg (c) (d) the corresponding particle size distribution of Blg-SeNPs. Without Blg as stabilizer, selenium particle was not stable in aqueous solutions, precipitated and turned into black after 2 days.

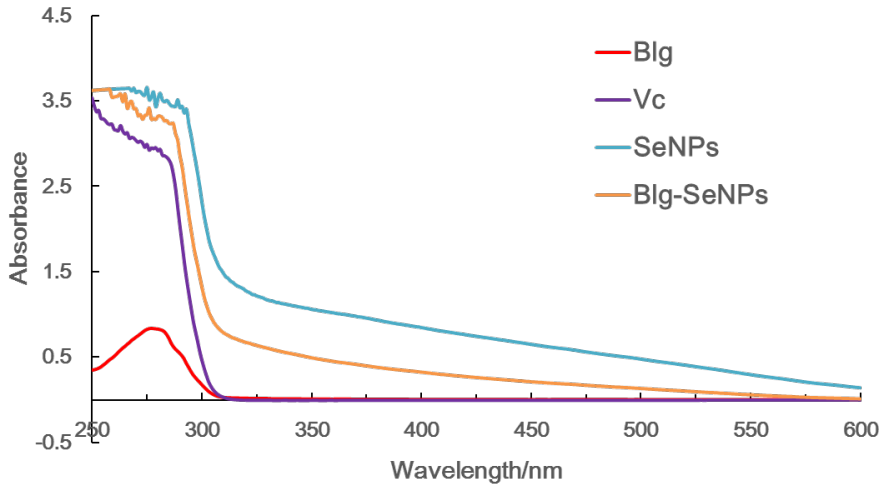

Figure 2.2 UV-vis spectra of Blg, ascorbic acid (Vc), SeNPs and Blg-SeNPs

Storage temperature showed a negative effect on the stability of Blg-SeNPs (Fig.2.1b). The Blg-SeNPs solution, which stored at 4ºC, remained transparent without any visible precipitation for the time duration of our experiments (i.e. 30 days). The orange-red Blg-SeNPs solution is expected to stay clear for an extended storage period at 4ºC, which needs to be confirmed by future experiments. However, for the one stored at room temperature (25±1ºC), solution became turbid and slightly phase separated. Particle size distributions measured by DLS showed that the particle diameter started to increase from day 1 under room temperature, and gradually increased to around 80 nm at Day 30 (Fig.2.1c). The increase of turbidity and particle size could be explained by the protein degradation and/or loss of activity. When stored at 4ºC, Blg was able to retain its structure and function, therefore the particle diameter of Blg-SeNPs was stable at around 40 nm (Fig.1d). The result indicated that refrigerating temperature is an appropriate storage condition for Blg-SeNPs solution, otherwise, preservatives may be added to prevent protein aggregation.

Represented images of TEM and diffraction patterns of the Blg-SeNPs were shown in Fig. 2. 3. Fig. 2.3a revealed that Blg-SeNPs had a homogeneous and spherical structure. Fig. 2.3b and Fig. 2.3c showed that the particle diameter was around 20 nm, which was smaller than that of the Blg-SeNPs in aqueous solution measured by DLS, maybe caused by a drying effect. Fig. 2.3d further confirmed that the orange-red selenium particles were amorphous, since there was no diffraction pattern consisting of concentric rings observed in the sample.

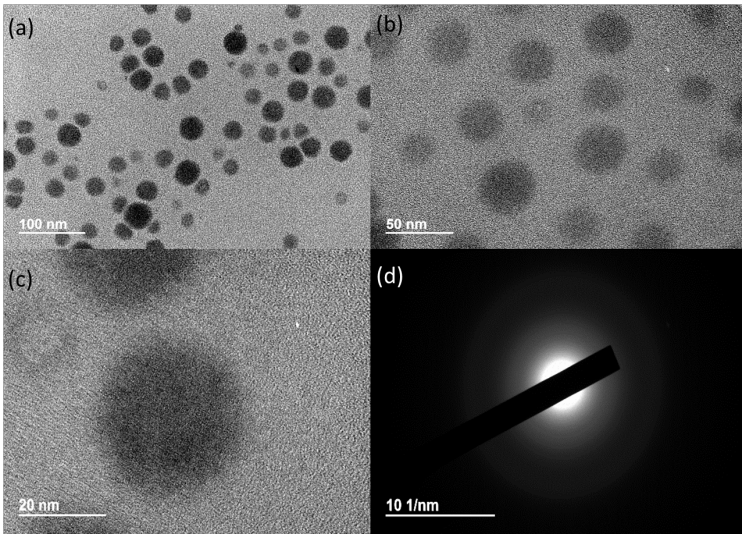

Figure 2.3 (a) (b) (c) Representative transmission electron microscope (TEM) images of Blg-SeNPs at different magnification and (d) 300K Diffraction Pattern of Blg-SeNPs. Round selenium particles were observed; Diffraction pattern indicated Blg-SeNPs were amorphous.

2.4.2 Se conversion rate

Se conversion yield was quantified by measuring unreacted sodium selenite by the DAN method. The sample first was dialyzed by a 10K Microsep™ Advance Centrifugal Filter to exclude interference of the Blg. After the dialysis, the intense orange-red solution remained in the upper part of the centrifugal filter tube that contained the concentrated Blg-SeNPs. In the filtrates, there were ascorbic acid and

ionic selenium, which have not participated in the redox reaction and not been encapsulated into nanoparticles. By adding DAN solution to the filtrates, selenium reacted with DAN to form the piazselenol which was a reddish colored precipitate. Using standard curve (Fig. 2.4), the Se concentration in the first filtrates were quantified as 4.43 and 5.40 μg/mL for Selenium without and with Blg, respectively. The Se conversion rate of Blg-SeNPs was 98.86%, which is comparable with that of SeNPs without Blg (i.e. 99.07%), indicating that Blg had little influence on the reduction reaction that selenite was reduced into elemental Se. The only function of Blg was to prevent the nano-sized elemental Se from growing into bigger particles *in situ*. This test also showed that there was a small amount of selenite remaining in the reduction system, therefore, second time dialysis with the centrifugal filter was performed. It was confirmed that there was no selenite (data not shown) remained after the second dialysis by the centrifugal filtering.

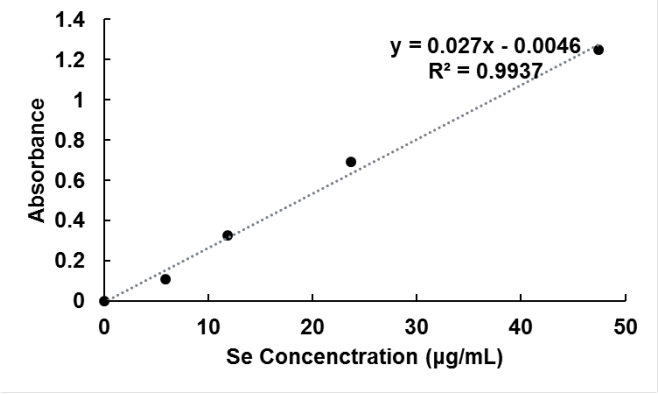

Figure 2.4 Standard curve of Se concentration determined by DAN method

2.4.3 Stability at different pH levels

Because of the ascorbic acid in the redox reaction, the initial pH of native Blg and freshly prepared Blg-SeNPs aqueous solutions was measured around 4.2 and 3.5, respectively. The effect of pH on the stability of SeNPs was examined through

observing the changes of zeta-potential, particle size, and turbidity (Table 2.1) upon adjusting pH to from 2.5 to 8.5. Blg-SeNPs demonstrated small changes on particle size, absolute value of zeta-potential, and turbidity at pH 2.5-3.5 and 6.5-8.5, indicating they had good stability at those pH levels. This was expected since proteins carried either positively or negatively charges when the pH was deviated from its isoelectric point (pI of Blg is near 5.1). Within the pH range of 4-6, the zeta-potential of nanoparticles was lower than ±10 mV, leading to the increase of both particle size and solution turbidity. Orange-red precipitate was observed in this pH range. The precipitate was thought to be contributed by the Blg, because in pH 4-6, net charge of the Blg molecules was close to zero (near its pI at 5.1), resulting in aggregation of Blg-SeNPs in the solution. The Blg-SeNPs formed reversible aggregate since adjusting pH to lower or higher values made the solution clear again. And this was also evidenced by DLS measurements. This confirmed that the main driving force involved in Blg-SeNPs stabilization is the electrostatic interactions. This experiment demonstrated that Blg-SeNPs were stable at pH 2.5-3.5 and 6.5-8.5 ranges, but became a precipitate at pH 4-6. A strategy such as alternation of Blg surface charge could be applied to modulate the stability of Blg-SeNPs within different pH ranges, since nanoparticles with high stability and solubility near neutral pH are of particular interest for their practical uses in industrial applications.

Table 2.1 Effect of pH on surface charge, particle size and turbidity of Blg-SeNPs*

pH	Zeta-potential (mV)	Particle Size (nm)	OD_{500}
2.5	29.03±0.59f	40.45±0.49a	0.37±0.02a
3.5	19.73±4.40e	41.35±0.49a	0.45±0.02b
4.5	9.19±0.28d	913.00±77.78c	0.83±0.07d
5.5	-9.39±0.79c	493.50±113.84b	0.58±0.05c
6.5	-19.73±0.72b	71.00±9.90a	0.46±0.02b
7.5	-27.40±2.39a	50.30±0.14a	0.33±0.04a
8.5	-30.07±3.26a	50.70±0.99a	0.36±0.04a

*Values with different letter are statistically different in the same column.

2.4.4 Binding mechanism

The FTIR spectra of Blg and Blg-SeNPs were displayed in Fig. 2.5 for further investigating the interaction between Blg and SeNPs. The characteristic peaks of the hydroxyl group (-OH stretching) were observed in both spectra, with slightly shifted from 3275 (Blg) to 3273 cm^{-1} (Blg-SeNPs). Native Blg exhibited three characteristic peaks: amide I (1630 cm^{-1}, C=O stretching), amide II (1523 cm^{-1}, C-N stretching and N-H bending), and amide III (1444 cm^{-1}, C-N stretching, N-H bending). In Blg-SeNPs, peak of amide I was observed with no significant shifting, while a weakening of relative intensity of amide II peak and slightly shifting of amide III peak were observed as compared with those in the Blg spectra. The results indicated that the interaction sites of Blg and SeNPs were on the functional groups of $–NH_2$ and –OH on protein molecules, which were consistent with recent studies showing that selenium was prone to interact with O- and N- containing groups. Yu, Zhang et al. observed the characteristic peak of −OH group in a Chitosan-SeNPs nanocomposites at 3426.2 cm^{-1} was relatively lower than that of Chitosan (3443.4 cm^{-1}), with blue-shift observed. Then, they concluded the conjugation of Se and –

OH group in their Chitosan-SeNPs.[67] Similar blue shift was also observed from another study on confirmation of covalent bonding of Se-N.[68] Therefore, it was concluded that Blg was not conjugated to SeNPs through covalent bonding in our study, since there is no significant shifting of characteristic peaks of the -OH group or amide group. The FTIR spectra of Blg-SeNPs presented characteristic peaks at 1112 and 1039 cm^{-1}, which is hard to be assigned to any Se related stretching vibration such as Se=O stretching vibration at 800-930 cm^{-1}. [69] They may belong to ascorbic acid residue in the system, which was confirmed by the FTIR spectra of ascorbic acid (Fig. 2.5c). Based on the above results, we proposed that the interactions of SeNPs with Blg might be simple physical adsorption and noncovalent association.

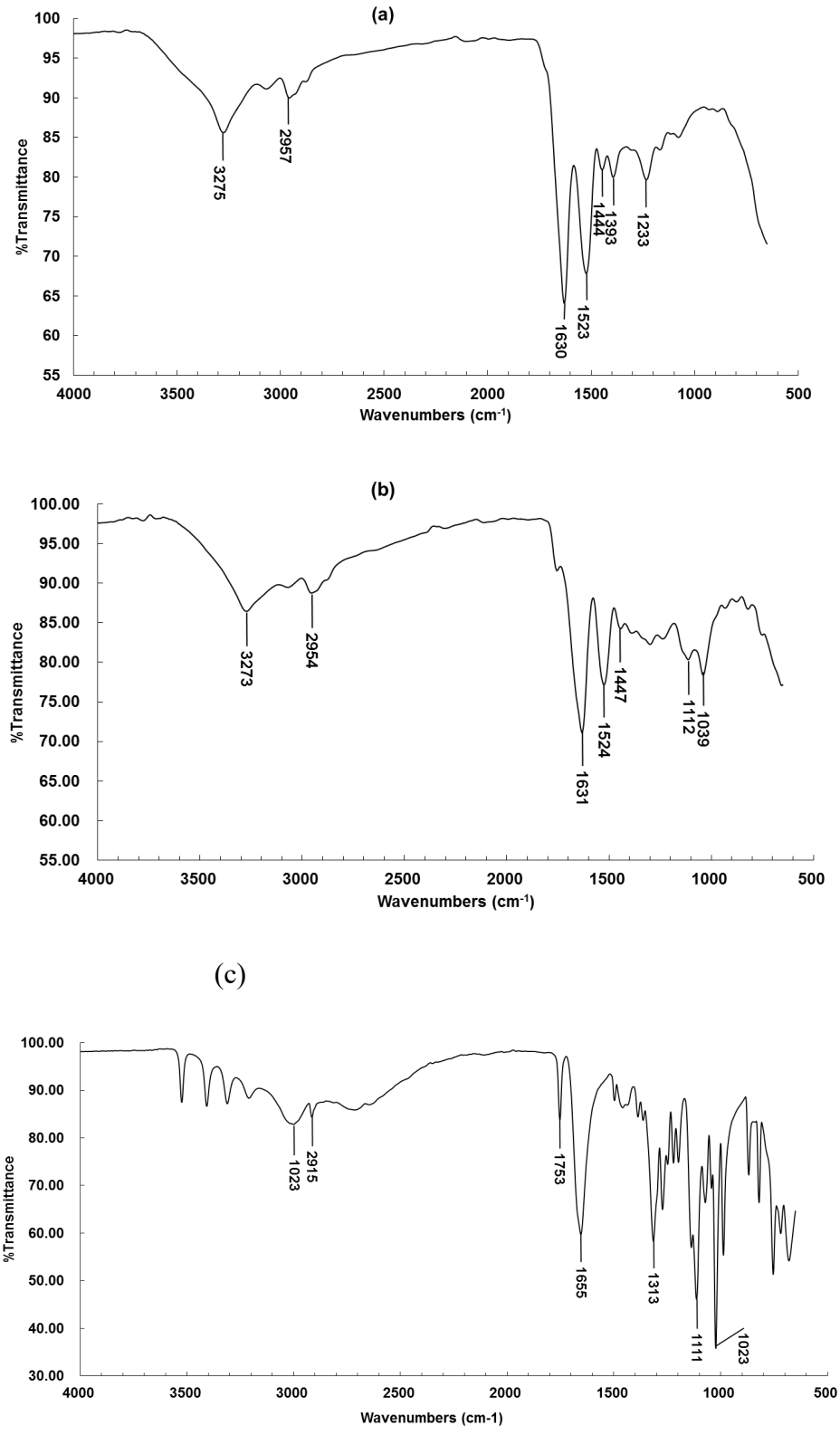

Figure 2.5 FTIR spectra for (a) Native Blg (b) Blg-SeNPs (c) ascorbic acid

The ANS fluorescence probe assay was conducted to study the surface hydrophobicity (S_o) of the Blg before and after Blg-SeNPs formation at pH 8.0 (Fig. 2.6). The native Blg exhibited a surface hydrophobicity of 126.98 in slightly basic solution, the value was consistent with a previous report.[65] For Blg-SeNPs, a lower surface hydrophobicity was detected, with the S_o value decreasing from 126.98 to 67.04. This was thought to be attributed to the following reasons. First, the binding of SeNPs and Blg may happen at the hydrophobic segments of the protein, competing with the binding of ANS to the same sites of protein molecules. Second, the association with SeNPs may cause Blg to have a conformational change, leading to the decrease in surface hydrophobicity.

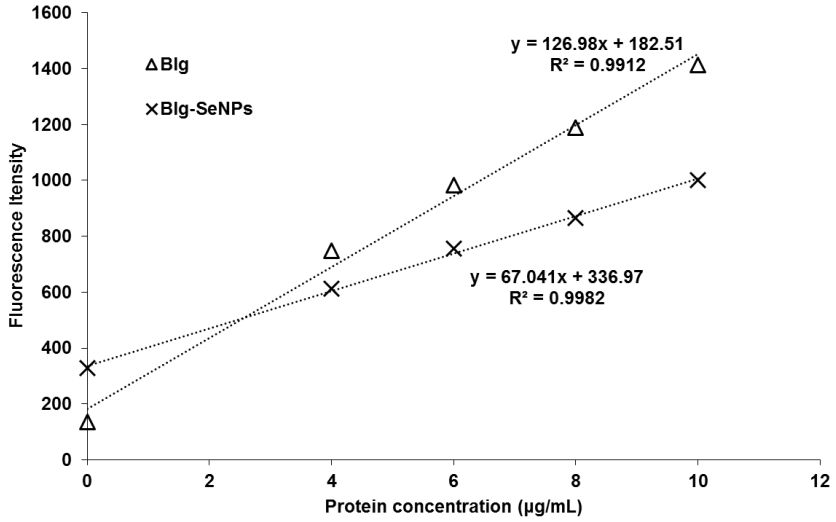

Figure 2.6 Fluorescence intensity (FI) of ANS bond to different concentration of Blg and Blg-SeNPs in tris/HCl buffer. The slope (S_o) of the linear regression line was used as an index for surface hydrophobicity.

Detailed discussion on the mechanisms of Blg-SeNPs formation, stabilization and growth are given as follows. The synthesis of Blg-SeNPs might begin with an attack of the precursor, $HSeO_3^-$ (pKa 2.62) by the protonated amino groups (NH_3^+) on Blg (pI 5.1) through the electrostatic attractions in the initial system at pH~3.5. This

may lead to distribution of $HSeO_3^-$ in the Blg molecular chain. Subsequently, $HSeO_3^-$ was reduced to Se^0 *in situ* once reacted with the ascorbic acid. With the increasing amount of elemental Se, it would agglomerate with each other to form a Se nucleus that continuously grow into SeNPs according to Gibbs-Thomson law.[70] Thus, Blg molecules, which intimately associated with the surface of the selenium particles, played an important role during particle nucleation and growth, leading to a uniform and stable nano-system. It was proposed that the association of SeNPs with Blg might be physical adsorptions and non-covalent interactions such as hydrophobic interaction.

2.4.5 *In vitro* cytotoxicity

In vitro cytotoxicity of Blg-SeNPs was evaluated and compared with that of sodium selenite using MTT method on both cancerous (HCT-116) and non-cancerous (CCD-112) cell lines. The cell viability after 24 and 48 h treatments were presented in Fig. 2.7. For HCT-116, selenite was highly toxic to the cells, only 22% viable cells were remained at the dose of 100 μM after 24 h treatment, whereas cells treated with Blg-SeNPs retained 54% of viable cells at 100 μM. The lower toxicity of Blg-SeNPs on HCT-116 stayed unchanged in prolonged cell incubation to 48 h. For CCD-112, similar inhibition effects on cell growth were observed after 48 h treatment, selenite showed high toxicity retaining 23% viability of cells at the dose of 100 μM, while Blg-SeNPs retained 44% of viable cells at the same concentration. The dose-dependent inhibition effects on cell growth from both selenite and Blg-SeNPs were observed on 24-48 h treatment of HCT-116, and 48 h treatment of CCD-112. However, Blg-SeNPs have shown significantly lower cytotoxicity than

selenite. Consistent with this finding, Zhang et al. reported that selenium in nanoscale has a 7-fold lower acute toxicity than sodium selenite in a mice model.[54]

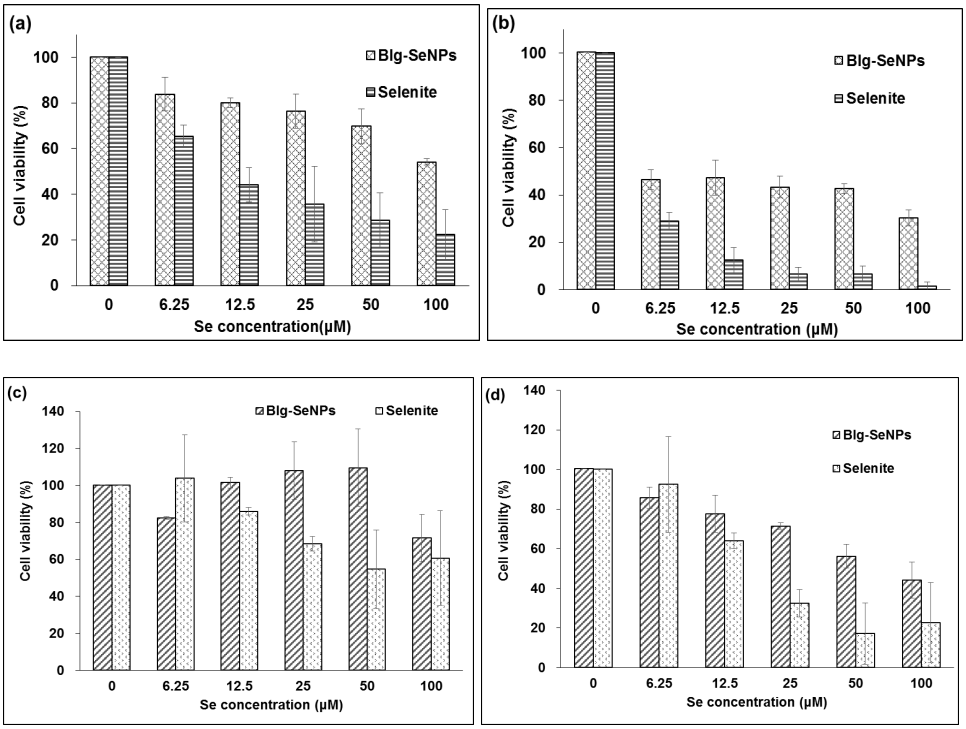

Figure 2.7 *In vitro* cytotoxicity of selenium in cancerous colon cells (HCT-116) (a) 24 h (b) 48 h and non-cancerous colon cells (CCD-112) (c) 24 h (d) 48 h. Cells were exposed to Blg-SeNPs and selenite at the indicated concentrations (0-100 μM) and incubated at 24 h and 48 h.

The differences between selenium-induced apoptosis of cancer and corresponding normal cells were a controversial topic. Some studies have reported that selenium compounds have preferential selection of killing cancer cells [71], while other researchers found that the cytotoxic effects of selenium compounds were more potent in normal hepatocytes and prostate cells as compared with their cancer cells.[72, 73] Selenium-induced apoptosis of cancer cells has been suggested to be an important mechanism for cancer prevention, but at the same time, the risk of selenium toxicity appears to be unavoidable. The Nano-Se synthesized in this study showed similar dose-dependent fashion and no significantly different cytotoxicity

(data no shown) on colon cancer cell and corresponding normal cell, indicating that Blg-SeNPs may pose the risk of toxicity to normal tissues when they are used for treating cancer.

In conclusion, SeNPs with mean particle size of 36.8±4.1 nm has been developed by using Blg as a stabilizer. The Blg-SeNPs were stable in acidic or neutral to basic solutions (pH 2.5-3.5 or 6.5-8.5) at 4ºC for 30 days as a result of electrostatic repulsions. Further, functional groups (i.e. $–NH_2$ and –OH) as well as hydrophobic domain on the protein molecules were responsible for binding with SeNPs. The cytotoxicity of Blg-SeNPs was lower than sodium selenite, but it showed similar cell growth inhibition on both colon cancer cell and corresponding normal cell. This work shed some light on developing Blg stabilized selenium nanoparticles, which need to be further evaluated for their applications as a medicine of cancer treatment.

3. Chapter III: Environmental Responsiveness of Microgels Stabilized Water-in-Water Emulsion

3.1 Abstract

A stable W/W emulsion was formed by mixing dextran and hydropropyl methylcellulose (HPMC) in an aqueous solution with addition of Blg microgels. The microstructure and stability of the W/W emulsion were investigated under different environmental conditions (i.e. changes of pH, ionic strength, and temperature). The pH effect on the W/W emulsion was the most significant, the microgels accumulating at the liquid-liquid interface led to a stable emulsion at pH 3–5, where the microgels carried positive charges. When pH was increased above the pI of the microgels (~pH 5), the emulsion was destabilized because the microgels tended to stay in the continuous phase (i.e., dextran) rather than the interface. The W/W emulsions were stable under ionic strength levels up to 300 mM though at ionic strength > 100 mM the droplets were incompletely coated by microgels. The W/W emulsion stabilized by protein microgels were thermally stable. The heat treatment promoted partial protein particle-particle fusion on the surface of droplet at 90°C, but the fusion had no protective effect on emulsion against demulsification. Electrostatic and hydrophobic interactions as well as interfacial tensions between dextran and HPMC phase were investigated to better understand the driving forces for microgels' accumulation at the interface.

3.2 Introduction

W/W emulsions can be formed by mixing two aqueous solutions containing incompatible polymers with droplets of one aqueous phase dispersed in another aqueous phase. Without any stabilizer, W/W emulsions exhibit thermodynamic

phase separation when the concentrations of the two incompatible polymers are above a critical point. These emulsions are characterized by extremely low interfacial tension, generally between 10^{-4} and 10^{-6} N/m (100–1000 times lower than the interfacial tension of a typical oil-water interface) [34]. The interfacial tension can be interpreted by energy or tension per unit area. A stable oil-water emulsion with small droplet size, which corresponding to large surface area, is usually obtained by applying high energy input into the emulsion system, for example high-pressure homogenization. Because of the ultralow interfacial tension of W/W interfaces, the droplet size of emulsions can be influenced by modest variations in the shear rate, such as through stirring and shaking. W/W emulsions have recently received a great deal of attention, owing to their potentials to be used in novel non-fat formulations for encapsulating sensitive hydrophilic ingredients.

Commonly used molecular surfactants cannot stabilize W/W emulsions against coalescence, because they are small relative to the correlation length of the polymer solutions and thus cannot span the entire water-water interface. Particle stabilization effects have long been known for the oil-in-water (O/W) emulsions known as Pickering emulsions. After a particle with radius r attaches to the oil-water interface, the free energy of spontaneous desorption, ΔG_d, can be estimated with the following equation:

$$\Delta G_d = \pi r^2 \gamma_{OW} (1 - |cos\theta|)^2 \qquad (1)$$

where γ_{OW} is the oil-water interfacial tension, and θ is the three-phase contact angle of the particle between the solid and two liquids. The stability of O/W Pickering emulsions can be understood on the basis of the following: for r > 10 nm particles, the binding energy is orders of magnitude larger than the thermal energy (if the

wetting angle is 90°), but for a water-water interface with an ultralow interfacial tension, the particle diameter must be at least 160 nm [74].

Accumulating evidence indicates Pickering stabilization of W/W emulsions through a diverse range of particulate entities such as biopolymer-based particles, bacterial cells and inorganic particles of various shapes and sizes [35, 41]. Among them, the most relevance food-based systems are W/W emulsions stabilized by protein particles [21, 42]. One advantage of using protein particles for emulsification is that protein-based microgels may have favorable properties because of their heat sensitivity [75]. On the other hand, protein particles are pH and ionic strength responsive. They have already been investigated for a model W/W emulsion formed through mixing dextran and poly(ethylene oxide) (PEO) [38, 76]. The protein particles showed a strong preference for the dextran phase at pH 7 and for the PEO phase at pH 3, thus influencing the contact angle of the particles at the interface and consequently the stability of W/W emulsions.

An important difference using proteins to stabilize O/W and W/W emulsions lies on that proteins are completely insoluble in the oil phase in O/W emulsions but are soluble in both water phases of W/W emulsions. Generally, for proteins, the preference is not the same for two phases, and partitioning occurs in aqueous two-phase systems [77]. Proteins, as polyelectrolyte macromolecules, carry charges in aqueous solutions. A consistent pattern has been observed in the partitioning of different polyelectrolytes in aqueous two-phase systems, reflecting the influence of charge on partitioning [78]. Moreover, the influence is not solely due to electrostatic effects: other properties of the system, such as hydrophobic interactions or the free

volume of the phases and interfacial tensions that are unrelated to the charge but change with pH, appear to be superimposed [79].

Herein, we used Blg microgels as particles for controlling the phase separation of a new food grade W/W system consisting of dextran and hydroxypropyl methylcellulose (HPMC). The protein microgels were produced by heat-induced aggregation of the native Blg molecules under specific conditions in which aggregation leads to the formation of self-assembled protein microgels, as extensively defined elsewhere [80].This study had two objectives. Objective 1 was to investigate the W/W emulsions under several emulsion and environmental conditions, i.e., microgel concentration, polysaccharide composition, pH, ionic strength and temperature, to gain a better understanding of the parameters that control the stabilization of W/W emulsions. Understanding and control of these phase phenomena are important because an excessive phase separation may cause unacceptable changes in the appearance or sensory properties of products in which W/W dispersions exist. Objective 2 was to measure surface charges, interfacial tension and hydrophobic interaction in the system, in order to improve our understanding of the forces driving microgels to accumulate at the interface.

3.3 Materials and Methods

The dextran and HPMC samples used for the study were purchased from Millipore Sigma. The nominal weight average molar mass was Mw=450,000-650,000 g/mol for the dextran and Mw=10,000 g/mol for the HPMC. HPMC has 1.8-2.0 mol methoxy per mol cellulose (D.S.), 0.2-0.3 mol propylene oxide per mol cellulose (M.S.), viscosity ~ 6 cP in 2 wt% aqueous solutions at 20°C, gel point 58-64°C.

Fluorescein isothiocyanate-dextran (average mol wt 500,000), rhodamine B (for fluorescence), sodium dodecyl sulfate (SDS; analytical grade powder) were also purchased from Millipore Sigma.

3.3.1 Preparation of protein microgel

Whey protein isolate was kindly donated by Davisco Foods International (Le Sueur, MN, USA) and further extracted for Blg was based on an established procedure [62]. Extracted Blg was used to prepare protein stock solutions in deionized water (DI), the final concentration of Blg stock solution was 2 wt%. Blg solution (2 wt%) was acidified to pH 5.85-5.95 using 0.1 M HCl solution. Microgels were formed by submerging a scintillation vial filled with 10 mL Blg solution in a hot-water bath at 85°C for 2 hours directly followed by submersion in an ice-water bath for 20 min. Samples were lyophilized and stored under 4°C before use. The Blg microgels (5 wt%) stock solution were prepared by dispersing the lyophilized samples in DI water under gentle magnetic stirring at room temperature for at least 2 hours. Solutions were stored overnight at 4°C to allow hydration of protein microgels. Before the microgels were characterized or mixed with the dextran and HPMC phases, the suspension was sonicated for 10-15 min using 30% amplitude pulses every 1 s. Particle size of dispersed microgels were confirmed at 190-200 nm with dynamic light scattering.

3.3.2 Preparation of W/W emulsion

The emulsions were prepared by mixing aqueous solutions of dextran (0-20 wt %), HPMC (1-10 wt %), and Blg microgels (0-1 wt %) at pH 3 using a magnetic stir

mixing for 30 min at 250 rpm. The order of mixing did not significantly influence the structure of the emulsion.

The criterion for stability of the emulsions was taken as the absence of a visible layer of the pure dispersed phase [21]. We considered the system unstable as soon as a thin (<1 mm) layer became noticeable. We considered that the formation of a layer of the pure continuous phase is not a sign of destabilization of the emulsion droplets, but of creaming or sedimentation of droplets of the dispersed phase.

3.3.3 Phase diagram

The phase diagram of mixture of Dextran and HPMC was constructed using a method reported previously [81]. Stock solutions of Dextran (10%) and HPMC (10%) were introduced to 96-well plates and mixed to form super-critical emulsions. All dispensing and mixing steps were performed with multichannel micropipettes. Each super-critical concentration was then titrated with DI water until emulsion characteristics (i.e., the presence of droplets) were no longer observed by a bright field microscopy. The concentration of each phase system after the point that a further dilution produced a droplet-free mixture was recorded as a critical concentration.

Tie lines were established based on a reported method [82] with minor modification. Mixtures with different concentrations of dextran and HPMC were prepared in the two-phase region, density of the top and bottom phases were analyzed using the gravimetric method. This was done by using a volumetric pipette and pipetting a known volume of sample (4 ml) and measuring its mass. Solutions of different total

mass ratios were tested until solutions had the same top phase density and bottom phase density (Fig. 3.1 red and blue symbols), which is a requirement for solutions on the same tie line. Polymer compositions on the same tie line have the same interfacial tension.

3.3.4 Confocal Laser Scanning Microscopy

The protein microgels and the dextran phase in W/W emulsion were visualized separately with a CLSM by utilizing different fluorescent labeling. The microgels were labeled with the fluorochrome rhodamine B isothiocyanate (rhodamine B) at a final concentration of 5 ppm. The dextran stock solution was labeled by adding a small portion (0.5%) of commercially available fluorescein isothiocyanate (FITC) labeled dextran with the same molecular weight as the dextran stock solution.

Confocal images of the microcapsule dispersion were obtained at 20°C with a Zeiss LSM 710 Confocal Microscope (Zeiss, Germany). An oil immersion objective lens (63×/1.2NA) was used. The incident light was emitted by a laser beam at 561 nm for rhodamine B and at 488 nm for FITC. The fluorescence intensity was recorded between 568 and 650 nm for rhodamine B and between 492 and 544 nm for FITC. Samples were inserted between a concave slide and a coverslip. The images were taken after 12 h, unless otherwise indicated. It was confirmed that the use of labeled dextran and proteins had no influence on the emulsions.

3.3.5 Emulsion stability to environmental stresses

In order to investigate the droplets morphology and creaming stability of emulsions under different environmental stresses, pH, ionic strength and temperature were adjusted as following:

pH: emulsions were formed at pH 3 and adjusted to pH 4, 5, 6, and 7 using 0.1M hydrochloric acid (HCl) solution and/or sodium hydroxide (NaOH).

Ionic strength: Emulsions with different ionic strengths were prepared by adding sodium chloride (NaCl) solution to obtain a final concentration of 50, 100 and 300 mM NaCl.

Temperature: for the thermal stability study, each 5 mL samples were poured into 25 mL glass vials and then submerged in a water bath set at 25, 60 or 90°C. The emulsions were held in the water bath for 30 min, and then cooled to the ambient temperature.

The emulsions were tested for droplet morphology by a CLMS shortly after treatment. For creaming stability, emulsions were stored at the refrigeration temperature and images were taken every day for a period of one week.

3.3.6 Zeta-potential measurement

The zeta-potentials of microgels and two polysaccharide phases were determined between pH 3 and 7 by a laser doppler micro-electrophoresis using a Zetasizer Nano ZS (Malvern Instruments, Worcestershire, UK). Each sample was measured three times in disposable folded capillary cells (DTS 1070, Malvern Instruments Ltd,

Worcestershire, UK) at a protein concentration of 0.1 wt% or polysaccharides concentration of 1%. At least 32 runs were performed per measurement.

3.3.7 Surface tension measurement

The surface tension of each phase with and without microgels under different pH levels were tested using an Attension Theta optimal tensiometer (Biolin Scientific, Gothenburg, Sweden) with pendant drop shape analysis. A drop of mixture containing 12 % dextran (or 2% HPMC) without or with 0.3% microgels was dispensed from a syringe needle into air. A constant drop volume was maintained in the air and the tension was recorded after 100 s of equilibrium. The tension was deduced from the drop shape by fitting with the Young-Laplace equation.

3.3.8 Demulsification of W/W emulsions by SDS

Demulsification of W/W emulsions was achieved by introducing SDS into the system. A 0.5 mL of stock SDS solutions were added to 0.5 mL of emulsions to obtain a final SDS concentration of 2, 4, and 10 mM. The mixtures were vortexed for 30 s and tested for droplet morphology by the CLMS shortly after treatment. As a control, 0.5 mL of DI Water was also mixed with 0.5 mL emulsion to exclude the effect of dilution on emulsion droplets.

3.4 Results and Discussion

3.4.1 Phase diagram

A phase diagram was produced for the dextran and HPMC in this study (Fig. 3.1). Because macroscopic phase separation between the two polymers was difficult to observe, the microplate estimation method, in which the phase separation was

detected through microscopy, was used instead of the traditional turbidometric titration method. When the concentrations of dextran and HPMC exceeded 5.8 wt% and 1.5 wt%, respectively, phase separation occurred in the absence of stabilizers. In these mixtures, droplets of one polysaccharide phase dispersed in the other polysaccharide as a continuous phase in a manner dependent on polymer composition. The red symbols in Fig. 3.1 correspond to the dextran-in-HPMC emulsions (dextran/HPMC), and the blue symbols correspond to the HPMC-in-dextran emulsions (HPMC/dextran). The polymer compositions at the same tie line have an identical interfacial tension. The interfacial tension between two aqueous phases increases with increasing polymer concentration [21] but remains orders of magnitude smaller than that for O/W emulsions, even at the high polymer concentrations studied herein (blue and red symbols).

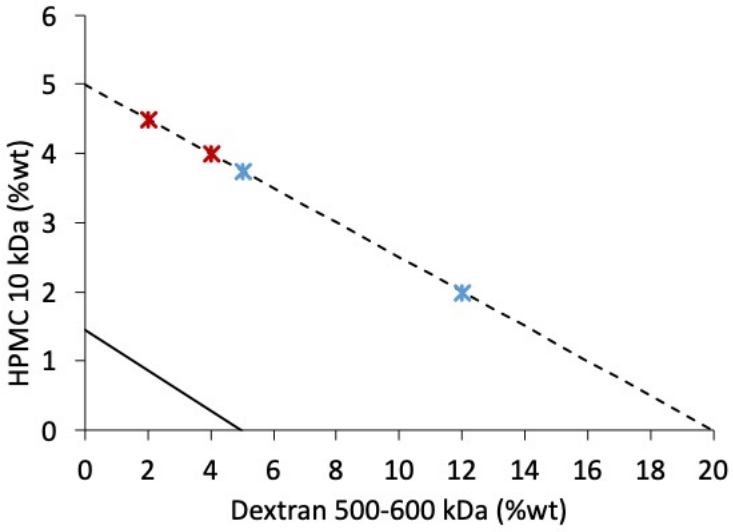

Figure 3.1 Phase diagram for aqueous mixtures of dextran and HPMC. The solid line indicates the binodal. A tie line is drawn for illustration as dashed dotted lines. Red and blue symbols indicate compositions leading to dextran/HPMC emulsions or HPMC/dextran emulsions, respectively.

3.4.2 Effect of protein microgels concentration

Stable W/W emulsions were achieved at pH 3.0; therefore, the pH of dispersion was set at 3.0 unless otherwise mentioned.

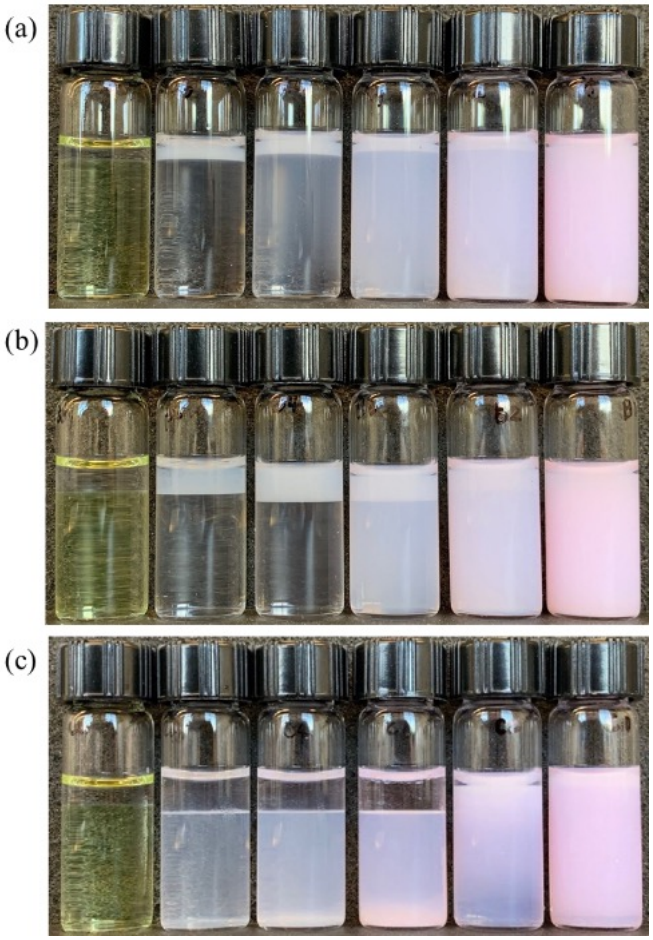

Figure 3.2 Emulsions of HPMC/dextran in the presence of different concentrations of protein microgels (C_{pro}=0, 0.05, 0.1, 0.25, 0.5, 1%, from left to right) after one week standing. (a)C_{dex}=12%, C_{HPMC}=1% (b) C_{dex}=12%, C_{HPMC}=2% (c) C_{dex}=8%, C_{HPMC}=2%. FITC labelled dextran (green) was only used in the first column to help visualize the phase separation; Protein microgels were dyed by rhodamine B (red)

Fig. 3.2 shows the effect of protein microgels (C_{pro}) concentration on the stability of HPMC/dextran emulsions after 1 week standing at the refrigerated temperature. Without stabilizer, all emulsions underwent phase separation within 1 day. With addition of protein microgels, the behaviors of the emulsions depended on the volume fraction of HPMC and dextran.

For emulsions containing 12% dextran and 1% or 2% HPMC, addition of protein microgels at C_{pro} > 0.05% stabilized the emulsions; i.e., the HPMC droplets did not merge or form a transparent HPMC top layer for at least 1 week. However, because of the size of the droplets and the action of buoyancy, the emulsions formed a creamed layer at the top and a subnatant aqueous phase. Depending on the C_{pro}, the subnatant was either (i) clear (for Fig. 3.2a C_{pro} < 0.1% or Fig. 3.2b <0.25%), suggesting complete adsorption of the microgels to droplet interfaces, or (ii) turbid, suggesting that a fraction of the microgels remained non-adsorbed in the continuous dextran phase.

At a higher HPMC concentration (2%) and a lower dextran concentration (8%), the emulsions were not stable against coalescence for $C_{pro} \leq 0.5\%$, and destabilization of the emulsion droplets resulted in a clear HPMC phase at the top, thus indicating that phase separation occurred even with the addition of protein microgels. The increase in the turbidity of the bottom dextran layer was caused by the presence of protein microgels with a preference for the dextran phase. However, increasing the protein concentration to C_{pro} > 0.5% prevented the phase separation, and the emulsions were stable for at least 1 week.

The effect of protein microgels' concentration on W/W emulsions is consistent with findings from a study on whey protein microgel (WPM) stabilized Pickering emulsions [13]. In Pickering emulsions, limited coalescence occurs in the emulsifier-poor régime, and the droplets are initially only partly covered by the emulsifier and undergo coalescence after agitation is stopped. This coalescence leads to a progressive decrease in the oil-water interfacial area until the adsorption density of

stabilizers become sufficiently high to prevent further coalescence. Consequently, the final droplet size is associated with the initial stabilizer concentration. In the presence of an excess of stabilizer (emulsifier-rich régime), the final droplet size of the emulsion is virtually independent of the initial stabilizer concentration and mainly depends on the stirring intensity, which controls droplet fragmentation.

The dependency of the W/W emulsion droplet size on protein microgels concentration was confirmed with CLSM images of emulsion droplet (Fig. 3.3) as well as a comparison of number-average droplet diameter for two emulsion compositions (Fig. 3.4). The number-average droplet diameter was determined by manually measuring the in-focus droplets from at least 3 images. The diameter of droplets in 12%:2% emulsions decreased with increasing C_{pro} up to 0.3%, and further increasing the C_{pro} did not significantly change the droplet size. With a larger volume fraction of the dispersed phase (8%:2%), the drop size was significantly larger, thus indicating that the emulsions underwent limited coalescence until C_{pro} of 0.5%. A good correlation was observed between the evolution of emulsion's droplet size and macroscopic observations of the emulsions, thus suggesting that the two-régime theory of emulsifier concentration for stabilization of Pickering emulsions is applicable to the W/W emulsions.

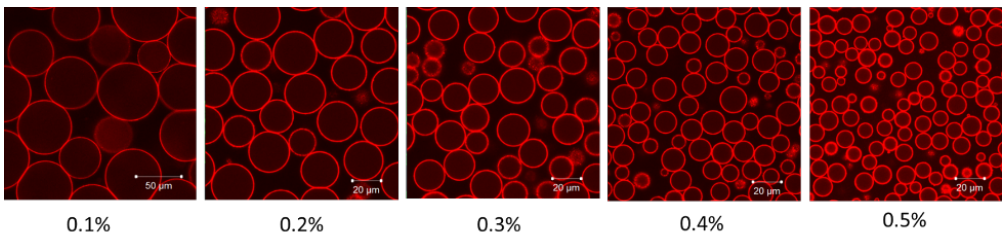

Figure 3.3 CLSM images of protein (red) signal showing the effect of the protein microgels concentration on the droplet size for an emulsion containing 12% dextran and 2% HPMC. The scale bar is 50 µm for the first image, and 20 µm for the others.

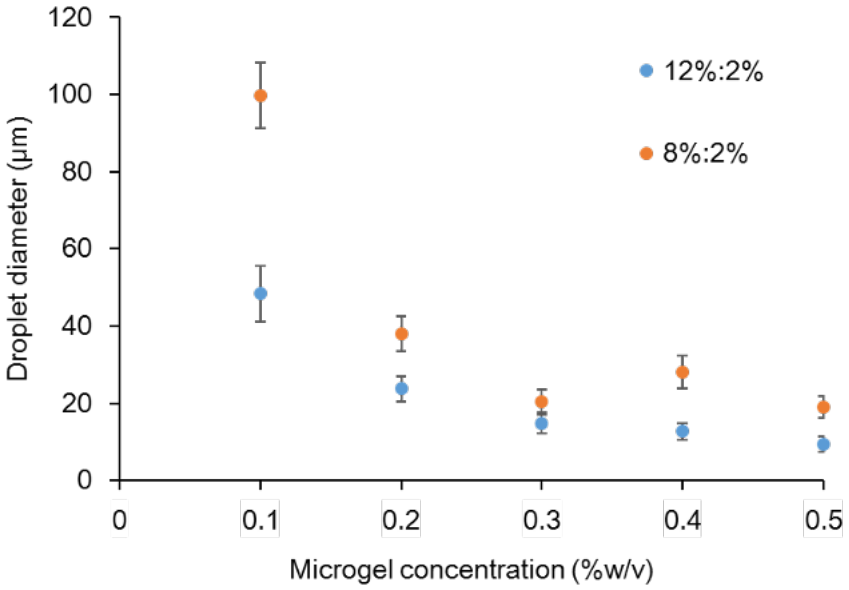

Figure 3.4 Dependence of number average droplet diameter on the protein concentration for two emulsion compositions: C_{dex} = 12% and C_{HPMC} =2% or C_{dex} = 8% and C_{HPMC} = 2%. The error bars represent the standard deviation of the size distribution.

3.4.3 Effect of composition

By tuning the ratio of HPMC and dextran in the mixture, we obtained either HPMC-in-Dex or Dex-in-HPMC emulsion, depending on the composition of polysaccharides. The emulsions of different polysaccharides ratio (C_{dex}/C_{HPMC} (%) 1.5/8; 1.5/2.9; 8/2; 12/2) showed different stability with the same 0.5% protein microgels addition (Fig. 3.5). The creaming of HPMC droplets began to be visible after 1 week (Fig. 3.5 two samples on the right), whereas sedimentation of dextran droplets was complete for C_{Dex}/C_{HPMC} (%) at 1.5/2.9 after only 1 day. CLSM images taken several minutes after preparation of the suspensions showed that dispersions of C_{Dex}/C_{HPMC} (%) at 1.5/8 and 1.5/2.9 comprised dextran droplets dispersed in the HPMC continuous phase, whereas dispersions of C_{Dex}/C_{HPMC} (%) at 8/2; 12/2 were HPMC droplets dispersed in dextran; protein microgels were situated at the

interface of two phases except in sample 1.5/2.9 (Fig. 3.6). Compared with other compositions, a ratio of 1.5/2.9 was closer to the binodal line in the phase diagram, representing a lower interfacial tension between the two polysaccharides. Therefore, the interfacial tension was considered one of driving forces for microgels accumulation on the interface.

Interestingly, for sample 1.5/8, even when covered with a layer of protein microgels, the droplets precipitated after 1 week. According to Nguyen [21], aggregation of dextran droplets is the reason for the relatively rapid sedimentation. By considering the higher density of dextran than HPMC, together with the preference of protein microgels for the dextran phase, the sedimentation or aggregation of dextran droplets can be explained.

Figure 3.5 Evolution with waiting time of emulsions formed by HPMC and dextran mixtures at different compositions containing 0.5% protein microgels. C_{dex}/C_{HPMC} (%) from left to right: 1.5/8; 1.5/2.9; 8/2; 12/2. The 2 samples on the left formed dextran droplets in the continuous HPMC phase and the 2 samples on the right formed HPMC droplets in the continuous dextran phase.

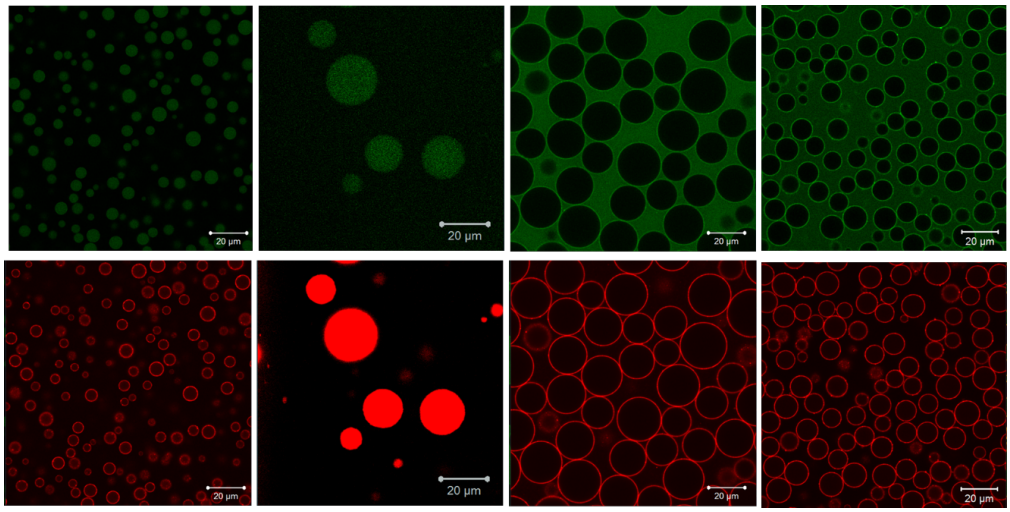

Figure 3.6 CLSM images of HPMC and dextran mixtures at different compositions containing 0.5% protein microgels dyed by rhodamine B (red) and dextran phase was FITC labelled (green). C_{dex}/C_{HPMC} (%) from left to right: 1.5/8; 1.5/2.9; 8/2; 12/2.

The emulsions contained several larger clusters of microgels that clearly protruded toward the dextran phase (Fig. 3.7), thus indicating that the protein microgels preferentially partitioned to the dextran phase in both dextran/HPMC and HPMC/dextran emulsions. The large clusters of microgels were formed through depletion interactions when entering the interface [22]. The relative preference of the microgels for one of the two phases influences the contact angle of the microgels at the interface and consequently the stability of W/W emulsions. Emulsions are well known to be more stable if the stabilizer prefers the continuous phase, in this case, HPMC/dextran emulsions.

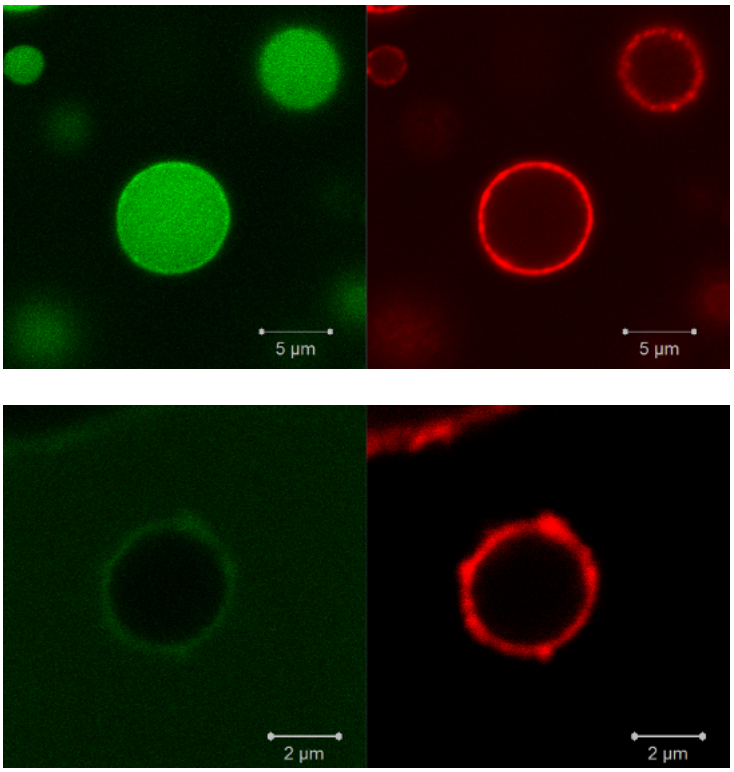

Figure 3.7 CLSM images of dextran in HPMC emulsion (top) and HPMC in dextran emulsion (bottom) in presence of protein microgels (0.5%). Protein was dyed by rhodamine B (red) and dextran phase was FITC labelled (green).

3.4.4 Effect of pH

We previously reported that the particle size distribution of Blg microgels is dependent on pH [83]. The microgels displayed a polyampholytic character with a pI around 5.2. Swelling of the soft and poorly cross-linked microgels was observed when the pH was far from the pI, thus indicating a flexible internal structure; increasing the internal charge density would cause protein strand or chain repulsion within the microgels.

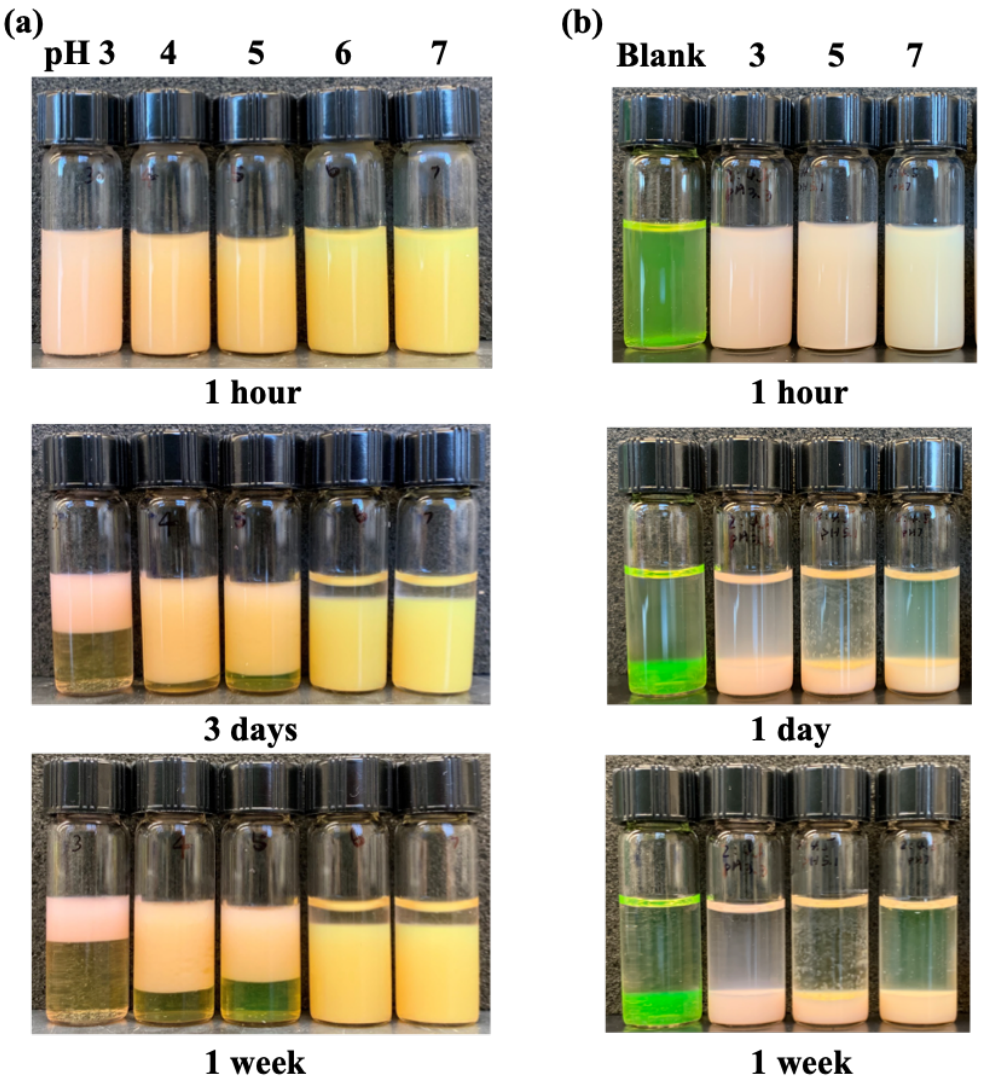

Figure 3.8 Evolution with waiting time of (a) HPMC/dextran (2%/12%) and (b) dextran/HPMC (2%/4.5%) emulsions at different pH containing 0 (Blank) or 0.3% protein microgels. The emulsion is colored by the presence of FITC-dextran (green) and rhodamine B dyed protein microgels (red), the intensity of green color is influenced by pH.

Fig. 3.8a shows the effects of pH on the visual appearance of HPMC/dextran (2%/12%) emulsions after 1 hour, 3 days and 1 week. Under pH 6 and 7, the emulsions formed a clear top layer consisting of the HPMC phase, thus indicating coalescence of the droplets. However, at pH < 5, the protein microgels completely inhibited coalescence but formed a creaming layer at the top. Creaming of dextran

droplets was observed to be faster and denser at pH 3 than at pH 4 and 5. The microstructure of the HPMC droplets and protein microgels is shown in Fig. 3.9a. CLSM images of the emulsions were taken right after the emulsion was mixed and revealed droplet morphologies before coalescence. Distinct layers of microgels were observed on the droplet surfaces at pH 3, 4 and 5, and the interfacial layers act as a barrier for inhibiting droplet coalescence. However, at pH 6 and 7, the microgel layer on the droplet surfaces disappeared, and the arrested HPMC droplets coalesced into larger droplets, thus ultimately resulting in the formation of a homogenous HPMC layer. The increasing pH also increased the FTIC intensity of dextran, which overwhelmed the protein signal in CLSM images. Macroscopic pictures (Fig. 3.8a) showed that the dextran bottom layer was turbid, indicating microgels situated in dextran phase under pH 6 and 7.

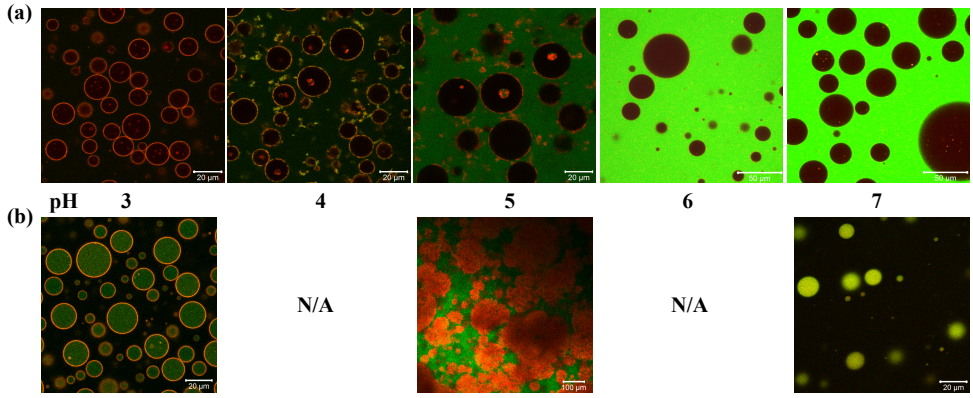

Figure 3.9 CLSM images of (a) HPMC/dextran (2%:12%) and (b) dextran/HPMC (2%/4.5%) emulsions with 0.3% protein microgels at different pH. The emulsion is colored by the presence of FITC-dextran (green) and rhodamine B dyed protein microgels (red). The FTIC-dextran concentration is identical in all samples, but the intensity of green color was influenced by pH.

The effects of pH on the visual appearance of dextran/HPMC (2%/4.5%) emulsion after 1 hour, 1 day and 1 week are shown in Fig. 3.8b. These dextran/HPMC emulsions were situated on the same tie-line as the HPMC/dextran (2%:12%)

emulsions, therefore the interfacial tension was the same for both emulsions. At all pH levels, rapid sedimentation of dextran droplets was observed, and the sedimented layers had the same height as those in the control sample; therefore, distinguishing whether the emulsion droplets coalesced was difficult. The microstructures of dextran droplets and protein microgels at different pH values are shown in Fig. 3.9b. Because both emulsions have the same interfacial tensions and microgels concentration, we expected to observe similar droplet size and a distinct layer of microgel on the surface, as seen with the HPMC/dextran emulsion; however, these aspects were observed only for dextran/HPMC emulsion at pH 3. At pH 5.0, microgels aggregated so aggressively that there was insufficient time for spherical dextran droplets to form. At pH 7.0, without the microgel layer on the surface, the dextran droplets remained small and sedimented into the dextran bottom layer.

The observed rapid creaming of HPMC droplets covered with microgels corresponded to the fast sedimentation of microgel-covered dextran droplets at pH 3, both of which are caused by the agglomeration of the droplets into larger clusters that cream or sediment rapidly [37]. When the pH was close to the microgels' pI, the creaming of the HPMC/dextran emulsion droplets slowed down, because protein aggregates led to the formation of a microgel network in the continuous phase. Inducing protein particle aggregation to prevent creaming has also been reported for a PEO-in-dextran emulsion by decreasing the net charge density of the protein, in a process called cold-gelation [38].

The microgels' preference to stay at the interface or in the continuous phase was influenced by the pH of emulsion systems. Blg protein particles have been found to prefer the dextran phase at pH > 4.0 but to prefer the PEO phase at lower pH [21]. Interestingly, in this study, Blg microgels preferred the dextran phase under all pH levels, thus simplifying our case and enabling us to further investigate the possible force driving microgels accumulation at the interface under different pH.

3.4.5 Effect of ionic strength

The effects of screening electrostatic interactions between the protein microgels and polysaccharide phases were investigated at pH 3.0 for emulsions with the same composition, through the addition of up to 300 mM NaCl. To understand the behavior of the mixtures, we first studied the behavior of Blg microgels as a function of ionic strength in pure dextran solutions at C_{dex}=12%, corresponding to the percentage of continuous phase in the emulsions. The microgels concentration was set at 0.3%, corresponding to the maximum concentration of microgels if all proteins partitioned to the dextran phase of the emulsions.

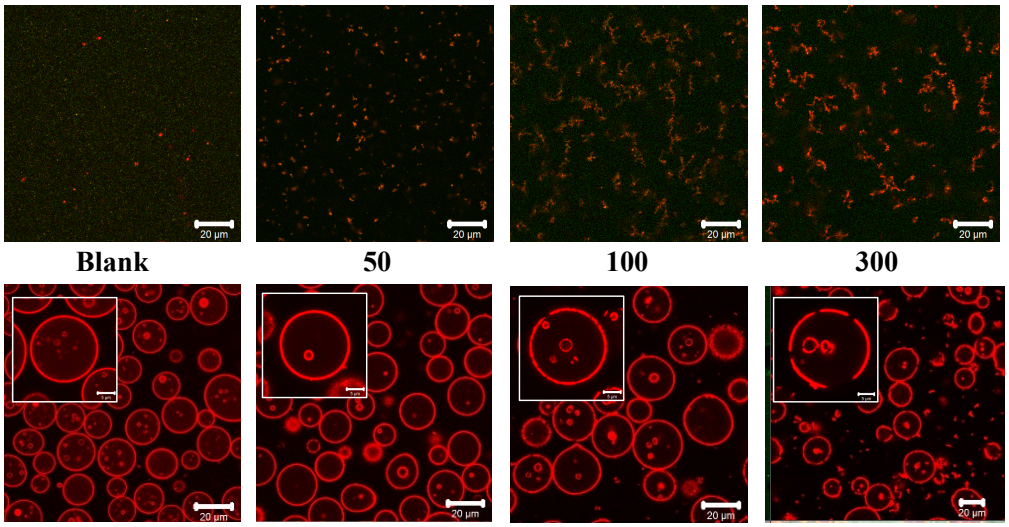

Figure 3.10 CLSM images of 0.3 % microgels in 12% dextran solutions (top) and HPMC/dextran (2%/12%) emulsions (bottom) at different ionic strength (mM) indicated in the figure. Microgels are dyed by rhodamine B (red), inserts are representative images for observing microgels coverage on surface. The scale bar of inserts is 5 μm.

The top row in Fig. 3.10 shows CLSM images of the microgels in a dextran solution at different ionic strengths. In the blank sample, individual microgels could scarcely be observed because of their nano-scale size (~200 nm). The microgels remained homogeneously distributed in the presence of 50 mM NaCl but formed flocs of dense protein clusters when 100 mM NaCl was added. Increasing the salt content to 300 mM did not cause these clusters to associate into larger flocs, thus indicating that the association was saturated around 100 mM.

CLSM images of emulsions (HPMC/dextran) with 0 to 300 mM NaCl taken shortly after mixing are shown in the bottom row of Fig. 3.10. Salt, at all concentrations tested, had no significant effect on the average droplet diameter. The microgels formed distinct layers at the droplet surfaces though at ionic strength > 100 mM coverages were not complete for some droplets. Aggregation of microgels with each

other and with microgels at the interface can be clearly seen at 300 mM. Nevertheless, the droplets do not coalesce, because the naked surfaces of droplets are maintained separated by the protein clusters. The ionic strength effect on droplet was very similar to that of pH 4 and 5. Therefore we suggest that the aggregation rate of protein microgels increases if the net charge of microgels decrease. Aggregated microgels can form bridges between the droplets and prevent the droplets from coalescence.

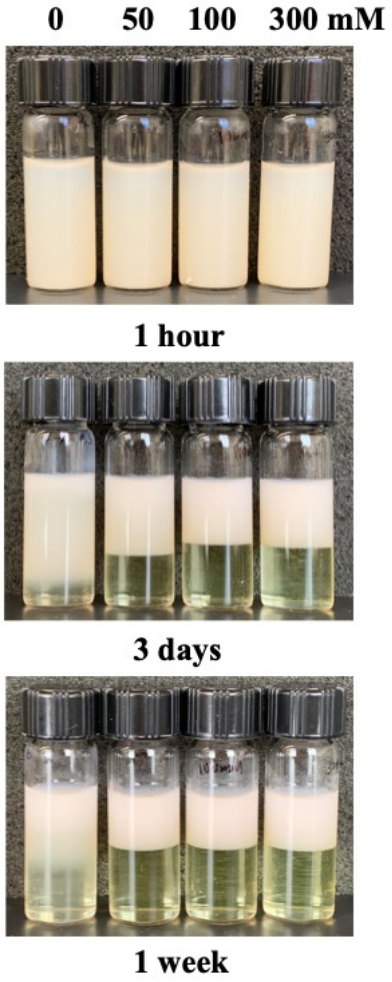

Figure 3.11 Evolution of HPMC/dextran (2%/12%) emulsions (pH 3.0) at different ionic strength (mM) containing 0.3% protein microgels with waiting time of 1 hour, 3 days and 1 week. The emulsion is colored by the presence of FITC-dextran (green) and rhodamine B dyed protein microgels (red).

The effects of ionic strength on emulsion stability after standing for 1 hour, 3 days and 1 week are shown in Fig. 3.11. With addition of NaCl, the emulsions underwent faster creaming. This finding was unexpected, according to the results of pH effect, we expected that creaming would be slowed down by aggregation of protein microgels. One possible reason for the fast creaming is that NaCl may slightly decrease the viscosity of the dextran phase. The slight decrease in the viscosity of polysaccharides had been reported for polysaccharides such as chia seed polysaccharide and seed gums with the addition of salt [84, 85]. Likewise, those reports have indicated a slight decrease in viscosity at 0.1 M NaCl but no further reduction in viscosity with salt concentrations increased to 0.5 M NaCl. The presence of salt could suppress inter- and intra- electrostatic repulsions of the microgels, thus causing shrinkage/collapse of the microgels, which could then lead to a slightly decrease in viscosity.

3.4.6 Thermal effect

Heat treatment of emulsions stabilized by whey proteins is known to accelerate creaming because of protein unfolding and an increase in hydrophobic attraction among droplets. Therefore, the stability of W/W emulsions was investigated at two different temperatures; i.e., temperatures resulting in partial (60°C) and full (90°C) protein unfolding.

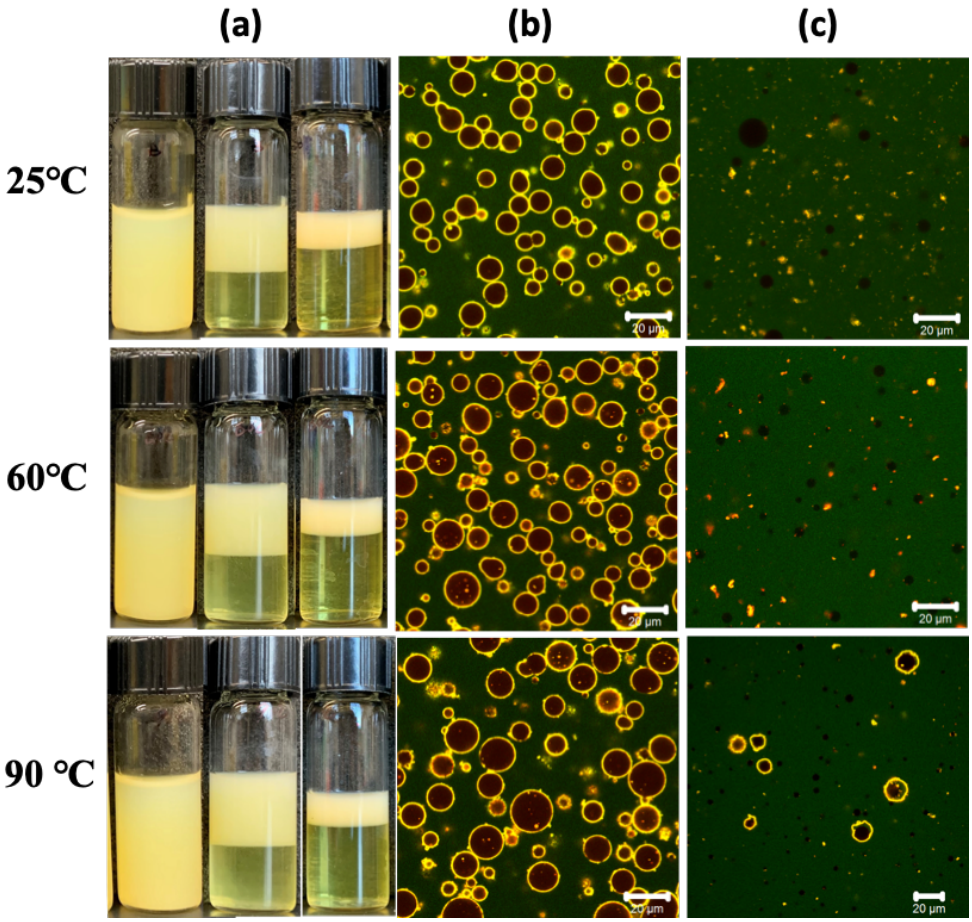

Figure 3.12 Thermal stability of HPMC/dextran (1%:12%) emulsions with 0.25% protein microgels after 30 min thermal treatment at 25°C, 60°C and 90°C. (a) Emulsions stored at 4°C for 0, 1, and 3 days (from left to right) (b) CLSM images of emulsions shortly after heating (c) CLSM images of heated emulsions with addition of 2 mM SDS solutions. The emulsion is colored by the presence of FITC-dextran (green) and rhodamine B dyed protein microgels (red).

As shown in Fig. 3.12a and Fig. 3.12b, thermal treatments had very little effect on the emulsion creaming stability and droplet morphology, as expected, because the protein microgels used in the systems were produced from a thermal treatment. The inter-droplet interactions or bridging of microgels were not observed after heat treatment, whereas the protein signal increased inside the HPMC droplets (Fig. 3.12b), possibly because more hydrophobic domains on protein microgels were exposed under heating, thus promoting their partitioning to the HPMC phase.

Interestingly, microgel adsorption on the HPMC droplets partially resisted SDS disruption after being heated at 90°C, as shown in Fig. 3.12c. In addition to exposing more hydrophobic sites on the microgels, the heat treatment promoted protein microgel particle–particle fusion on the surfaces of the droplets. Similar particle fusion has been reported for WPM on the Pickering emulsion surface [75]. SDS did not dissociate the structures that formed after heating, thus indicating that the particle-particle fusion was caused by covalent bindings between microgels on the surface. In the 90°C heated emulsion, the spherical microgel layer shrank with the decrease in droplet surface after addition of SDS (Fig. 3.13) and partially lost contact with the surface. The results indicated that the protein microgels were not "fused" or "gelled" with the HPMC phase, and therefore would not protect the emulsion from demulsification.

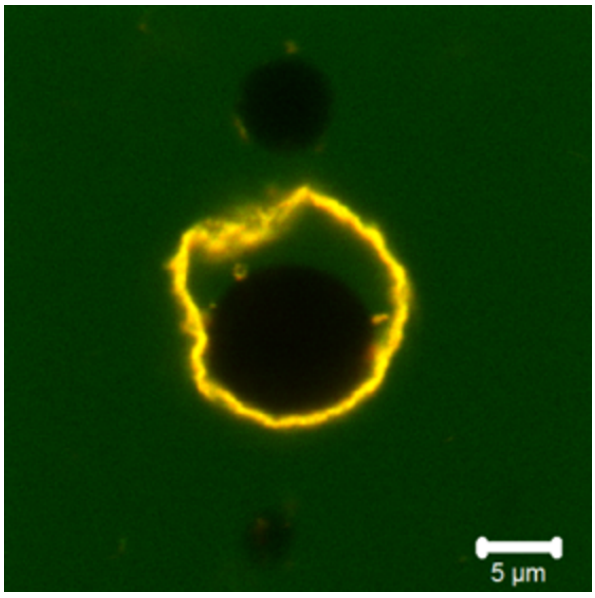

Figure 3.13 CLSM images of heated HPMC/dextran (1%:12%) emulsion with 0.25% protein microgels after 30 min thermal treatment at 90°C with addition of 2 mM SDS solutions. The emulsion is colored by the presence of FITC-dextran (green) and rhodamine B dyed protein microgels (red).

3.4.7 Surface charges of the emulsion constituents

To elucidate the effect of charge on protein preference for the interface or dextran phase, zeta-potential of pristine protein microgels and pure dextran and HPMC solution was measured. Dextran and HPMC showed little surface charge in both pH 3 and 7 (Table 3.1) as expected because of the absence of ionic side groups on their chemical structures. The zeta-potentials for protein microgels were 21.37 mV and -27.21 mV at pH 3.0 and 7.0, respectively. There was no significant difference in the zeta-potentials of the mixtures of microgel and dextran or microgel and HPMC, in comparison with the microgels alone, thus indicating absent or very weak electrostatic interactions among the emulsion constituents. A similar finding has been reported by Camino *et al.*, who have found that HPMC and Blg exhibited weak complex formation under acidic conditions [86]. Nevertheless, owing to the very small differences in the electrical potential, we conclude that electrostatic interactions are not the predominant driving force for microgels accumulation on the interface.

Table 3.1 Zeta-potential of dextran, HPMC and BM mixtures under different pH values.

Components	Zeta potential/mV			
	pH 3		pH 7	
	Avg.	Std.	Avg.	Std.
Dextran (Dex)	0.27	0.14	0.43	0.27
HPMC	0.48	0.18	0.70	0.50
Blg Microgels (BM)	21.37	2.10	-27.21	0.80
BM+Dex	20.40	0.14	-28.60	0.43
BM+HPMC	20.03	0.29	-27.13	0.83

3.4.8 Interfacial tension

Since the effect of pH on the surface charge of the microgels cannot explain changes of the protein preference, we further investigated the effect of pH on interfacial tension. The pendant drop method was used to measure the interfacial tension between dextran and HPMC under different pH values. Unfortunately, the intrinsic ultralow interfacial tension between the two phases in the W/W emulsion prevented the direct measurement by this technique. However, it was found that interfacial tension can be interpreted as the difference between the surface tension of each of the phases against a common medium, for example, air [79]. Therefore, the surface tension of both single phases with and without microgels at 25°C was measured at three different pH values, and the "interfacial tension" between the two phases was obtained by subtracting the surface tension of HPMC from that of dextran as shown in Table 3.2. Of note, although this method cannot measure the interfacial tension quantitatively, it can provide insight into the pattern of pH-induced changes.

Table 3.2 Surface tension of dextran, HPMC and Blg microgels (BM) mixture under different pH values.

Components	Surface tension (mN/m)		
	pH3	pH5	pH7
σ1(Dextran)	95.3±0.3	107.7±0.5	116.8±0.3
σ2(HPMC)	76.0±0.6	75.4±1.2	77.5±1.6
σ3(BM+Dex)	75.1±0.8	82.0±2.6	91.2±0.2
σ4(BM+HPMC)	68.2±0.4	75.2±0.8	76.8±1.2
σ1-σ2	19.3	31.6	39.3
σ3-σ4	6.8	6.8	15

We compared the "interfacial tension" between two phases with and without microgels and found changes in interfacial tension from pH 3 to 7. Without addition

of microgels, the interfacial tension between dextran and HPMC was 19.3 mN/m at pH 3, and increased to 31.6 mN/m and 39.3 mN/m at pH 5 and 7, respectively; when the microgels were included, the interfacial tension was 15 mN/m at pH 7, and decrease to a same level of 6.8 mN/m at pH 3 and 5. The influence of pH on interfacial tension can be related to the partition coefficient of charged macromolecules in W/W system [79], therefore the pattern of pH-induced changes on "interfacial tension" with microgels may explain the observation in section 3.4.4 that microgels accumulated on the droplets interface at pH 3-5, but not at pH 6-7. If there is no specific interaction between the microgels and either polysaccharides, the microgels' preference for the interface may be due to the difference in interfacial tension resulting from the polymer-depleted regions around the particles in the two thermodynamic incompatible phases [87]. The difference in interfacial tension resulting from pH changes was considered one of the driving forces inducing microgels to stay on the interface or partition into the dextran phase.

However, there might be an interaction between microgels and HPMC phase at pH 3. The addition of microgel did not change the surface tensions of HPMC solutions at pH 5 and 7, but induced a slight decrease in the value of surface tension at pH 3, thus indicating that the microgels may have interaction with HPMC under this condition. The exposure of the hydrophobic units on the surface of the proteins may play a role in the pH dependence of the interaction [37]. Blg microgels have been reported to undergo conformational changes exposing more hydrophobic domains under pH 3 [83], therefore it is possible that there is hydrophobic interactions between microgels and HPMC at pH 3.

3.4.9 SDS effect

To investigate the hydrophobic interaction in W/W emulsions, we introduced SDS into the W/W system at pH 3. SDS is usually used to induce protein denaturation by binding to the protein hydrophobic patch with its hydrocarbon tail in the critical micelle concentration range, which is approximately 8 mM in water [88]. Although the microgels, as a protein structure, might be assumed to be destroyed by SDS, Schmitt et al. [12] have demonstrated that the particle size of microgel is not affected solely by SDS, thus indicating that the microgels do not dissociate into protein molecules by addition of SDS. Effective demulsification of W/W emulsions occurs when the emulsion is sufficiently diluted, because the phase diagram of dextran/HPMC features only a two-phase region under high polymer concentrations. Control groups confirmed the dilution by an equivalent DI water did not cause demulsification. It is expected that SDS addition would disrupt the hydrophobic interaction between microgels and HPMC, which would trigger demulsification of the emulsions.

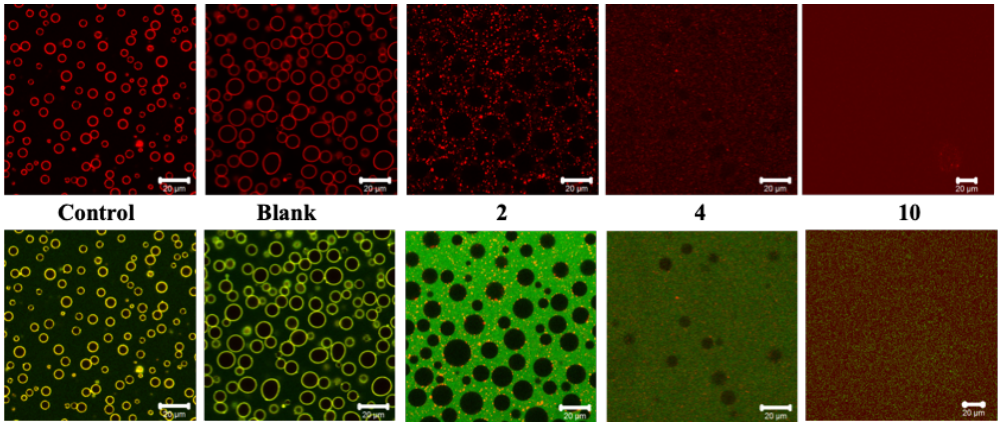

Figure 3.14 CLSM images of HPMC/dextran (1%:12%) emulsions with 0.25% protein microgels with addition of SDS at concentrations of 0 (Control), 2, 4, and 10 mM. Blank is the original emulsion without any dilution and mixing treatment. The emulsion is colored by the presence of FITC-dextran (green) and rhodamine B dyed protein microgels (red). The FTIC-dextran concentration is identical in all

samples, but the intensity of green color was influenced by strong negative charges of SDS.

The effect of the anionic surfactant SDS on emulsion stability is shown in Fig. 3.14. With the addition of 2 mM SDS, the confocal images showed that the microgels left the interface and formed small aggregates (red dots) in the dextran (continuous) phase. It was obvious that SDS fully disrupted the interaction between microgels and the HPMC phase. This disruption can be explained by two types of interactions between protein microgels and SDS. At pH 3.0, microgels with positive surface charges are neutralized by negatively charged SDS molecules, and protein microgels tend to aggregate when their surface charges are close to zero. Moreover, SDS competes with HPMC for interactions with microgels through merging of hydrophobic domains on the microgel surface and the SDS alkyl tails. Further increasing concentration of SDS to 4 and 10 mM resulted in disappearance of the small protein aggregate as well as the HPMC droplets. These results are consistent with those from previous reports [10]. SDS-microgels aggregates acquire a large amount of total negative charge, which is capable of re-dispersing the aggregate in water. Interestingly, high concentration (> 4 mM) of SDS also disrupt the cellulose network structure, thus resulting in a loss of rheological characteristics and the formation of a fluid-like and diluted cellulose solution [89, 90]. In the case of W/W emulsions, the interaction between SDS and HPMC causes the incompatible aqueous phases to become miscible.

The mechanism of how SDS demulsifies W/W emulsions involves both electrostatic and hydrophobic interactions in the presence of low concentrations of

SDS. Therefore, electrostatic and hydrophobic force may both contribute to the microgels' preference for the interface at pH 3. However, the previous results showed the electrostatic interaction between microgels and interface is weak, thus indicating the hydrophobic force predominates the interaction.

3.5 Conclusion

HPMC/dextran emulsions formed by mixing dextran and HPMC solutions were stabilized by the addition of Blg microgels (size 190–200 nm). Increased microgel concentration prevented the droplet coalescence in the emulsion but did not inhibit creaming. The droplet size of the dispersed phase was found to decrease with increasing protein concentration. At pH 3, sufficient interfacial tension between two phases drove the microgels spontaneously accumulating at the interface of the two polymer phases in both HPMC/dextran and dextran/HPMC emulsions, and the interfacial microgels clearly protruded toward the dextran phase.

The stability of W/W emulsions was influenced by pH. The HPMC/dextran emulsion was stable under pH 3–5, whereas increasing the pH above the microgel pI (~pH 5) destabilized the emulsion by driving the interfacially adsorbed microgels into the continuous phase. The W/W emulsions were stable under high ionic strength levels though at ionic strength > 100 mM the microgels coverages at the surface were not complete for some droplets. The W/W emulsions stabilized by protein microgels were thermally stable. Heat treatment promoted partial protein particle-particle fusion on the droplet surface at 90°C, but this fusion had no protective effects against demulsification.

The interfacial tension between dextran and HPMC, which is unrelated to charge, changed with pH. This change in interfacial tension may be one factor underlying the protein preference for the interface at pH 3. Moreover, our results indicated that specific interactions may occur between microgels and HPMC at pH 3. Addition of SDS at 2 mM disrupted interaction between microgels and the HPMC phase, leading to microgel aggregation in the dextran phase through neutralization of the positively charged microgel surfaces as well as competing with HPMC for hydrophobic interactions. The microgels' preference for the interface at pH 3 was driven by electrostatic and hydrophobic force, whereas hydrophobic force predominated the interaction.

4. Chapter IV: Study on β-Lactoglobulin Microgels Adsorption onto A Hydrophobic Solid Surface by QCM-D

Adapted from Zhang J.L., Mei L., Chen N.N., Yuan Y., Zeng Q.Z., Wang Q, 2020. Study on β-lactoglobulin microgels adsorption onto a hydrophobic solid surface by QCM-D. *Food Hydrocolloids*, 98, 105320

4.1 Abstract

Microgel particles formed from β-lactoglobulin (Blg) are able to stabilize Pickering emulsions, yet their interfacial properties have not been fully characterized. In this study, quartz crystal microbalance with dissipation (QCM-D) was employed to investigate adsorption behavior of Blg microgels on a hydrophobic solid surface. The QCM-D results showed that adsorption efficiency of the microgels was strongly dependent on the particle charge and the ionic strength of the aqueous phase. The adsorption of weakly charged Blg microgels (pH 5.6) was characterized by highly covered particles, producing a relatively rigid monolayer at the interface. Significantly fewer amount of the microgels was adsorbed when they were strongly charged (pH 3.2 and 7.4) with surface being covered by discrete particles. Those estimations were supported by the direct visualization of sensor surfaces by atomic force microscopy (AFM). Addition of salt effectively screened the electrostatic repulsion between microgel particles, which resulted in a more densely packed layer. QCM-D showed the ability to characterize the microgels interfacial properties and viscoelasticity of absorbed layer on solid surface, which may be used

to predict microgels' interfacial behavior at oil-water interface and provide insights in their stabilization effect in Pickering emulsions.

Key words: QCM-D, Microgel, Pickering emulsion, β-Lactoglobulin

4.2 Introduction

Emulsions are widely used in many different fields including but not limited to pharmaceutics, cosmetics, and food industry. It is commonly known that emulsions can be stabilized by small molecular surfactants through reduction of interfacial tension or amphiphilic macromolecules (e.g. proteins and polysaccharides) via formation of the steric elastic film in addition to the reduction of interfacial tension. Dispersed colloidal particles, which accumulate at the interface between two immiscible liquids (typically denoted as oil and water phases), were discovered to be able to stabilize emulsions[14], and this kind of emulsion is recognized as "Pickering emulsion".

Theories that demonstrate the mechanism of stabilization in Pickering emulsions have been proposed. The commonly accepted one considers that colloidal particles are adsorbed at the oil-water interface to form a particle monolayer acting as a rigid film and providing a mechanical barrier to coalescence[91, 92]. Once a particle with radius r is attached to the oil-water interface, the free energy of spontaneous desorption, ΔG_d, can be estimated through the following equation:

$$\Delta G_d = \pi r^2 \gamma_{OW} (1 - |cos\theta|)^2$$

Where γ_{OW} is the oil-water interfacial tension, and θ is the three-phase contact angle of the particle between the solid and two liquids. Although the particle-surface binding energy is influenced somewhat by the compositions of the oil and aqueous

phases, the most important controlling factor is particle size[15]. It has been confirmed that even for small nanoparticles (r ~ 5-10 nm), as long as the contact angle is not too far away from 90°, the process of particle adsorption at the oil-water interface is essentially irreversible ($\Delta G_d \gg 10\ kT$)[15]. This characteristic associated with the ability of particles to form rigid films that protects the droplets from coalescence is critical for forming a highly stabilized Pickering emulsion. Research into rigid particles composed of compounds such as silica, clay, and metal oxides as Pickering emulsion stabilizer has been well studied and recently reviewed [93-95]. However, growing attention has been directed toward the use of deformable biopolymer-based particles, including microgels derived from protein, which usually have low toxicity as well as great biodegradability and biocompatibility for usage in food systems.

Beta-lactoglobulin (Blg) is the most abundant whey protein in cow's milk, accounting for about 58% of whey and 10% of total milk protein. Consisting of 162 amino acids in its sequence, Blg exhibits an average molecular weight of 18 kDa and an isoelectric point (pI) of pH 5.1-5.2. On heating dilute Blg solutions, at temperatures up to 85ºC under mildly acidic conditions (pH 5.8-6.2), the protein has been found to produce stable microgel particles of 100-300 nm in size[80, 96]. The individual microgel particle (simply called "microgel" for short) consists of a cross-linked network of polymer molecules[8]. In fact, synthetic microgels, have been well studied for stabilization of Pickering emulsions[97]. Recent studies have shown that biopolymer microgels, especially whey protein based microgels, were able to stabilize oil-in-water emulsions[13, 98], as well as water-in-water emulsions[21]. However, there is very limited information on the interfacial behaviors based on those biopolymer microgels.

In a Pickering emulsion system, the contact angle is a parameter usually used to determine particle interfacial wettability on the oil-water interface, but for the microgel particle which is deformable and porous, the contact angle concept is ill-defined and inappropriate[17]. Along with widely acclaimed dynamic light scattering (DLS) or AFM, the nano-scaled and deformable microgels need a more precise measurement for the interfacial property. Quartz crystal microbalance with dissipation monitoring (QCM-D) is a technology that enables real time measurements of biological materials adsorption and/or interactions on various surfaces. Relied on a voltage being applied to a quartz crystal causing it to oscillate at a specific frequency, QCM-D is able to characterize two individual properties e.g. adsorbed mass by changes in frequency (Δf) of the quartz crystal and structural (viscoelastic) properties of adsorbed layers provided by the energy dissipation parameter (ΔD). Also, by monitoring both Δf and ΔD it is possible to quantify and separate the viscoelastic variables relating to the shear viscosity and storage modulus of the adsorbed biological materials[26]. QCM-D has been shown to be a powerful tool for its ability to monitor the adsorption of microgel particles to gold surface, their subsequent swelling and collapse due to changing on system pH, and uptake of other functional particles by the microgels[27-29]. Therefore, we proposed to use QCM-D to study the interfacial performance of microgels on a model hydrophobic surface, which might represent the oil-water interface, so that the adsorption of microgels is characterized, not only by a single point (or line) of contact, but rather by a dynamic polymer profile. Simultaneously, the viscoelastic properties of the adsorbed film of microgels are evaluated by the combination of the two parameters (Δf and ΔD) from QCM-D.

The objective of this work was to evaluate the interfacial properties of Blg microgels by QCM-D under different pH and ionic strength conditions. The gold coated quartz crystals used in the QCM-D experiments were modified using an alkane thiol molecule i.e. $(CH_3CH_2)_{14}CH_2SH$ to mimic the oil-water interface in real emulsions. The thiol group in this molecule was immobilized onto gold surfaces through a covalent bond[31], therefore a hydrophobic self-assembled monolayer (SAM) containing CH_3 terminated groups on the quartz crystal surface was formed. This model surface has been used to study whey protein and lactoferrin interaction at oil-water interface by QCM-D[30]. Particle size and electrophoretic mobility of microgels were characterized using light scattering techniques and conformational structure of microgels was investigated by Fourier-transform infrared spectroscopy (FTIR). Atomic force microscopy (AFM) was used to obtain the morphology/topography of microgels as a complementary technique to QCM-D providing direct information on particle-surface coverage.

4.3 Materials and Methods

4.3.1 Materials

1-hexadecanethiol (95% GC) was purchased from Sigma Aldrich (St. Louis, MO, USA); Ammonia (ACS 28.0-30.0%) was purchased from Alfa Aesar (Heysham, England); Hydrogen peroxide (ACS 30%) was purchased from Fisher Scientific; Hydrochloric Acid (HCl, 36.5-38%), sodium hydroxide, sodium phosphate monobasic monohydrate and sodium phosphate dibasic heptahydrate were of ACS grade and purchased from VWR (Radnor, PA, USA). Citric acid (ACS) was purchased from Amresco (Solon, OH, USA).

4.3.2 Preparation of protein microgel particles

Whey protein isolate was kindly donated by Davisco Foods International (Le Sueur, MN, USA) and further extracted for Blg was based on an established procedure [62]. Extracted Blg has initial pH of ~6.5 and high similarity compared to commercial pure Blg powder according to preliminary tests on FTIR and SDS-PAGE. Blg solution was prepared by dispersing the Blg powder in deionized water under gentle magnetic stirring at room temperature for at least 2 h. Solutions were stored overnight at 4±1ºC to allow complete protein hydration. Then, Blg solution was filtered through a 0.22 μm Acrodisc syringe filter membrane (Pall Co., Newquay, UK) to remove impurity. The concentration of Blg solution was checked by UV/Vis spectrophotometer (Beckman Coulter, DU-730, Fullerton, CA) at 278 nm, using an extinction coefficient of 0.96 $Lg^{-1}cm^{-1}$[199]. The final concentration of Blg stock solution was 2 wt%.

The 2 wt% Blg solution was acidified to pH 5.95 using 0.1 M HCl solution. Microgels were formed by submerging scintillation vial filled with 10 mL Blg solution in a hot-water bath at 80°C for 60 min directly followed by submersion in an ice-water bath for 20 min. To isolate the microgels from free protein and small aggregates, samples were centrifuged at 50000 g for 30 min. The supernatant was removed and replaced with DI water, or citrate-phosphate buffer (CP buffer, pH3-7, 20 mM), and the microgels were re-suspended by vortexing for 1-3 mins. Small amount of large aggregates formed during centrifugation were not re-suspended, as this would have a negative impact on particle size and polydispersity. Samples were

either analyzed on the same day or stored overnight at 4°C and warmed to 25°C prior to characterization.

After heating, the protein solutions were turbid, while the turbidity decreased to negligible with mixture of 0.5 M NaOH at ratio of 1:10 (microgels to NaOH). Protein content of the isolated microgels sample was measured afterwards by a spectrophotometer at 278 nm using an extinction coefficient of 0.96 $Lg^{-1}cm^{-1}$ [99].

4.3.3 Characterization of Blg microgel particles

Hydrodynamic diameters of microgels samples were measured by a dynamic light scattering (DLS) instrument (BI-200SM, Brookhaven Instruments Corp., Holtsville, NY), which was equipped with a 35 mW HeNe laser beam at a wavelength of 637 nm. All DLS measurements were performed at 25 °C with triplicates.

The electrophoretic mobility of microgels samples was determined between pH 3.2 to 7.4 using a Zetasizer Nano ZS (Malvern Instruments, Worcestershire, UK). Each sample was measured three times in disposable folded capillary cells ((DTS 1070, Malvern Instruments Ltd, Worcestershire, UK)) at a protein concentration of 0.1 wt%, and at least 32 runs were performed per measurement. The values of the electrophoretic mobility were not converted to a zeta-potential. The usual hard-sphere model is not applicable for microgels, because they are porous, soft, and swollen by the solvent[100].

4.3.4 Quartz crystal microbalance with dissipation (QCM-D) measurements

Preparation of hydrophobic gold surfaces

QCM-D crystals, AT-cut quartz crystals with a fundamental resonance frequency of ~4.95 MHz, were purchased from Q-Sense (Biolin Scientific, Gothenburg, Sweden) with bare gold electrodes (QSX 301). The gold sensors were cleaned with "Piranha" solution (a mixture of 5:1:1 ratio of deionized (DI) water, 25% ammonia and 30% hydrogen peroxide) at 75°C for 10 min and rinsed with hot DI water. The sensors were dried with nitrogen gas.

After cleaning and drying, the gold surface of the sensors was rendered hydrophobic by introducing a self-assembled monolayer (SAM) according to a previous report[30]. Briefly, the cleaned gold surface was immersed overnight in a pure hexadecanethiol to form SAM. After overnight treatment, gold sensors were transferred into ethanol, ultra-sonicated for 5 min and then rinsed thoroughly with ethanol and DI water to remove unabsorbed hexadecanethiol.

Contact angle measurement to confirm the formation of hydrophobic surface was performed by the sessile drop method using an Attension Theta optical tensiometer (Biolin Scientific, Linthicum Heights, MD, USA). Placement of drop was controlled by a C201 automatic liquid dispenser (Biolin Scientific). An aliquot of 20 μL pure DI water was dropped onto either modified or bare gold surfaces. Data collection (60 fps) was manually triggered by an initial contact of a liquid drop with a solid surface. Captured images were automatically analyzed by an OneAttension software, Version 1.8 (Biolin Scientific) to identify the baseline and calculate contact angles.

QCM-D experiment

Protein microgels adsorption on the SAM hydrophobic surfaces was carried out using a QCM-D system (Q-Sense E1 system, Q-Sense, Biolin Scientific, Gothenburg, Sweden) equipped with a temperature controlled chamber and a peristaltic pump (ISMATEC® ISM Single Channel Dispenser, IDEX Health & Science, Germany). Each QCM-D experiment started with pre-equilibration with DI water or buffer solution for at least 15 min to obtain a signal baseline. The test solutions were then fed to the SAM hydrophobic QCM-D sensors at a flow rate of 0.08 mL/ min. All experiments were measured at 25 ± 1°C. At least three measurements were performed for each sample.

Data analysis of QCM-D results

QCM is a sensitive mass sensor which measures a mass per unit area by measuring the change in frequency of a quartz crystal resonator[27]. The Sauerbrey equation describes the relation between frequency shift and coupled mass to the QCM crystal, and is given by

$$\Delta m = -\frac{C}{n}\Delta f$$

Where n is the number of the resonance overtone and C (=17.7 ng cm^{-2} Hz^{-1} for the AT-cut crystal used) is the mass sensitivity constant. Note that the frequency shift obtained from QCM-D (Q-Sense) is already normalized, i.e., divided by the overtone number (n). In the present study, all results were from the frequency shift in the third overtone (n=3), since under the third overtone, the resonator is less affected by mechanical forces associated with mounting the resonator. The Sauerbrey equation is valid under a number of assumptions, including that the

adsorbed film must be thin, rigid, and couple perfectly to the quartz crystal. In the case of microgels adsorption, the calculated adsorbed mass is expected to be higher than that actually adsorbed, because the mass calculated by Sauerbrey equation includes a certain amount of water.

The dissipation value is a measurement of the energy loss in the oscillating quartz crystal system and defined by the following equation:

$$D = \frac{E_{dissipated}}{2\pi E_{stored}}$$

The shift in dissipation is due to changes in the damping of the quartz crystal during measurements, which occurs if viscoelastic properties of an attached layer changes[101]. A soft material attached to the sensor crystal usually has more deformation during the oscillation, resulting in a higher dissipation value, whereas a rigid material will give a lower dissipation value[27].

4.3.5 Atomic force microscopy (AFM)

Upon completion of the QCM-D measurement, the sensor crystals were removed, and air-dried under hood overnight. Prior to studying in the AFM, the quartz crystals were glued onto metal disks and attached to a magnetic sample holder, located on top of the scanner tube. AFM imaging was carried out using a Cypher ES Enviromental AFM (Asylum Research, Santa Barbara, CA) in an AC Air mode. The Asylum Research HQ-300-Au probe was used, which has 4-sided silicon tip on rectangular cantilevers with Ti/Au reflex coating. The probe has nominal spring constants of 40 N/m and driving frequencies of 300 kHz. The images were collected with a scan size of 5 μm at a scan-rate of 1 Hz. Standard imaging procedures and

setting parameters were used and images of height and phase were recorded. Height images and phase images from AFM data were produced by Argyle Light software and surface coverage analysis were obtained with Gwyddion software using the grain threshold marking and grain statistics function.

4.3.6 Fourier-transform infrared spectroscopy (FTIR)

FTIR studies were conducted to monitor the secondary structural changes of Blg microgels under different pH conditions. The lyophilized samples (3 to 5 mg) were mounted onto a Jasco FT/IR 4100 spectrometer (Jasco Inc., Easton, MD, USA) coupled with Attenuated total reflection (ATR). The infrared transmittance was acquired at the wavenumbers from 1000 to 4000 cm^{-1} with a resolution of 2 cm^{-1}. Sixty-four repeated scans were undertaken for each sample. The spectra were averaged, smoothed, corrected for their baselines and converted to absorbance with a Spectra Manager software (Jasco Inc., Easton, MD, USA).

For obtaining information of secondary structures, the IR spectra were further subjected to Fourier self-deconvolution (FSD) using the OMNIC software (Thermo Scientific, West Palm Beach, FL, USA). A bandwidth at half height of 23 cm^{-1} and an enhance factor (K value) of 2.7 were adopted over the wavenumbers ranging from 2000 to 1300 cm^{-1}, according to a previous study[65]. The FSD spectra were then curve fitted assuming a Gaussian band profile. The resolved peaks were validated only when they were found on the inverted secondary derivative (ISD) spectra obtained over the same wavenumber range. Peak assignment was carried out on the FSD spectra, and the content of each secondary structure was expressed as the percentage of area for the corresponding peak.

4.4 Results

4.4.1 Characterization of microgels formation

The formation of microgels from thermal treatment of Blg by controlled aggregation process was previously established in a literature[96], which claimed that when the pH was set within 5.75 and 6.00, stable suspensions of spherical protein microgels can be formed by heating Blg at concentrations ranging from 10 and 50 g/L. In order to obtain acceptable microgels particle size and concentration, the condition of pH 5.95 and Blg concentration of 20 g/L were selected.

About 36% of the initial proteins were converted into Blg microgels (BM) while using DI water to resuspend microgels from centrifugation at 50000 g for 30 min. The yield rate was relatively low comparing to other study[96]. This maybe because the large protein aggregation as well as undenatured native protein were eliminated from this mixture during the centrifugation step. The BM exhibited an average hydrodynamic radius of 138 nm and a polydispersity index of 0.071. The formation of the microgels causes an increase of the pH (data not shown), which in turn increases the electrostatic repulsion between the microgels. The spontaneous increase of the pH during microgels formation is a necessary condition to obtain stable suspensions[96].

We investigated the colloidal stability of BM dispersion at various pH levels (adjusted between 3.2 and 7.4 by using CP buffer to resuspend microgels from centrifugation). As can be seen in Fig.4.1, the size change of the microgels was found to be related to the aqueous pH value, and this behavior was correlated with

the variation of the surface charge of the particles. Ohshima[102] has derived an equation describing the electrophoretic mobility of colloid particles, but a fitting of microgel mobility with the model is complicated and not the purpose of this study. Therefore, figures showing ζ-potential of the microgels derived from the Smoluchowski model were also provided in Fig.4.2, even though the hypotheses behind the Smoluchowski equation aren't fully satisfied for microgel particles.

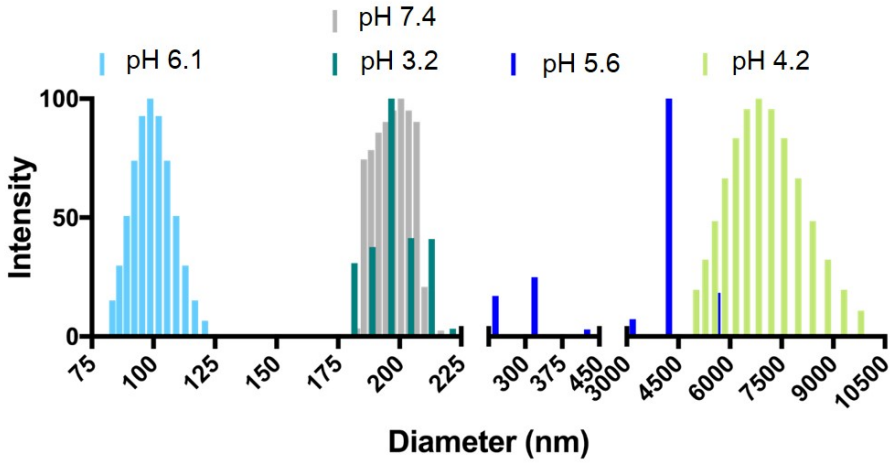

Figure 4.1 Particle size distribution of Blg microgels at various pH

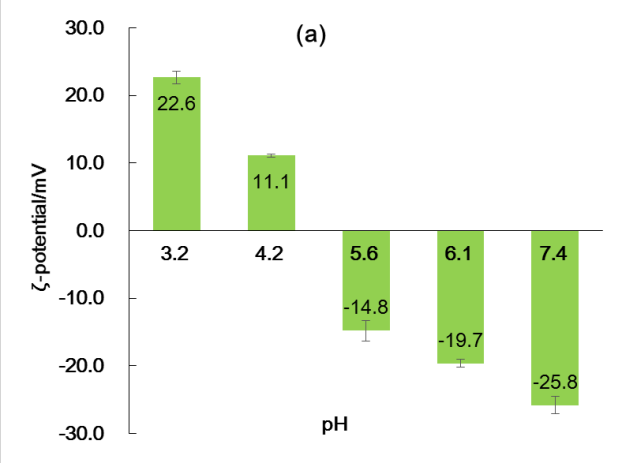

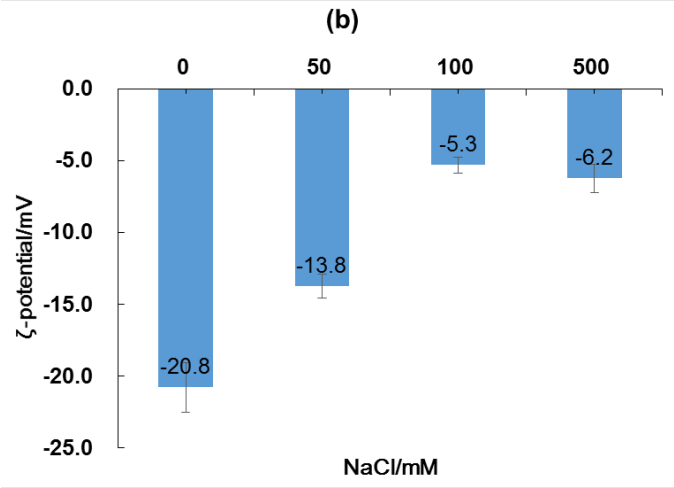

Figure 4.2 (a) Zeta-potential of Blg microgels at various pH and (b) ionic strength effect on zeta-potential of Blg microgels in pH7.0 20 mM CPBuffer

The microgel particles displayed a polyampholytic character with an isoelectric point (pI) between 4.2 and 5.6, where their overall charge was zero. The microgel particles were negatively or positively charged, at two pH domains above or below range of 4.2-5.6. As a single particle, microgel should have smallest hydrodynamic size at its pI[12], however, the microgel particles exhibited large particle size distribution at pH 4.2 and 5.6. This is because the microgel particles were unstable and precipitated when their surface charges were low. The surface charges of microgels were related to the balance between the dissociation of the carboxylic and amino groups of the microgels consisting of Blg proteins. At pH of 4.2-5.6, the electrostatic repulsion between microgel particles were too low to counterbalance the attractive interactions that lead to aggregation and ultimately sedimentation.

Since the stability of microgels dispersion was dependent on the electrostatic force, the sodium contents is expected to play a role on the colloid stability. The decreasing trend of electrophoretic mobility was observed in the presence of NaCl

(Fig.4.2b) due to a screening effect of charge caused by Na^+ and Cl^- ions. However, the colloidal stability was retained with more addition of NaCl, no sedimentation was observed for BM at pH 7.0 in the presence of 500 mM NaCl.

To be noted, when the pH value of the solvent increased from 6.1 to 7.4, the hydrodynamic diameter of the particles was also increased, which was thought to be caused by swelling of individual microgel. It was reported that whey proteins or Blg microgels exhibited swelling ability when increasing their net charges [12]. Because the microgels are soft and poorly cross-linked particles, their internal structure is flexible enough to respond to changes in the solvent pH. Therefore, the large internal charge density would cause the protein strands or chains repel from each other within the microgels, leading to the swelling.

4.4.2 Adsorption of Blg microgels on hydrophobic surfaces

In order to study the interfacial performance of microgels in the Pickering emulsion, adsorption dynamic of BM on a hydrophobic SAM surface was investigated by the QCM-D. The hydrophobic SAM containing CH_3 terminated groups has been used to mimic the interface in oil-in-water emulsion[30]. The contact angle (Fig.4.3) of DI water on the SAM modified surface was confirmed at 105°, while on the unmodified gold surface it was 52°, indicating a hydrophobic layer was successfully formed.

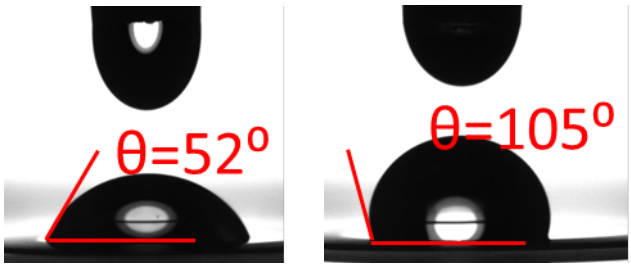

Figure 4.3 Contact angles of gold surface (left) and modified hydrophobic surface (right)

The effect of BM concentration on adsorption process was investigated by the QCM-D firstly. The typical shift in frequency and dissipation from QCM-D measurement of BM at various concentrations (0.2, 0.75, and 1.5%) on SAM modified gold crystal are shown in Fig.4. When a stable baseline was obtained, fresh BM (directly after centrifugation and being re-suspended with DI water, pH 6) was introduced and left to adsorb for 1 h, the surface was then rinsed with DI water for another 1 h.

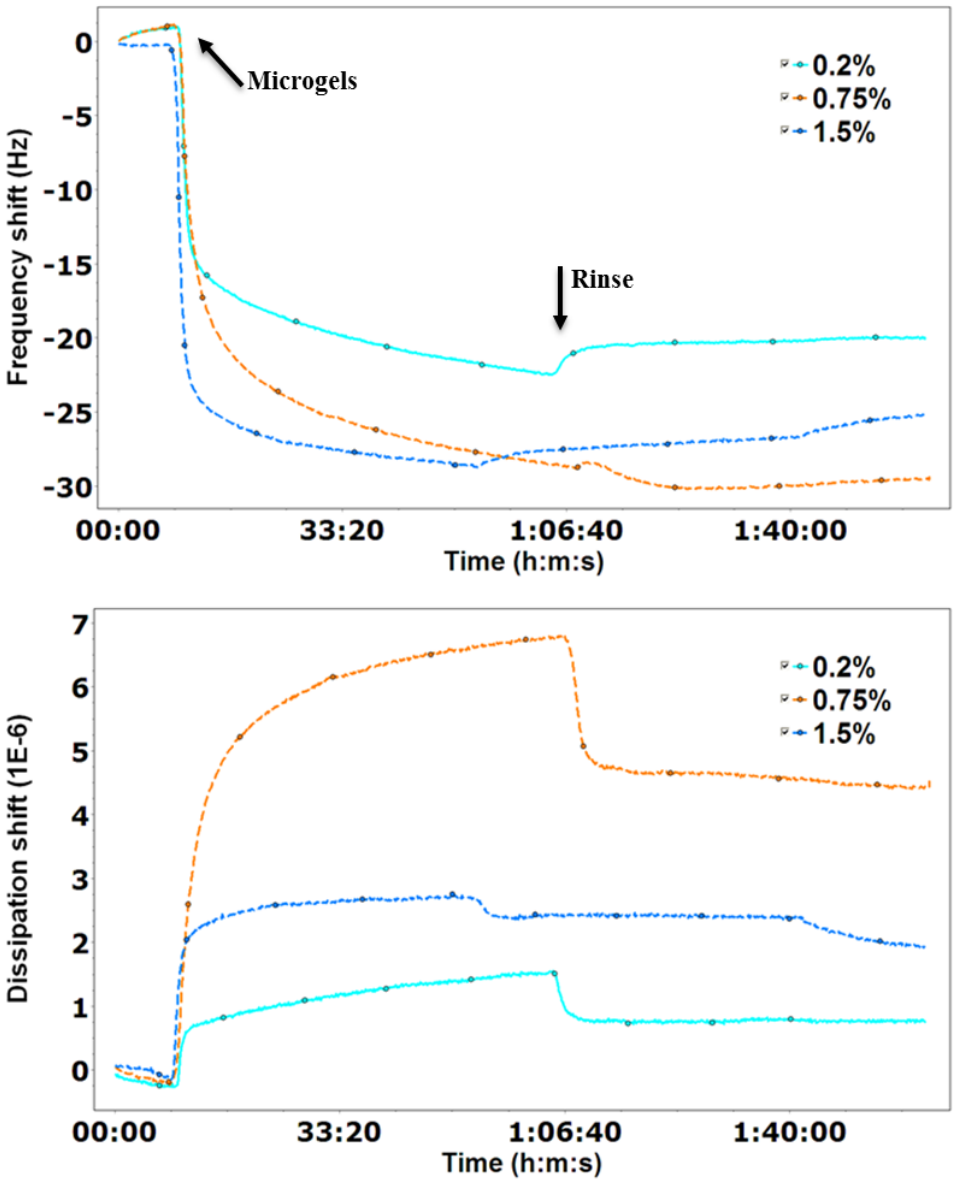

Figure 4.4 Shift in frequency and dissipation from QCM-D measurement of Blg microgels at various concentrations (0.2, 0.75, and 1.5%). The data is of the third overtone.

The magnitudes of Δf increased with BM concentration from 0.2 to 0.75%. At concentration of 1.5%, the Δf reached to the same magnitude as 0.75% but more rapidly, indicating that the adsorption of BM reached a saturation at the concentration of 0.75%. Murphy RW *et al.*[25] has proposed that the adsorption of

protein-based microgels should be considered as a diffusion-limited process, and the saturation occurred more rapidly at a higher concentration. Interestingly, a relatively high dissipation signal was observed from microgels adsorption at concentration of 0.75%, indicating that the microgels absorbed layer is softer and having more water than that of 1.5%.

The energy dissipation decreased during rinsing steps under all concentrations. Removal of loosely bond microgels during rinsing can be used to explain the decrease of dissipation, because the ad-layer become more densely packed. It is true in the case of 0.2 and 1.5% microgels adsorption since their absorbed mass amount decreased simultaneously during rinsing. On the contrary, when the dissipation signal of 0.75% microgels was rapidly dropped upon rinsing, the magnitude of Δf kept stable or even slightly increased. The decreased dissipation was thought to be related to the surface rearrangement of adsorbed microgels at relatively low concentration. When surface is not fully absorbed by soft microgels, they will undergo conformational change[25]. A more rigid layer was formed evidenced by the changes in the dissipation signal, while minor changes in frequency indicating very little desorption of this microgels layer. Since we are interested in knowing the interfacial behavior of BM as well as properties of the absorbed layer, BM at the concentration of 0.75% with significant changes of frequency and dissipation signals was chosen for later investigation.

4.4.3 Effects of pH

The adsorption of BM was studied for pH values of 3.2, 5.6 and 7.4, representatives of BM carrying positive (22.63 mV at pH 3.2), low negative (-14.80 mV at pH 5.6)

and negative (-25.83 mV at pH 7.4) surface charge, respectively. As shown in Fig.4.5, the frequency shift of microgels in those pH levels differed significantly, indicating that the amount of BM adsorbed on the hydrophobic surface is strongly dependent on pH values of the solution. The highest frequency shift was found for BM solution at pH 5.6, while that of pH 3.2 was about 2 times lower, and the lowest Δf was observed from solution at pH 7.4, only having 1/6 of that at pH 5.6. Maximum adsorption of BM on hydrophobic surface was found at pH 5.6, where BM carried least net surface charge. This corresponded well with the literature on the adsorption of proteins on surfaces, which in general exhibited pH dependency with a higher adsorption rate near its pI [30, 101]. When microgel particles carried less surface charge, the hydrophobicity of the particles were enhanced, which favored their interaction on the hydrophobic surface.

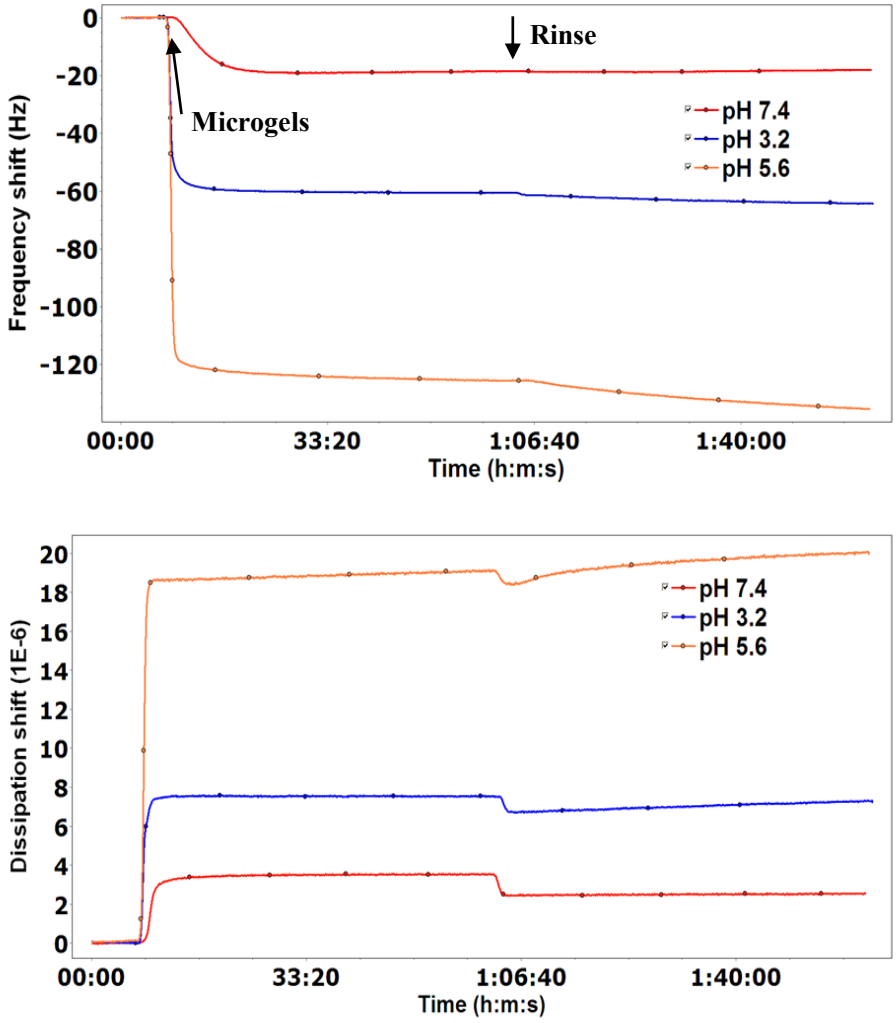

Figure 4.5 Shift in frequency and dissipation from QCM-D measurement of Blg microgels at pH 3.2, 5.5 and 7.4. The data is of the third overtone.

Dissipation shift (ΔD) shows the similar trend as that of the frequency shift for BM under different pH values. Based on Mivehi L. *et al.*[103], the rigid film assumption for Sauerbrey equation is only valid when dissipation remains below 1×10^{-6}. Therefore, all of the three protein microgels ad-layers were not considered as rigid films, but viscoelastic ones. However, unlike the case in the different concentrations of BM, the magnitudes of Δf changed dramatically at different pH of BM solution. Therefore, an alternative presentation of the QCM-D data, namely $\Delta D/\Delta f$ plot, was

introduced below to better explain the interfacial behavior of microgels. In this plot, it is possible to directly compare the ratio between ΔD and Δf, that is, the induced energy dissipation per coupled unit mass. By comparing the ratio of $\Delta D/\Delta f$, it is able to explain the influence of the microgels adsorption on the damping of the crystals resonance and thus infer the viscoelastic properties of the adsorbed layer[104]. A small $\Delta D/\Delta f$ value indicates a mass addition without significant dissipation increase, which is a characteristic of a rigid layer. In contrast, a large $\Delta D/\Delta f$ value indicates a soft viscoelastic layer.

As shown in Fig.4.6, there is a clear linear relationship between ΔD and Δf during adsorption of the BM at pH 7.4, but trends are less clear in conditions at pH 3.2 and 5.6. Nonetheless, the slope of $\Delta D/\Delta f$ for the BM at pH 7.4 is much steeper than that at pH 3.2 or 5.6, indicating the ad-layer formed under pH 7.4 is softer. It should be noted that when pH value of the solvent increased from 5.6 to 7.4, there is a swelling effect of single microgel, as we discussed in section 3.1. The adsorption of swollen microgels that entrapped more water in its internal structure resulted in the softer viscoelastic layer. Another possible reason is that the BM were loosely packed on the surface under pH 7.4. This could be evidenced by the more significant effect of buffer rinsing step on the change of $\Delta D/\Delta f$ gradients for pH7.4 than others.

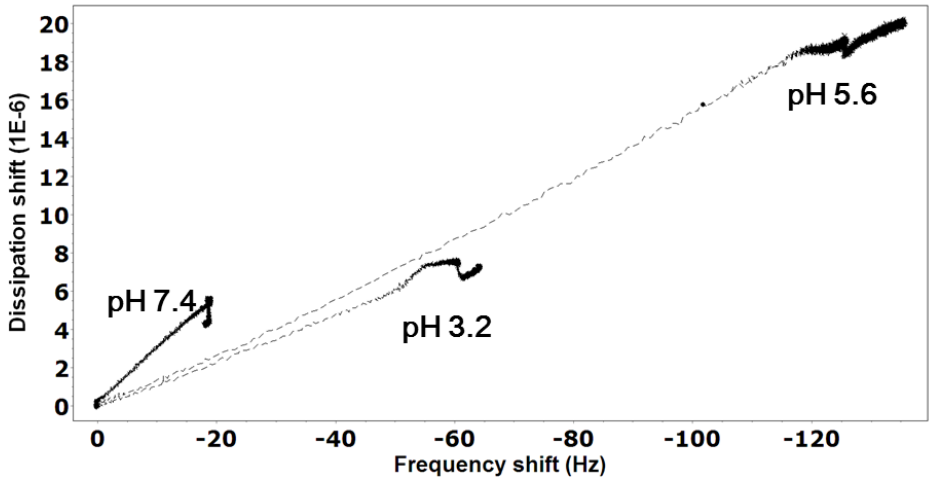

Figure 4.6 Changes of dissipation shift versus frequency shift (*ΔD/Δf* plot) during the adsorption of Blg microgels at pH 3.2, 5.6 and 7.4. The data is of the third overtone.

Of particular interest is that the $\Delta D/\Delta f$ gradients are almost identical from the adsorption at pH 3.2 and 5.6, which indicated that the resulted microgels layers might have similar viscoelastic properties. It brings out another factor, conformational structure of the BM under different conditions, which may influence the microgel adsorption onto the hydrophobic surface, and it will be discussed further in AFM and FTIR sections.

4.4.4 Effect of ionic strength

The adsorbing surface, which incubated in methyl-terminated thiol (hexadecanethiol), is a well-defined, electrically inert hydrophobic surface. The electrostatic interactions between the surface and the substrates were expected to be minimum, and the adsorption should be relatively unaffected by the ionic strength of the solution. On the other hand, the strong influence of NaCl concentration on BM adsorption was obvious, as shown in Fig.4.7. The saturation shifts of *f* and *D*

increased rapidly with increasing ionic strength in the range of 50-100 mM and was then independent of ionic strength at >100 mM. The microgels at pH 7.0 was negatively charged, and at low NaCl concentration (0-50 mM) these charges were poorly screened. When adsorbed onto the surface, electrostatic repulsion effectively repelled the BM from each other and became widely spaced on the surface. As the NaCl concentration increased from 50 to 100 mM, screening became successively more effective, and BM might move to closer distances on the surface, resulted in the increased absorption of BM. It was reported that after a critical salt concentration, screening effect eventually resulted in overall dominance of attractive forces between protein, causing protein clustering on solution and adsorbing surface[105]. In our case, the critical concentration is around 100 mM.

$\Delta D/\Delta f$ plot (Fig.4.7c) also shows that at low NaCl concentration, the BM adsorption induced more energy dissipation per coupled unit mass. In other word, with increased ionic strength, BM formed a more rigid layer on the hydrophobic surface. It has been previously demonstrated with the QCM-D technique, by controlling the packing density of ferritin molecules with the salt concentration, a more densely packed protein layer led to a lower $\Delta D/\Delta f$ value[105].

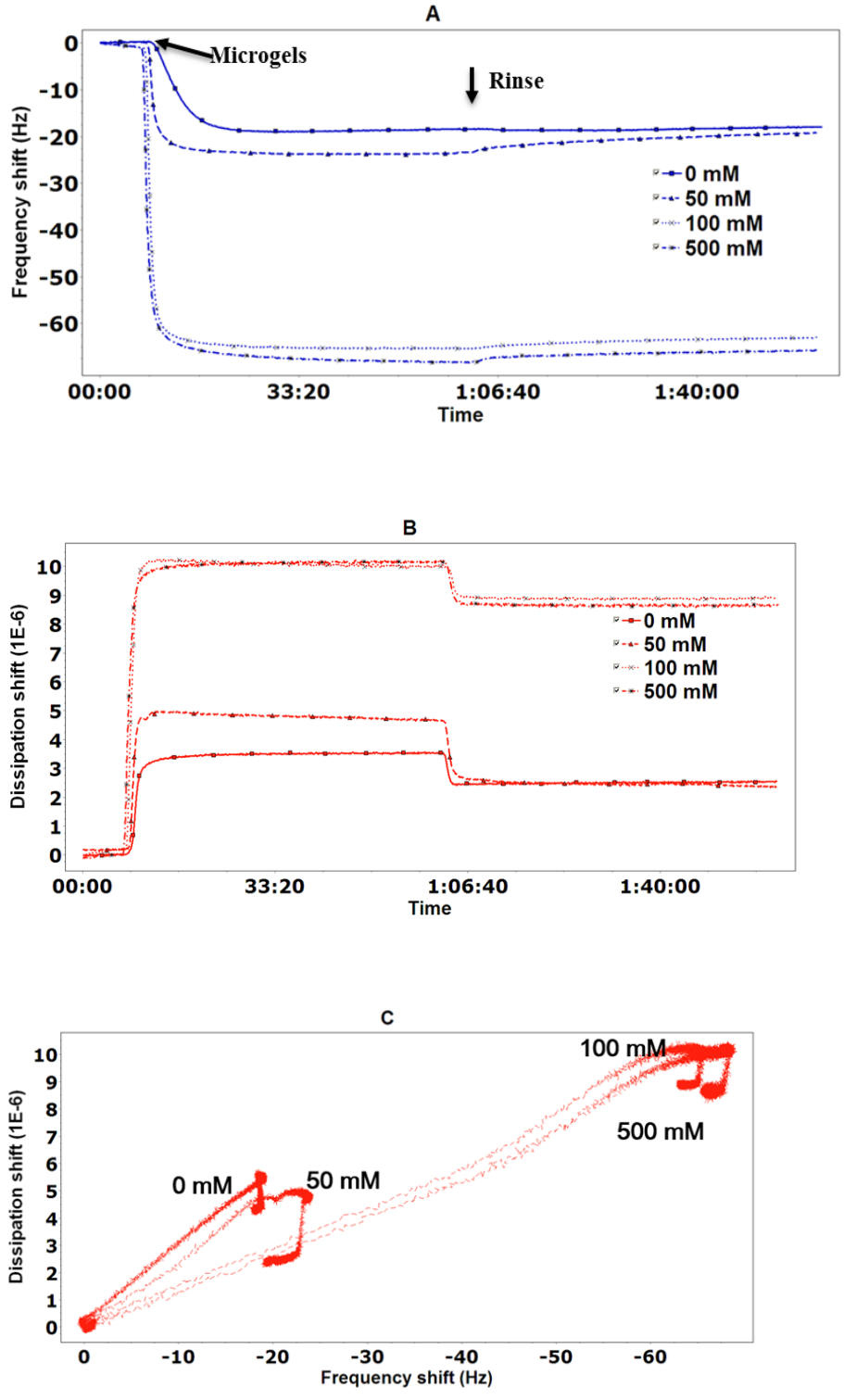

Figure 4.7 Frequency shifts (A) and dissipation shifts (B) vs time for Blg microgels adsorption on hydrophobic surface, in a 20 mM CP buffer at pH 7.0 with 0, 50, 100, and 500 mM NaCl addition. (C) $\Delta D/\Delta f$ plot using the data of (A, B). The data is of the third overtone.

4.4.5 Morphology microgels upon adsorption

Combining *in situ* QCM-D with AFM[27, 101] has enabled the examination of the QCM-D response as a function of independently measured surface morphology and coverage of absorbing substrate. The observation from AFM is essential, because it decides how to quantitatively interpret QCM-D data, that is usually dependent on the type of adsorbed layer as well as dissipative response (D)[106]. The hydrophobic self-assembled monolayer was imaged as a homogenous thin layer on the top of the gold surface of quartz crystal, and its height was around 20-30 nm (Fig.4.8). While as shown in Fig.4.9 and Fig.4.10, the BM adsorbed as monolayers of discrete particles on the surface in all conditions, rather than forming laterally homogeneous films as generally assumed in the QCM-D studies, therefore using viscoelastic model to interpret frequency and dissipation shift is not applicable in the present case.

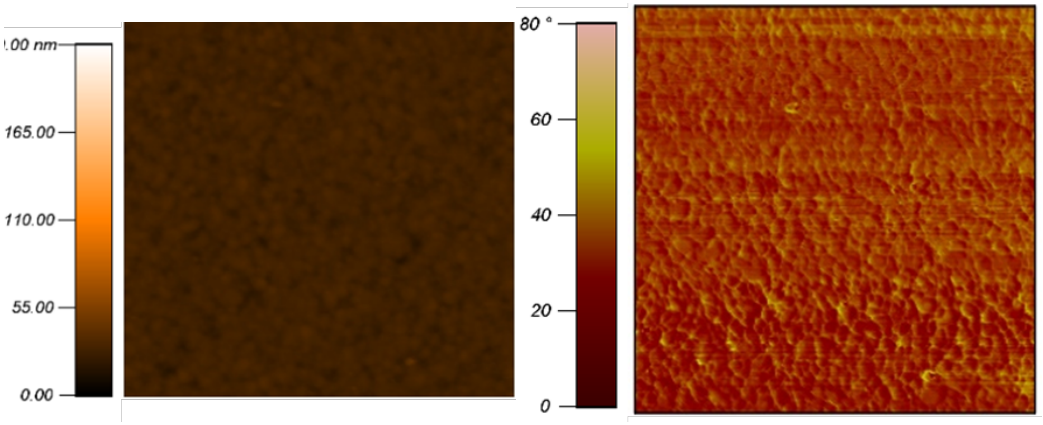

Figure 4.8 Height (left) and phase (right) AFM images of self-assemble monolayer on QCM-D quartz crystal. The images are 2×2 μm^2.

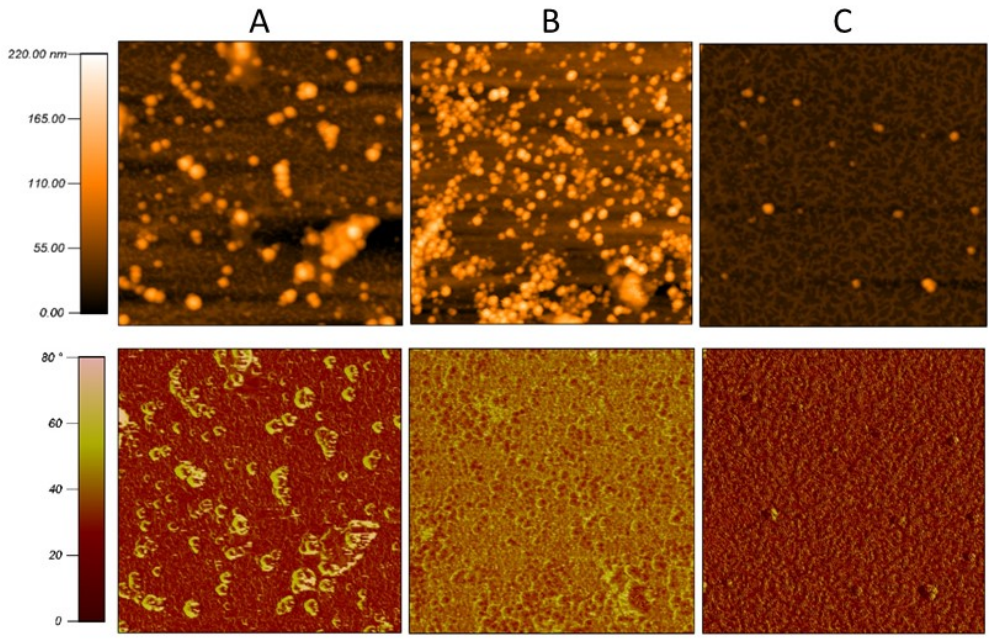

Figure 4.9 Height (top row) and phase (bottom row) AFM images of Blg microgels adorption on hydrophobic surface at A) pH 3.2, B) pH 5.6 and C) pH 7.4. The images are 5×5 μm^2.

The surface coverage for pH 5.6 and 3.2 were 35.9% and 13%, whereas that for BM of pH 7.4 was merely 1.7%, and it agreed well with the results on frequency shift from QCM-D (Fig. 4.9). Microgels adsorption under different ionic strength show similar trend as QCM-D results (Fig.4.10). To be noted, at pH 5.6 and 3.2 and NaCl concentration of 500 mM, the AFM phase images (second row of Fig. 4.9A, 9B, and 10C) shown significantly higher contrast than in other conditions, indicating that the adsorbed microgels layers have higher stiffness.

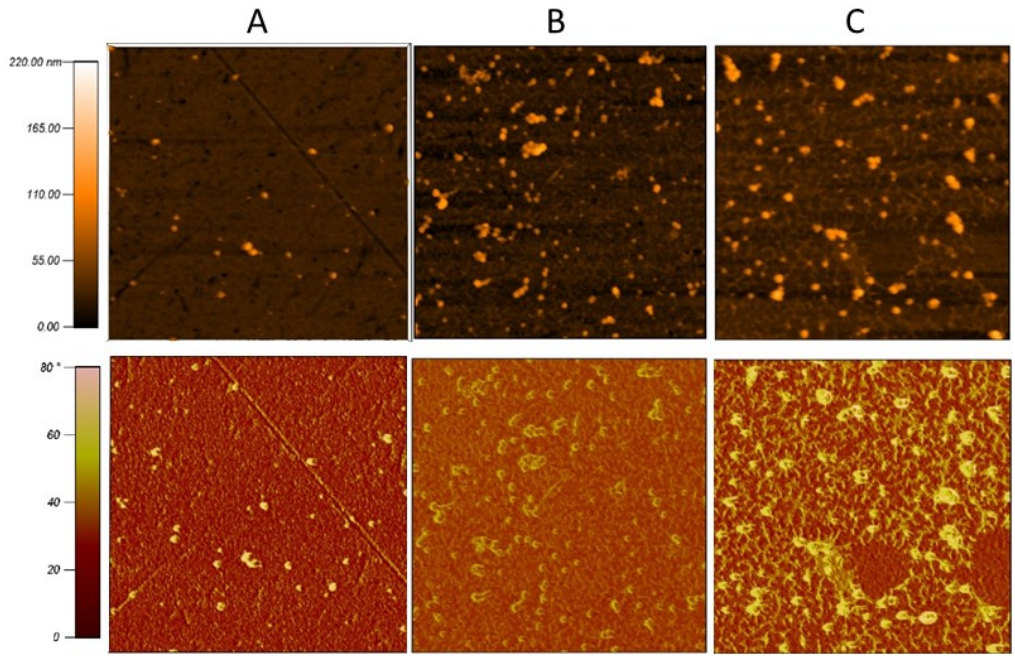

Figure 4.10 Height (top row) and phase (bottom row) AFM images of Blg microgels adorption on hydrophobic surface at pH 7.0 with different ionic strength A) 50 mM, B) 100 mM and C) 500mM. The images are 5×5 μm^2.

4.4.6 Conformational change of microgel under pH

To further investigate the interfacial affinity of BM, conformational changes of BM under different pH levels (i.e. 3.2, 4.2, 5.6, 6.1 and 7.4) were studied by ATR-FTIR. BM particles, after purification by centrifugation, were re-suspended in buffer at different pH levels. The re-suspended microgels dispersions were lyophilized and tested immediately. The spectra profiles of BM did not show significant difference from pH changes (Fig.4.11), except for the peak at 1716 cm^{-1} (i.e. -COOH group) for BM under pH 4.2 and 3.2. Three characteristic peaks of protein were found at 1626-1631 (amide I, C=O stretching), 1531-1536 (amide II, C−N stretching and N−H bending) and 1444-1446 (amide III, C−N stretching, N−H bending) cm^{-1}. These observation were consistent with a previous literature on the native Blg protein[65]. The secondary structural changes of protein, which alter stretching

patterns and consequentially change the IR absorbance of corresponding peaks, exhibited the highest sensitivity on amide I (C=O stretching)[107]. Therefore, the spectra were further processed to FSD and Gaussian curve fitting procedure in the spectra range of 1600-1700 cm^{-1}. Ten peaks were resolved and confirmed for all pH conditions, which were assigned to different secondary structure components according to previous studies both on the Blg and Blg microgels [65, 80]. As shown in Table 4.1, when pH decreased to 3.2, the key spectral features had the highest increase in the bands at 1617, 1624 and 1633 cm^{-1} corresponding to β-sheets, but one characteristic peak of β-sheet at 1693 cm^{-1} was disappeared. The total percentage of secondary structures did not show a trend differed from the tested pH range, but at pH 3.2, the percentage of β-sheet significantly increased. The increased degree of β-sheets at pH 3.2 may favor the microgels adsorption onto hydrophobic surface, because the exposed β-sheets are thought to contribute most to conformational change of proteins when adsorbing at oil-water interface[108]. We believe that microgels at pH 3.2 underwent significant conformational changes when adsorbing on the surface, therefore formed the stiffer ad-layer as indicated by QCM-D and AFM measurements. Further studies are needed to investigate the possible deformation and structural rearrangement of BM at pH 3.2 at the interface, and the findings may be valuable to future application of protein microgels in an acidic environment.

Table 4.1 Secondary structure assignments and area percentage of the amide I wavenumbers in the ATR-FTIR spectra of Blg microgels under different pH.

Peak No.	Wavenumber (cm^{-1})	Band assignments	Area% pH 3.2	4.2	5.6	6.1	7.4
1	1610.3	Side chain	-	-	-	-	-
2	1617.5	β-sheet	19.07	8.69	7.76	10.74	9.81
3	1624.1	β-sheet	21.19	15.69	15.50	14.07	16.56
4	1633.2	β-sheet	17.46	13.49	14.68	15.02	14.04
5	1643.2	Random coil	10.83	11.11	11.32	12.29	12.35
6	1651.3	α-helix	12.66	10.31	10.83	10.56	11.56
7	1660.4	Turns	9.11	10.25	10.27	10.89	10.37
8	1669.4	Turns	5.91	8.96	9.53	8.72	9.19
9	1680.9	Turns	3.78	10.66	10.25	9.07	9.04
10	1693.7	β-sheet	0.00	10.85	9.85	8.62	7.07

	Area% pH 3.2	4.2	5.6	6.1	7.4
Total β-sheet	57.72	48.716	47.797	48.459	47.482
Total turns	18.793	29.87	30.055	28.688	28.604
α-helix	12.661	10.308	10.831	10.561	11.564

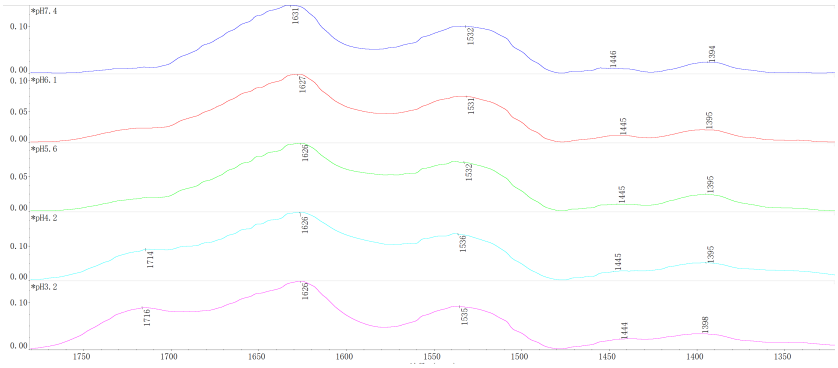

Figure 4.11 FTIR spectra of Blg microgels at pH 3.2, 4.2, 5.6, 6.1 and 7.4

4.5 Discussion

Mechanism of stabilization in Pickering emulsions has been well studied for many years. There are both similarities and differences in relation to Pickering emulsions

stabilization by solid particles and soft microgel particles. Dickinson[8] provided a good review highlighted the special properties of microgels and described studies in the use of microgels for the stabilization of oil-in-water emulsions. Special attributes of microgels including swelling ability, interfacial deformation and structural rearrangement, and inherently surface activity at both oil-water and air-water interfaces, contribute to the mechanistic basis of Pickering emulsion stabilization. The mechanistic interplay between microgels interfacial structure and oil-in-water emulsion stability is concluded by Schmitt and Ravaine[19]. The formation of a tightly packed monolayer of microgels particles mainly contributes to the production of stable dispersed droplets without flocculation. If the particle packing in the microgels layer is loose and heterogeneous, then the microgels layers tend to flocculate by protein particle bridging, but they would not coalesce. However, these mechanistic insights are derived from research on synthetic polymer microgels[97].

It is commonly assumed that the same general principles also apply to microgel particles based on biopolymers. Investigations showed interrelationship among formation parameter, interfacial structure, and emulsion stability. The ability of whey protein microgels to stabilize oil-in-water emulsions over a wide range of pH and ionic strength has been studied with optical microscopy, spectrophotometry and cryogenic scanning electron microscopy (Cryo-SEM) [13]. For conditions where microgel particles were weakly charged (absolute value of ζ-potential <20 mV) or when their charges were screened by salt addition, they stabilized fluid emulsions with relatively large droplets. However, when they were strongly charged, the resulting emulsions were constituted of small and flocculated droplets. The high

resolution of Cryo-SEM system enables the discovery of different packing structures of particles at interface. Recently, the techniques of surface pressure, interfacial rheology and AFM monolayer characterizations have been exploited to study the interfacial behavior of Blg microgels at heptane-water interface[25]. The study focused on the influence of size distribution on the interfacial properties. Small microgels were found to adsorb to and deform at the interface more rapidly than large particles, resulting in interfaces that are more elastic.

In current work, it is clear that the adsorption efficiency of microgels on hydrophobic surface was dependent on the particle charge or the ionic strength of the aqueous phase. Under different pH, BM showed different adsorption affinity and properties of adsorbed layers on hydrophobic surface, as evidenced by QCM-D. With addition of salt, increased adsorption of microgels and strengthening of the adsorbing layer were also indicated by combination of Δf and ΔD measurement. The rigid interfacial protein films has been proven to favor the stability of Pickering emulsion as well as its freeze-thaw stability[109].

The estimations of microgels adsorption were supported by direct visualization of QCM-D crystal surfaces by AFM imaging. The microgels coverages in AFM images agreed well with QCM-D results. However, many studies [110-112] have clearly demonstrated that the frequency shift is not a linear function of the surface coverage. Instead, the relative contribution of the surrounding liquid to the frequency response decreases with increasing coverage. By applying an appropriate method of modeling or simulation, the dissipation characteristics induced by the adsorbed heterogeneous films under different pH conditions can be interpreted.

According to the summary from Reviakine *et al.*[106], when ΔD is low, the case of monolayer of discrete particles is rather simple (Sauerbrey equation is applied) at high coverage. However, it is still complicated at low coverage, which involved an empirical trapped-liquid coat model. The model relies on an independent measurement, such as reflectometry or ellipsometry, to calculate the real mass density of the adsorbed particles. When $\Delta D>0$, true for BM adsorption at those three pH levels, the situation should be rationalized in terms of coatings of hydrodynamically trapped liquid that surround each adsorbed particle. Based on studies about the hydrodynamic effects[110, 113], the amount of dissipation strongly depended on 1) the stiffness of the particle-surface contact region (also called "linker") and 2) the surface coverage of absorbed particles. Naturally, energy dissipation decreases as the stiffness increases. With increasing coverage, the overall dissipation decreases, resulting in a decrease in the $\Delta D/\Delta f$ ratio[113]. By far, we are able to further explain the identical gradients of $\Delta D/\Delta f$ obtained at pH 3.2 and pH 5.6. BM adsorption under pH 5.6 achieving the highest coverage should have resulted in lowest $\Delta D/\Delta f$ value, because hydrodynamic interactions between adjacent microgel particles would reduce the amplitude of absorbed particles motion. BM absorbed under pH 3.2 may have stiffer particle-surface contact region so that decreased the energy dissipation around the particles. Therefore even with lower coverage, the microgels adsorption in pH 3.2 resulted in almost the same gradients of $\Delta D/\Delta f$ with that of pH 5.6.

For heterogeneous films, quantitative calculation of QCM outputs is possible by applying finite element method (FEM) simulation[113], in which the stress distribution around the surface-bound particles is calculated and used to derive the

f and *D* changes. But there is a computationally demanding, so further research is needed to extend it to soft particles such as microgels.

Overall, microgels morphology and coverage on modified hydrophobic surface showed consistency with Cryo-SEM observation of the emulsion droplet interface[13]. QCM-D showed the ability to characterize the microgels interfacial properties and viscoelasticity of the adsorbed layer on solid surface, which may provide insights in their relationship with the oil-in-water emulsion stability. However, differences between solid/liquid and liquid/liquid interface should be considered, when transfer the QCM-D findings to the microgels at oil-water interface. One of main differences between solid/liquid and liquid/liquid interfaces lies in a fact that in the latter case the microgels slightly protrude to the oil phase[114]. Another factor affecting microgels packing at the oil-water interface is the intensity of hydrodynamic disturbance during emulsification. The setting-up of QCM-D system only allows for studying the diffusion adsorption, so when applied into the real emulsion, the shearing induced interfacial changes also need to be taken into consideration for soft particles. Besides, since microgels have porous structure, one could expect that a small amount of oil will be adsorbed by the microgel particles at the liquid interface in the real oil-water emulsion. Further study is needed to better support the validity of the modified hydrophobic surface as a mimic to the real oil-water interface.

4.6 Conclusion

We have investigated the ability of QCM-D to study the Blg microgels adsorption onto a model hydrophobic surface. The Blg microgels adsorption under different

BM concentration, pH values, and ionic strength conditions were explored. The QCM-D results showed that the adsorption efficiency was strongly dependent on the particle charge and the ionic strength of the aqueous phase. The adsorption of weakly charged Blg microgels (pH 5.6) was characterized by highly covered particles, producing a relative rigid monolayer at the interface. Fewer amount of the microgels adsorbed when they were strongly charged (pH 3.2 and 7.4) with surface being covered by discrete particles. The particle packing in the ad-layer was loose at pH 7.4, while secondary structural changes in Blg microgels at pH 3.2 may favor the structural rearrangement on interface, resulted in formation of a stiff monolayer. Those estimations were supported by the direct visualization of sensor surfaces by AFM. Addition of salt effectively screened the electrostatic repulsion between microgel particles, resulted in a more densely packed layer. The application of QCM-D enables us to generate insights into the fundamental behavior of soft particles at a solid-liquid interface. We have examined a possible technique to study interfacial properties of microgels in Pickering emulsions, while further study is needed to better support the transferability from interfacial activity of microgels at solid hydrophobic interface to the microgels at oil-water interface.

5. Chapter V Perspectives

The application of QCM-D and AFM enabled us to generate insights on the fundamental behavior of soft particles at a hydrophobic surface, however, the microgels behavior at the flat solid-liquid interface may not completely resemble that at the curved liquid-liquid interface of emulsion droplets. Further study is needed to better support the transferability from interfacial activity of microgels at the solid-liquid interface to the liquid-liquid interface. Furthermore, the solid surface of QCM-D chip can be modified with hydrophilic polysaccharide. The technique of QCM-D will provide detailed information about particle-polysaccharide and particle-particle interactions on the hydrophilic surface under different conditions. Viscoelastic models may be valid to quantitatively analyze the rheological properties of adsorbing layer, which could be used to obtain the stabilization mechanism of W/W emulsion.

We demonstrated that microgels particle-particle fusion is formed on the surface of W/W droplet after thermal treatment. It points toward a potential strategy to fabricate protein microcapsules via water-in-water emulsions. Protein microcapsules, also named as “colloidosomes”, are hollow, elastic capsules with easily adjusted and highly controllable permeability and elasticity [115]. Precise control of several parameters would allow a strategic design of new protein structures with possible controlled release properties. The microcapsule surfaces composed of a crosslinked layer of protein microgels will link together to form an elastic shell. The size of the microcapsule can be easily adjusted based on the size of droplet of the W/W emulsion. The interstices between the microgels as well as

polyelectrolyte nature of protein can provide the microcapsules with pH responsive permeability. The biocompatibility of protein allows microcapsules' encapsulation of food-grade ingredients as well as sensitive ingredients, such as biomolecules and cells.

From a more practical perspective, several issues must be addressed before the W/W can be used in food applications. In this study, the stability of W/W emulsion is highly dependent on the pH, increasing pH above the pI of microgels leads to phase separation. Altering the microgels' pI is feasible by conjugating Blg microgels with polyamines via carbodiimide coupling reaction[116]. The pI of modified Blg microgels may be increased to pH 7-10, thus providing the microgels stabilized W/W emulsions desirable stability at a wide range of pH. Although many works have focused on the mechanism and stability of particle-stabilized W/W emulsions, their applications such as delivery for bioactive compounds was seldom reported. As the features of the two aqueous phases are so similar, how to enrich the bioactive compounds in either of the phases rather than dispersing in both two phases is a problem to be solved. Further study is needed to turn this W/W emulsion into an efficient vehicle for loading hydrophilic bioactive compounds.

References

1. Wang, Y.-J.; Pan, M.-H.; Cheng, A.-L.; Lin, L.-I.; Ho, Y.-S.; Hsieh, C.-Y.; Lin, J.-K., Stability of curcumin in buffer solutions and characterization of its degradation products. *Journal of pharmaceutical and biomedical analysis* **1997,** *15* (12), 1867-1876.
2. Yang, M. C.; Guan, H.-H.; Yang, J.-M.; Ko, C.-N.; Liu, M.-Y.; Lin, Y.-H.; Huang, Y.-C.; Chen, C.-J.; Mao, S. J., Rational design for crystallization of β-lactoglobulin and vitamin D3 complex: revealing a secondary binding site. *Crystal Growth and Design* **2008,** *8* (12), 4268-4276.
3. Teng, Z.; Xu, R.; Wang, Q., Beta-lactoglobulin-based encapsulating systems as emerging bioavailability enhancers for nutraceuticals: a review. *RSC Advances* **2015,** *5* (44), 35138-35154.
4. Elzoghby, A. O.; Hemasa, A. L.; Freag, M. S., Hybrid protein-inorganic nanoparticles: From tumor-targeted drug delivery to cancer imaging. *Journal of Controlled Release* **2016,** *243*, 303-322. DOI: 10.1016/j.jconrel.2016.10.023.
5. Kayani, Z.; Bordbar, A. K.; Firuzi, O., Novel folic acid-conjugated doxorubicin loaded beta-lactoglobulin nanoparticles induce apoptosis in breast cancer cells. *Biomedicine & Pharmacotherapy* **2018,** *107*, 945-956. DOI: 10.1016/j.biopha.2018.08.047.
6. Guillet-Nicolas, R.; Popat, A.; Bridot, J. L.; Monteith, G.; Qiao, S. Z.; Kleitz, F., pH-Responsive NutraceuticalMesoporous Silica Nanoconjugates with Enhanced Colloidal Stability. *Angewandte Chemie-International Edition* **2013,** *52* (8), 2318-2322. DOI: 10.1002/anie.201208840.
7. Izadi, Z.; Divsalar, A.; Saboury, A. A.; Sawyer, L., beta-lactoglobulin-pectin Nanoparticle-based Oral Drug Delivery System for Potential Treatment of Colon Cancer. *Chemical Biology & Drug Design* **2016,** *88* (2), 209-216. DOI: 10.1111/cbdd.12748.
8. Dickinson, E., Microgels—An alternative colloidal ingredient for stabilization of food emulsions. *Trends in Food Science & Technology* **2015,** *43* (2), 178-188.
9. Nicolai, T.; Britten, M.; Schmitt, C., beta-Lactoglobulin and WPI aggregates: Formation, structure and applications. *Food Hydrocolloids* **2011,** *25* (8), 1945-1962. DOI: 10.1016/j.foodhyd.2011.02.006.
10. Jung, J. M.; Savin, G.; Pouzot, M.; Schmitt, C.; Mezzenga, R., Structure of heat-induced beta-lactoglobulin aggregates and their complexes with sodium-dodecyl sulfate. *Biomacromolecules* **2008,** *9* (9), 2477-2486. DOI: 10.1021/bm800502j.
11. Tuan, P. X.; Durand, D.; Nicolai, T.; Donato, L.; Schmitt, C.; Bovetto, L., On the Crucial Importance of the pH for the Formation and Self-Stabilization of Protein Microgels and Strands. *Langmuir* **2011,** *27* (24), 15092-15101. DOI: 10.1021/la203357p.
12. Schmitt, C.; Moitzi, C.; Bovay, C.; Rouvet, M.; Bovetto, L.; Donato, L.; Leser, M. E.; Schurtenberger, P.; Stradner, A., Internal structure and colloidal behaviour of covalent whey protein microgels obtained by heat treatment. *Soft Matter* **2010,** *6* (19), 4876-4884.
13. Destribats, M.; Rouvet, M.; Gehin-Delval, C.; Schmitt, C.; Binks, B. P., Emulsions stabilised by whey protein microgel particles: towards food-grade Pickering emulsions. *Soft Matter* **2014,** *10* (36), 6941-6954. DOI: 10.1039/C4SM00179F.
14. Pickering, S. U., Cxcvi.—emulsions. *Journal of the Chemical Society, Transactions* **1907,** *91*, 2001-2021.
15. Dickinson, E., Use of nanoparticles and microparticles in the formation and stabilization of food emulsions. *Trends in Food Science & Technology* **2012,** *24* (1), 4-12.
16. Xiao, J.; Li, Y.; Huang, Q., Recent advances on food-grade particles stabilized Pickering emulsions: fabrication, characterization and research trends. *Trends in Food Science & Technology* **2016,** *55*, 48-60.
17. Schmidt, S.; Liu, T.; Rütten, S.; Phan, K.-H.; Möller, M.; Richtering, W., Influence of microgel architecture and oil polarity on stabilization of emulsions by stimuli-sensitive core–shell poly (N-isopropylacrylamide-co-methacrylic acid) microgels: Mickering versus Pickering behavior? *Langmuir* **2011,** *27* (16), 9801-9806.
18. Geisel, K.; Isa, L.; Richtering, W., The Compressibility of pH- Sensitive Microgels at the Oil-Water Interface: Higher Charge Leads to Less Repulsion. *Angewandte Chemie-International Edition* **2014,** *53* (19), 4905-4909. DOI: 10.1002/anie.201402254.

19. Schmitt, V.; Ravaine, V., Surface compaction versus stretching in Pickering emulsions stabilised by microgels. *Current Opinion in Colloid & Interface Science* **2013,** *18* (6), 532-541. DOI: 10.1016/j.cocis.2013.11.004.
20. de Folter, J. W.; van Ruijven, M. W.; Velikov, K. P., Oil-in-water Pickering emulsions stabilized by colloidal particles from the water-insoluble protein zein. *Soft Matter* **2012,** *8* (25), 6807-6815.
21. Nguyen, B. T.; Nicolai, T.; Benyahia, L., Stabilization of water-in-water emulsions by addition of protein particles. *Langmuir* **2013,** *29* (34), 10658-10664.
22. Balakrishnan, G.; Nicolai, T.; Benyahia, L.; Durand, D., Particles Trapped at the Droplet Interface in Water-in-Water Emulsions. *Langmuir* **2012,** *28* (14), 5921-5926. DOI: 10.1021/la204825f.
23. FitzGerald, P. A.; Dupin, D.; Armes, S. P.; Wanless, E. J., In situ observations of adsorbed microgel particles. *Soft Matter* **2007,** *3* (5), 580-586. DOI: 10.1039/b613981g.
24. Bahri, A.; Chevalier-Lucia, D.; Marchesseau, S.; Schmitt, C.; Gergely, C.; Martin, M., Effect of pH change on size and nanomechanical behavior of whey protein microgels. *Journal of Colloid and Interface Science* **2019,** *555*, 558-568. DOI: 10.1016/j.jcis.2019.07.083.
25. Murphy, R. W.; Farkas, B. E.; Jones, O. G., Dynamic and viscoelastic interfacial behavior of β-lactoglobulin microgels of varying sizes at fluid interfaces. *Journal of colloid and interface science* **2016,** *466*, 12-19.
26. Dixon, M. C., Quartz crystal microbalance with dissipation monitoring: enabling real-time characterization of biological materials and their interactions. *Journal of biomolecular techniques: JBT* **2008,** *19* (3), 151.
27. Feiler, A. A.; Davies, P. T.; Vincent, B., Adsorption of anionic gold nanoparticles by a layer of cationic microgel particles deposited on a gold-coated, quartz surface: studied by quartz crystal microbalance and atomic force microscopy. *Soft Matter* **2011,** *7* (14), 6660-6670.
28. Howard, S. C.; Craig, V.; FitzGerald, P. A.; Wanless, E. J., Swelling and collapse of an adsorbed pH-responsive film-forming microgel measured by optical reflectometry and QCM. *Langmuir* **2010,** *26* (18), 14615-14623.
29. Serpe, M. J.; Yarmey, K. A.; Nolan, C. M.; Lyon, L. A., Doxorubicin uptake and release from microgel thin films. *Biomacromolecules* **2005,** *6* (1), 408-413.
30. Teo, A.; Dimartino, S.; Lee, S. J.; Goh, K. K.; Wen, J.; Oey, I.; Ko, S.; Kwak, H.-S., Interfacial structures of whey protein isolate (WPI) and lactoferrin on hydrophobic surfaces in a model system monitored by quartz crystal microbalance with dissipation (QCM-D) and their formation on nanoemulsions. *Food Hydrocolloids* **2016,** *56*, 150-160.
31. Ito, E.; Arai, T.; Hara, M.; Noh, J., Surface potential change depending on molecular orientation of hexadecanethiol self-assembled monolayers on AU (111). *Bulletin of the Korean Chemical Society* **2009,** *30* (6), 1309-1312.
32. Vrij, A., POLYMERS AT INTERFACES AND INTERACTIONS IN COLLOIDAL DISPERSIONS. *Pure and Applied Chemistry* **1976,** *48* (4), 471-483. DOI: 10.1351/pac197648040471.
33. Semenova, M.; Dickinson, E., Biopolymers in Food Colloids: Thermodynamics and Molecular Interactions. *Biopolymers in Food Colloids: Thermodynamics and Molecular Interactions* **2010**, 1-369. DOI: 10.1163/ej.9789004171862.i-370.
34. Poortinga, A. T., Microcapsules from self-assembled colloidal particles using aqueous phase-separated polymer solutions. *Langmuir* **2008,** *24* (5), 1644-1647.
35. Nicolai, T.; Murray, B., Particle stabilized water in water emulsions. *Food Hydrocolloids* **2017,** *68*, 157-163.
36. Firoozmand, H.; Murray, B. S.; Dickinson, E., Interfacial Structuring in a Phase-Separating Mixed Biopolymer Solution Containing Colloidal Particles. *Langmuir* **2009,** *25* (3), 1300-1305. DOI: 10.1021/la8037389.
37. Gonzalez-Jordan, A.; Nicolai, T.; Benyahia, L., Influence of the Protein Particle Morphology and Partitioning on the Behavior of Particle-Stabilized Water-in-Water Emulsions. *Langmuir* **2016,** *32* (28), 7189-7197. DOI: 10.1021/acs.langmuir.6b01993.
38. Gonzalez-Jordan, A.; Benyahia, L.; Nicolai, T., Cold gelation of water in water emulsions stabilized by protein particles. *Colloids and Surfaces a-Physicochemical and Engineering Aspects* **2017,** *532*, 332-341. DOI: 10.1016/j.colsurfa.2017.04.073.
39. Khemissi, H.; Bassani, H.; Aschi, A.; Capron, I.; Benyahia, L.; Nicolai, T., Exploiting complex

formation between polysaccharides and protein microgels to influence particle stabilization of W/W emulsions. *Langmuir* **2018,** *34* (39), 11806-11813.
40. de Freitas, R. A.; Nicolai, T.; Chassenieux, C.; Benyahia, L., Stabilization of water-in-water emulsions by polysaccharide-coated protein particles. *Langmuir* **2016,** *32* (5), 1227-1232.
41. Dickinson, E., Particle-based stabilization of water-in-water emulsions containing mixed biopolymers. *Trends in Food Science & Technology* **2019,** *83*, 31-40. DOI: 10.1016/j.tifs.2018.11.004.
42. Chatsisvili, N.; Philipse, A. P.; Loppinet, B.; Tromp, R. H., Colloidal zein particles at water-water interfaces. *Food Hydrocolloids* **2017,** *65*, 17-23. DOI: 10.1016/j.foodhyd.2016.10.036.
43. Sinn, N.; Alishahi, M.; Hardt, S., Detachment of particles and particle clusters from liquid/liquid interfaces. *Journal of Colloid and Interface Science* **2015,** *458*, 62-68. DOI: 10.1016/j.jcis.2015.06.050.
44. Papp, L. V.; Lu, J.; Holmgren, A.; Khanna, K. K., From selenium to selenoproteins: synthesis, identity, and their role in human health. *Antioxidants & redox signaling* **2007,** *9* (7), 775-806.
45. Yang, G.; Yin, S.; Zhou, R.; Gu, L.; Yan, B.; Liu, Y., Studies of safe maximal daily dietary Se-intake in a seleniferous area in China. Part II: Relation between Se-intake and the manifestation of clinical signs and certain biochemical alterations in blood and urine. *Journal of trace elements and electrolytes in health and disease* **1989,** *3* (3), 123-130.
46. Ip, C.; Hayes, C.; Budnick, R. M.; Ganther, H. E., Chemical form of selenium, critical metabolites, and cancer prevention. *Cancer research* **1991,** *51* (2), 595-600.
47. Van Overschelde, O.; Guisbiers, G.; Snyders, R., Green synthesis of selenium nanoparticles by excimer pulsed laser ablation in water. *Apl Materials* **2013,** *1* (4), 042114.
48. Mees, D. R.; Pysto, W.; Tarcha, P. J., Formation of selenium colloids using sodium ascorbate as the reducing agent. *Journal of colloid and interface science* **1995,** *170* (1), 254-260.
49. Shakibaie, M.; Khorramizadeh, M. R.; Faramarzi, M. A.; Sabzevari, O.; Shahverdi, A. R., Biosynthesis and recovery of selenium nanoparticles and the effects on matrix metalloproteinase‐2 expression. *Biotechnology and applied biochemistry* **2010,** *56* (1), 7-15.
50. Bannerjee, I., The spontaneous formation of selenium nanoparticles on gallic acid assemblies and their antioxidant properties. *Fordham Undergraduate Research Journal* **2013,** *1* (1), 3.
51. Wu, S.; Sun, K.; Wang, X.; Wang, D.; Wan, X.; Zhang, J., Protonation of epigallocatechin-3-gallate (EGCG) results in massive aggregation and reduced oral bioavailability of EGCG-dispersed selenium nanoparticles. *Journal of agricultural and food chemistry* **2013,** *61* (30), 7268-7275.
52. Kong, H.; Yang, J.; Zhang, Y.; Fang, Y.; Nishinari, K.; Phillips, G. O., Synthesis and antioxidant properties of gum arabic-stabilized selenium nanoparticles. *International journal of biological macromolecules* **2014,** *65*, 155-162.
53. Zhang, C.; Zhai, X.; Zhao, G.; Ren, F.; Leng, X., Synthesis, characterization, and controlled release of selenium nanoparticles stabilized by chitosan of different molecular weights. *Carbohydrate polymers* **2015,** *134*, 158-166.
54. Zhang, J.-S.; Gao, X.-Y.; Zhang, L.-D.; Bao, Y.-P., Biological effects of a nano red elemental selenium. *BioFactors* **2001,** *15* (1), 27-38. DOI: 10.1002/biof.5520150103.
55. Xia, Y.-Y., Synthesis of selenium nanoparticles in the presence of silk fibroin. *Materials Letters* **2007,** *61* (21), 4321-4324.
56. Wang, H.; Zhang, J.; Yu, H., Elemental selenium at nano size possesses lower toxicity without compromising the fundamental effect on selenoenzymes: comparison with selenomethionine in mice. *Free Radical Biology and Medicine* **2007,** *42* (10), 1524-1533.
57. Yamada, C.; Yamashita, Y.; Seki, R.; Izumi, H.; Matsuda, T.; Kato, Y., Digestion and gastrointestinal absorption of the 14–16-kDa rice allergens. *Bioscience, biotechnology, and biochemistry* **2006,** *70* (8), 1890-1897.
58. Reddy, I. M.; Kella, N. K.; Kinsella, J. E., Structural and conformational basis of the resistance of β-lactoglobulin to pectic and chymotryptic digestion. *Journal of agricultural and food chemistry* **1988,** *36* (4), 737-741.
59. Given, P. S., Encapsulation of flavors in emulsions for beverages. *Current Opinion in Colloid & Interface Science* **2009,** *14* (1), 43-47.
60. Chen, L.; Subirade, M., Chitosan/β-lactoglobulin core–shell nanoparticles as nutraceutical carriers. *Biomaterials* **2005,** *26* (30), 6041-6053.

61. Zimet, P.; Livney, Y. D., Beta-lactoglobulin and its nanocomplexes with pectin as vehicles for ω-3 polyunsaturated fatty acids. *Food Hydrocolloids* **2009,** *23* (4), 1120-1126.
62. Alomirah, H.; Alli, I., Separation and characterization of β-lactoglobulin and α-lactalbumin from whey and whey protein preparations. *International Dairy Journal* **2004,** *14* (5), 411-419.
63. Viseu, M. I.; Carvalho, T. I.; Costa, S. M., Conformational transitions in β-lactoglobulin induced by cationic amphiphiles: equilibrium studies. *Biophysical journal* **2004,** *86* (4), 2392-2402.
64. Lott, P. F.; Cukor, P.; Moriber, G.; Solga, J., 2, 3-Diaminonaphthalene as a Reagent for the Determination of Milligram to Submicrogram Amounts of Selenium. *Analytical Chemistry* **1963,** *35* (9), 1159-1163.
65. Teng, Z.; Li, Y.; Luo, Y.; Zhang, B.; Wang, Q., Cationic beta-lactoglobulin nanoparticles as a bioavailability enhancer: protein characterization and particle formation. *Biomacromolecules* **2013,** *14* (8), 2848-56. DOI: 10.1021/bm4006886.
66. Shah, C.; Kumar, M.; Bajaj, P., Acid-induced synthesis of polyvinyl alcohol-stabilized selenium nanoparticles. *Nanotechnology* **2007,** *18* (38), 385607.
67. Yu, B.; Zhang, Y.; Zheng, W.; Fan, C.; Chen, T., Positive surface charge enhances selective cellular uptake and anticancer efficacy of selenium nanoparticles. *Inorganic chemistry* **2012,** *51* (16), 8956-8963.
68. Liu, W.; Li, X.; Wong, Y.-S.; Zheng, W.; Zhang, Y.; Cao, W.; Chen, T., Selenium nanoparticles as a carrier of 5-fluorouracil to achieve anticancer synergism. *ACS nano* **2012,** *6* (8), 6578-6591.
69. Zheng, G.; Liu, H.; Zhu, Z.; Zheng, J.; Liu, A., Selenium modification of β-lactoglobulin (β-Lg) and its biological activity. *Food chemistry* **2016,** *204*, 246-251.
70. Yang, F.; Tang, Q.; Zhong, X.; Bai, Y.; Chen, T.; Zhang, Y.; Li, Y.; Zheng, W., Surface decoration by Spirulina polysaccharide enhances the cellular uptake and anticancer efficacy of selenium nanoparticles. *Int J Nanomedicine* **2012,** *7*, 835-844.
71. Ghose, A.; Fleming, J.; El-Bayoumy, K.; Harrison, P. R., Enhanced sensitivity of human oral carcinomas to induction of apoptosis by selenium compounds. *Cancer research* **2001,** *61* (20), 7479-7487.
72. Weiller, M.; Latta, M.; Kresse, M.; Lucas, R.; Wendel, A., Toxicity of nutritionally available selenium compounds in primary and transformed hepatocytes. *Toxicology* **2004,** *201* (1), 21-30.
73. Rebsch, C. M.; Penna, F. J.; Copeland, P. R., Selenoprotein expression is regulated at multiple levels in prostate cells. *Cell research* **2006,** *16* (12), 940-948.
74. Vis, M.; Opdam, J.; van 't Oor, I. S. J.; Soligno, G.; van Roij, R.; Tromp, R. H.; Erne, B. H., Water-in-Water Emulsions Stabilized by Nanoplates. *Acs Macro Letters* **2015,** *4* (9), 965-968. DOI: 10.1021/acsmacrolett.5b00480.
75. Sarkar, A.; Murray, B.; Holmes, M.; Ettelaie, R.; Abdalla, A.; Yang, X. Y., In vitro digestion of Pickering emulsions stabilized by soft whey protein microgel particles: influence of thermal treatment. *Soft Matter* **2016,** *12* (15), 3558-3569. DOI: 10.1039/c5sm02998h.
76. Nguyen, B. T.; Wang, W. K.; Saunders, B. R.; Benyahia, L.; Nicolai, T., pH-Responsive Water-in-Water Pickering Emulsions. *Langmuir* **2015,** *31* (12), 3605-3611. DOI: 10.1021/la5049024.
77. Asenjo, J. A.; Andrews, B. A., Aqueous two-phase systems for protein separation: A perspective. *Journal of Chromatography A* **2011,** *1218* (49), 8826-8835. DOI: 10.1016/j.chroma.2011.06.051.
78. Schluck, A.; Maurer, G.; Kula, M. R., INFLUENCE OF ELECTROSTATIC INTERACTIONS ON PARTITIONING IN AQUEOUS POLYETHYLENE-GLYCOL DEXTRAN BIPHASIC SYSTEMS .1. *Biotechnology and Bioengineering* **1995,** *46* (5), 443-451. DOI: 10.1002/bit.260460508.
79. Schluck, A.; Maurer, G.; Kula, M. R., THE INFLUENCE OF ELECTROSTATIC INTERACTIONS ON PARTITION IN AQUEOUS POLYETHYLENE GLYCOL/DEXTRAN BIPHASIC SYSTEMS .2. *Biotechnology and Bioengineering* **1995,** *47* (2), 252-260. DOI: 10.1002/bit.260470217.
80. Schmitt, C.; Bovay, C.; Vuilliomenet, A.-M.; Rouvet, M.; Bovetto, L.; Barbar, R.; Sanchez, C., Multiscale characterization of individualized β-lactoglobulin microgels formed upon heat treatment under narrow pH range conditions. *Langmuir* **2009,** *25* (14), 7899-7909.
81. Ruthven, M.; Ko, K. R.; Agarwal, R.; Frampton, J. P., Microscopic evaluation of aqueous two-phase system emulsion characteristics enables rapid determination of critical polymer concentrations for solution micropatterning. *Analyst* **2017,** *142* (11), 1938-1945.
82. Griffith, C.; Daigle, H., On the shear stability of water-in-water Pickering emulsions

stabilized with silica nanoparticles. *Journal of colloid and interface science* **2018,** *532*, 83-91.
83. Zhang, J. L.; Mei, L.; Chen, N. N.; Yuan, Y.; Zeng, Q. Z.; Wang, Q., Study on beta-lactoglobulin microgels adsorption onto a hydrophobic solid surface by QCM-D. *Food Hydrocolloids* **2020,** *98*. DOI: 10.1016/j.foodhyd.2019.105320.
84. Goh, K. K. T.; Matia-Merino, L.; Chiang, J. H.; Quek, R.; Soh, S. J. B.; Lentle, R. G., The physico-chemical properties of chia seed polysaccharide and its microgel dispersion rheology. *Carbohydrate Polymers* **2016,** *149*, 297-307. DOI: 10.1016/j.carbpol.2016.04.126.
85. Koocheki, A.; Taherian, A. R.; Bostan, A., Studies on the steady shear flow behavior and functional properties of Lepidium perfoliatum seed gum. *Food Research International* **2013,** *50* (1), 446-456. DOI: 10.1016/j.foodres.2011.05.002.
86. Camino, N. A.; Sanchez, C. C.; Patino, J. M. R.; Pilosof, A. M. R., Hydroxypropylmethylcellulose-beta-lactoglobulin mixtures at the oil-water interface. Bulk, interfacial and emulsification behavior as affected by pH. *Food Hydrocolloids* **2012,** *27* (2), 464-474. DOI: 10.1016/j.foodhyd.2011.09.006.
87. Ettelaie, R.; Murray, B. S.; Liu, S. J., On the Origin of Seemingly Nonsurface-Active Particles Partitioning between Phase-Separated Solutions of Incompatible Nonadsorbing Polymers and Their Adsorption at the Phase Boundary. *Langmuir* **2019,** *35* (29), 9493-9503. DOI: 10.1021/acs.langmuir.9b00892.
88. Bhuyan, A. K., On the Mechanism of SDS-Induced Protein Denaturation. *Biopolymers* **2010,** *93* (2), 186-199. DOI: 10.1002/bip.21318.
89. Nilsson, S., INTERACTIONS BETWEEN WATER-SOLUBLE CELLULOSE DERIVATIVES AND SURFACTANTS .1. THE HPMC/SDS/WATER SYSTEM. *Macromolecules* **1995,** *28* (23), 7837-7844. DOI: 10.1021/ma00127a034.
90. Tanaka, R.; Meadows, J.; Williams, P. A.; Phillips, G. O., INTERACTION OF HYDROPHOBICALLY MODIFIED (HYDROXYETHYL)CELLULOSE WITH VARIOUS ADDED SURFACTANTS. *Macromolecules* **1992,** *25* (4), 1304-1310. DOI: 10.1021/ma00030a016.
91. Arditty, S.; Whitby, C. P.; Binks, B.; Schmitt, V.; Leal-Calderon, F., Some general features of limited coalescence in solid-stabilized emulsions. *The European Physical Journal E* **2003,** *11* (3), 273-281.
92. Whitesides, T. H.; Ross, D. S., Experimental and theoretical analysis of the limited coalescence process: stepwise limited coalescence. *Journal of colloid and interface science* **1995,** *169* (1), 48-59.
93. Yang, Y.; Fang, Z.; Chen, X.; Zhang, W.; Xie, Y.; Chen, Y.; Liu, Z.; Yuan, W., An overview of pickering emulsions: solid-particle materials, classification, morphology, and applications. *Frontiers in pharmacology* **2017,** *8*, 287.
94. Chevalier, Y.; Bolzinger, M.-A., Emulsions stabilized with solid nanoparticles: Pickering emulsions. *Colloids and Surfaces A: Physicochemical and Engineering Aspects* **2013,** *439*, 23-34.
95. Whitby, C.; Wanless, E., Controlling Pickering emulsion destabilisation: A route to fabricating new materials by phase inversion. *Materials* **2016,** *9* (8), 626.
96. Phan-Xuan, T.; Durand, D.; Nicolai, T.; Donato, L.; Schmitt, C.; Bovetto, L., On the crucial importance of the pH for the formation and self-stabilization of protein microgels and strands. *Langmuir* **2011,** *27* (24), 15092-15101.
97. Destribats, M.; Lapeyre, V.; Sellier, E.; Leal-Calderon, F.; Ravaine, V.; Schmitt, V., Origin and control of adhesion between emulsion drops stabilized by thermally sensitive soft colloidal particles. *Langmuir* **2012,** *28* (8), 3744-3755.
98. Zimmerer, L.; Jones, O. G., Emulsification capacity of microgels assembled from β-lactoglobulin and pectin. *Food biophysics* **2014,** *9* (3), 229-237.
99. Townend, R.; Winterbottom, R.; Timasheff, S. N., Molecular Interactions in β-Lactoglobulin. II. Ultracentrifugal and Electrophoretic Studies of the Association of β-Lactoglobulin below its Isoelectric Point2. *Journal of the American Chemical society* **1960,** *82* (12), 3161-3168.
100. Kleinen, J.; Richtering, W., Rearrangements in and release from responsive microgel–polyelectrolyte complexes induced by temperature and time. *The Journal of Physical Chemistry B* **2011,** *115* (14), 3804-3810.
101. Hemmersam, A. G.; Rechendorff, K.; Besenbacher, F.; Kasemo, B.; Sutherland, D. S., pH-dependent adsorption and conformational change of ferritin studied on metal oxide surfaces by a

combination of QCM-D and AFM. *The Journal of Physical Chemistry C* **2008,** *112* (11), 4180-4186.
102. Ohshima, H., Electrophoresis of soft particles. *Advances in colloid and interface science* **1995,** *62* (2-3), 189-235.
103. Mivehi, L.; Bordes, R.; Holmberg, K., Adsorption of cationic gemini surfactants at solid surfaces studied by QCM-D and SPR—Effect of the presence of hydroxyl groups in the spacer. *Colloids and Surfaces A: Physicochemical and Engineering Aspects* **2013,** *419*, 21-27. DOI: https://doi.org/10.1016/j.colsurfa.2012.11.044.
104. Feiler, A. A.; Sahlholm, A.; Sandberg, T.; Caldwell, K. D., Adsorption and viscoelastic properties of fractionated mucin (BSM) and bovine serum albumin (BSA) studied with quartz crystal microbalance (QCM-D). *Journal of Colloid and Interface Science* **2007,** *315* (2), 475-481. DOI: https://doi.org/10.1016/j.jcis.2007.07.029.
105. Höök, F.; Rodahl, M.; Brzezinski, P.; Kasemo, B., Measurements Using the Quartz Crystal Microbalance Technique of Ferritin Monolayers on Methyl-Thiolated Gold: Dependence of Energy Dissipation and Saturation Coverage on Salt Concentration. *Journal of Colloid and Interface Science* **1998,** *208* (1), 63-67. DOI: https://doi.org/10.1006/jcis.1998.5774.
106. Reviakine, I.; Johannsmann, D.; Richter, R. P., Hearing what you cannot see and visualizing what you hear: interpreting quartz crystal microbalance data from solvated interfaces. ACS Publications: 2011.
107. Kong, J.; Yu, S., Fourier transform infrared spectroscopic analysis of protein secondary structures. *Acta biochimica et biophysica Sinica* **2007,** *39* (8), 549-559.
108. Fang, Y.; Dalgleish, D. G., Conformation of β-lactoglobulin studied by FTIR: effect of pH, temperature, and adsorption to the oil–water interface. *Journal of Colloid and Interface Science* **1997,** *196* (2), 292-298.
109. Zhu, X.-F.; Zheng, J.; Liu, F.; Qiu, C.-Y.; Lin, W.-F.; Tang, C.-H., Freeze-thaw stability of Pickering emulsions stabilized by soy protein nanoparticles. Influence of ionic strength before or after emulsification. *Food Hydrocolloids* **2018,** *74*, 37-45.
110. Johannsmann, D.; Reviakine, I.; Rojas, E.; Gallego, M., Effect of Sample Heterogeneity on the Interpretation of QCM(-D) Data: Comparison of Combined Quartz Crystal Microbalance/Atomic Force Microscopy Measurements with Finite Element Method Modeling. *Analytical Chemistry* **2008,** *80* (23), 8891-8899. DOI: 10.1021/ac8013115.
111. Rojas, E.; Gallego, M.; Reviakine, I., Effect of sample heterogeneity on the interpretation of quartz crystal microbalance data: impurity effects. *Analytical chemistry* **2008,** *80* (23), 8982-8990.
112. Choi, K.-H.; Friedt, J.-M.; Frederix, F.; Campitelli, A.; Borghs, G., Simultaneous atomic force microscope and quartz crystal microbalance measurements: Investigation of human plasma fibrinogen adsorption. *Applied Physics Letters* **2002,** *81* (7), 1335-1337.
113. Johannsmann, D.; Reviakine, I.; Richter, R. P., Dissipation in films of adsorbed nanospheres studied by quartz crystal microbalance (QCM). *Analytical chemistry* **2009,** *81* (19), 8167-8176.
114. Pinaud, F.; Geisel, K.; Massé, P.; Catargi, B.; Isa, L.; Richtering, W.; Ravaine, V.; Schmitt, V., Adsorption of microgels at an oil–water interface: correlation between packing and 2D elasticity. *Soft Matter* **2014,** *10* (36), 6963-6974.
115. Dinsmore, A.; Hsu, M. F.; Nikolaides, M.; Marquez, M.; Bausch, A.; Weitz, D., Colloidosomes: selectively permeable capsules composed of colloidal particles. *Science* **2002,** *298* (5595), 1006-1009.
116. Teng, Z.; Luo, Y. C.; Li, Y.; Wang, Q., Cationic beta-lactoglobulin nanoparticles as a bioavailability enhancer: Effect of surface properties and size on the transport and delivery in vitro. *Food Chemistry* **2016,** *204*, 391-399. DOI: 10.1016/j.foodchem.2016.02.139.